Structural and Topological Basis of Glass Properties and Diffusion

Smedskjær, Morten Mattrup

Publication date:
2011

Document Version
Publisher's PDF, also known as Version of record

Structural and Topological Basis of Glass Properties and Diffusion

Morten Mattrup Smedskjær

Section of Chemistry
Aalborg University

ISBN: 978-87-90033-81-1
Ph.D. Dissertation, 2011

AALBORG UNIVERSITY

Ph.D. Dissertation

Structural and Topological Basis of Glass Properties and Diffusion

by

Morten Mattrup Smedskjær

Section of Chemistry
Department of Biotechnology, Chemistry,
and Environmental Engineering
Aalborg University, Denmark

Date of Defense
April 28th, 2011

Assessment committee

Thorkild Hvitved-Jacobsen
Professor Emeritus
Aalborg University, Denmark

Xiujian Zhao
Professor
Wuhan University of Technology, China

Pierre Lucas
Associate Professor
University of Arizona, USA

Supervisor

Yuanzheng Yue
Professor
Aalborg University, Denmark

Preface and Acknowledgements

This thesis is submitted in partial fulfillment of the requirements for obtaining the Ph.D. degree. The Ph.D. study was carried out from August 1st 2008 to March 15th 2011. The work was primarily done at the Section of Chemistry at Aalborg University with external stays at Zhejiang University (China) for 2½ months, National University of Singapore (Singapore) for 2 months, and Clausthal University of Technology (Germany) for 2 weeks. The study was financed by Aalborg University.

I am truly grateful to my supervisor Yuanzheng Yue for his dedicated supervision, support, and commitment to the project. I have really enjoyed our collaboration and I look forward to working on more fascinating aspects of the glassy state with you in the future. I also take great pleasure in acknowledging my unofficial co-supervisor John C. Mauro from Corning Inc., who has been an outstanding role model for me. I am deeply humbled by all of your support and encouragement, and I look forward to working even closer with you in the future, when I start at Corning. My kind acknowledgements also go to Iván A. Cornejo from Corning Inc. for providing me access to Corning's research facilities during the final period of my Ph.D. study, and to the Advanced Materials Processing Laboratory and Characterization Sciences and Services Directorate at Corning for the experimental work.

I would like to thank Joachim Deubener and his glass group at Clausthal University of Technology for providing me access to their laboratory, whenever I needed it. Thomas Peter deserves special mentioning for always performing my countless SNMS measurements with great dedication and enthusiasm. My kind acknowledgements also go to Sabyasachi Sen (University of California-Davis) and Randall E. Youngman (Corning Inc.) for performing NMR spectroscopy measurements, Steen Mørup (Technical University of Denmark) and Haraldur P. Gunnlaugsson (Aarhus University) for performing Mössbauer spectroscopy measurements, and Mette Solvang and Dorthe Lybye (Rockwool International A/S) for providing samples and for valuable discussions in relation to the work on glass fibers.

I owe special thanks to Jianrong Qiu and John Wang for supporting my stays at Zhejiang University and National University of Singapore, respectively. I have really enjoyed working in your groups, and I have learned so much. In this regard, I thank the Danish Ministry of Science, Technology and Innovation for granting me an Elite Research Scholarship that financially supported my external stays.

I would also like to thank the present and former members of the inorganic amorphous materials group at Aalborg University for many fruitful scientific discussions and assistance in the laboratory. Ralf Keding, Martin Jensen, Qiuju Zheng, Mette Moesgaard, and Xiaoju Guo deserve special mentioning. Finally, my warm thanks go to my fellow Ph.D. students at Aalborg, Clausthal, Zhejiang, and Singapore for providing enjoyable working and social environments.

Abstract

Owing to the complicated non-crystalline structure of glasses and the long time scales involved in the glass transition process, the accurate quantitative design of glassy materials with specific properties has hitherto been impossible. The properties of glasses are determined by their structure (spatial arrangements of atoms) and topology (connectivity of individual atoms). Establishing the structural and topological basis of glass properties is therefore of practical significance, but a challenge. Conquering this challenge is the subject of the present thesis.

The transport properties are a particularly important issue of glass science, and control of these properties plays a crucial role in glass technology. To understand the microscopic mechanisms of transport properties of glass, we investigate the so-called inward and outward diffusion processes. At the same time, we apply these processes as potential tools to enhance various physical and chemical performances of both surface and bulk of glasses. To explore the origins of one mechanical (hardness H) and two dynamical (glass transition temperature T_g and liquid fragility m) properties of glasses, we also apply and extend the topological constraint theory. This approach can be used to isolate the key physics governing macroscopic glass properties.

The inward (from surface toward interior) and outward (from interior toward surface) diffusion of network-modifying cations occur during thermal reduction and oxidation, respectively, of polyvalent element-containing oxide glasses. The redox mechanism depends on temperature and type and partial pressure of the reducing or oxidizing gas. For sufficiently low partial pressure of the oxidizing or reducing gas at sufficiently low temperature, chemical diffusion of the network-modifying cations dominates the dissipation of the driving force for the redox reaction. The cationic diffusion occurs to charge-compensate the flux of electron holes (i.e., charge transfer between, e.g., Fe^{2+} and Fe^{3+}) in the opposite direction. In this work, we focus on the inward diffusion process. The mechanism and kinetics of the outward diffusion process have already been studied in the glass literature.

We reveal that the inward diffusion can occur in a wide range of oxide glass systems and can be driven by reduction of various polyvalent ions, i.e., it is a universal phenomenon in oxide glasses. By characterizing the spatial extent of the inward diffusion as a function of diffusion time and temperature, the kinetics and temperature dependence of the diffusion have been established. Using these data, diffusion coefficients of the network-modifying cations can be calculated based on Fick's first law derived for ionic materials. In similarly polymerized glasses, there is good agreement between the inward diffusion coefficient and the tracer diffusion coefficient of alkaline earth ions, whereas the alkali inward diffusivity is several orders of magnitude lower than the alkali tracer diffusivity. In fact, we find that the inward diffusivity of alkaline earth ions is larger than that of alkali ions. This is unexpected, because the monovalent alkali ions are generally much more mobile than the divalent alkaline earth ions due to the charge difference. The origin of this discrepancy might be attributed to the fact that for alkali inward diffusion, the charge-compensation of electron holes is a rather slow process, which rate-limits the diffusion.

The glass composition and structure affect the degree of diffusion. We demonstrate how size of diffusing cations, type and concentration of polyvalent element, boron speciation, network

polymerization, and crystallization affect the inward diffusion. Among the alkaline earth ions, Mg^{2+} has the lowest activation energy of inward diffusion, whereas copper is the polyvalent element that causes the most intense inward diffusion. In borate and boroaluminosilicate glasses, we show that the diffusivity of the diffusing cations depends on their structural role in the network and the atomic packing fraction of the network. We find that the inward diffusion occurs only in glass and not in crystals, i.e., the diffusion degree decreases with increasing crystallization degree. Finally, we show how liquid fragility (extent of the non-Arrhenius viscous flow behavior) affects the inward diffusion process. In detail, the activation energy of inward diffusion is lower in "strong" compared to "fragile" glass systems.

We also demonstrate how the surface redox reactions and diffusion processes modify various surface and bulk properties of glasses. The crystallization behavior and high temperature stability of glass fibers can be modified by these processes. For example, thermal oxidation (i.e., outward diffusion) enhances the high temperature stability due to the formation of a nano-crystalline oxide surface layer. A silica-rich surface layer is created as a result of inward diffusion in silicate glasses, since the Si^{4+} ions are virtually immobile. This layer enhances the chemical durability and mechanical properties of bulk glasses. This can be combined with improved photoluminescence properties of, e.g., Eu-Yb doped glasses. Reduction of Eu^{3+} to Eu^{2+} allows one ultraviolet-excited Eu^{2+} ion to transfer its energy to two Yb^{3+} ions that emit photons around 1000 nm, which is in the region where crystalline Si solar cells exhibit their greatest spectral response. Hence, Eu-Yb doped glasses subjected to thermal reduction may potentially act as interesting solar cell substrate materials.

Finally, we apply temperature-dependent constraint theory to understand and predict three important glass properties (T_g, m, and H). According to this approach, the glass network can be considered as a network of bond constraints and the number of these constraints decreases with increasing temperature. A key feature of the modeling approach is that it is analytical, i.e., it avoids the costly computations associated with first principle calculations. Using this approach, we demonstrate the universal role of network topology in governing liquid fragility, and we quantitatively predict the composition dependence of T_g, m, and H. This knowledge provides valuable insights into the topological and microstructural origins of glass properties and the approach can be used to quantitatively design new glassy materials with optimized properties.

Resume (Danish Abstract)

Som konsekvens af den komplicerede ikke-krystallinske struktur af glas og de lange tidsskalaer involveret i glasovergangen er det fortsat umuligt at kvantitativt designe glasmaterialer med forudbestemte egenskaber. Egenskaberne af glas er bestemt af glassets struktur (rumligt arrangement af atomer) og topologi (forbindelse mellem individuelle atomer). Fastlæggelse af det strukturelle og topologiske grundlag for glasegenskaber er derfor af stor praktisk betydning, men samtidig en stor udfordring. Løsningen af denne udfordring er emnet for indeværende afhandling.

Transportegenskaberne er et særligt vigtigt emne indenfor glasvidenskab, og kontrol af disse egenskaber spiller en afgørende rolle i glasteknologien. For at forstå de mikroskopiske mekanismer bag transportegenskaberne af glas undersøger vi de såkaldte indadrettede og udadrettede diffusionsprocesser. Samtidig anvender vi disse processer som mulige redskaber til at forbedre forskellige fysiske og kemiske egenskaber af både overflade og bulk af glas. For at udforske baggrunden for én mekanisk (hårdhed H) og to dynamiske (glasovergangstemperatur T_g og væske skrøbelighed m) egenskaber af glas anvender og udbygger vi desuden den topologiske begrænsningsteori. Denne teori kan bruges til at isolere den afgørende fysik, der bestemmer makroskopiske glasegenskaber.

Indadrettet (fra overflade mod indre) og udadrettet (fra indre mod overflade) diffusion af netværksmodificerende kationer forekommer under henholdsvis termisk reduktion og oxidation af oxid glas indeholdende polyvalente elementer. Redox-mekanismen afhænger af temperatur samt type og partialtryk af den reducerende eller oxiderende gas. Ved tilstrækkeligt lavt partialtryk af den reducerende eller oxiderende gas og ved tilstrækkelig lav temperatur er kemisk diffusion af de netværksmodificerende kationer den dominerende redox-mekanisme. Diffusionen af kationer foregår for at ladningsbalancere en modsatrettet bevægelse af elektronhuller (dvs. ladningsoverførsel mellem eksempelvis Fe^{2+} og Fe^{3+}). I denne afhandling fokuserer vi på den indadrettede diffusionsproces. Mekanismen og kinetikken bag udadrettet diffusion er allerede blevet undersøgt i glaslitteraturen.

Vi viser, at indadrettet diffusion kan forekomme i en lang række forskellige oxid glassystemer, og den kan fremkaldes ved reduktion af forskellige polyvalente ioner. Det er med andre ord et universelt fænomen i oxid glas. Ved at kortlægge diffusionsgraden som funktion af tid og temperatur har vi fastlagt kinetik og temperaturafhængighed af diffusionsprocessen. Diffusionskoefficienter for de netværksmodificerende kationer kan beregnes ud fra disse data ved brug af Ficks første lov udledt for ioniske materialer. Der er god overensstemmelse mellem den indadrettede diffusionskoefficient og sporstof diffusionskoefficienten for de jordalkaliske ioner i glas med sammenlignelig polymerisationsgrad. Derimod er den indadrettede alkali diffusionskoefficient meget, meget mindre end alkali sporstof diffusionskoefficienten. Vi har således fundet ud af, at indadrettede diffusion af jordalkaliske ioner er hurtigere end indadrettet diffusion af alkali ioner. Dette er overraskende, da de monovalente alkali ioner generelt er meget mere mobile end de divalente jordalkaliske ioner på grund af forskellen i ladning. Årsagen til denne uoverensstemmelse skal muligvis findes i, at ladningsbalanceringen af elektronhuller er en relativ langsom proces, der hastighedsbegrænser den indadrettet alkali diffusion.

Sammensætningen og strukturen af glas påvirker graden af diffusion i glasset. Vi påviser, hvordan størrelsen af de diffunderende kationer, typen og koncentrationen af det polyvalente

element, bor speciering, netværkspolymerisation samt krystallisation påvirker den indadrettede diffusion. Mg^{2+} har den lavest aktiveringsenergi for indadrettet diffusion blandt de jordalkaliske ioner, mens kobber er det polyvalente element, der fremkalder den mest intense indadrettede diffusion. I borat og boraluminiumsilikat glas afhænger kationernes diffusionshastighed af deres strukturelle rolle i glasnetværket samt den atomare pakningsgrad af netværket. Den indadrettede diffusion finder kun sted i glas og ikke i krystaller, dvs. diffusionsgraden falder med stigende krystallisationsgrad. Endelig viser vi, hvordan væske skrøbelighed (grad af væskens ikke-Arrhenius viskøse flow karakter) påvirker den indadrettede diffusionsproces. Aktiveringsenergien for indadrettet diffusion er således mindre i "stærke" sammenlignet med "skrøbelige" glassystemer.

Vi demonstrerer også, hvordan overflade redox reaktioner og diffusionsprocesser kan bruges til at ændre forskellige overflade og bulk egenskaber af glas. Vi viser, hvordan krystallisationsopførslen og høj temperatur stabiliteten af glasfibre kan modificeres. Eksempelvis forbedrer termisk oxidation høj temperatur stabiliteten på grund af dannelsen af et nanokrystallinsk oxid overfladelag som følge af udadrettet diffusion. Et overfladelag beriget i silika dannes som konsekvens af indadrettet diffusion i silikat glas, fordi Si^{4+} ionerne er næsten ubevægelige. Laget forbedrer den kemiske modstandsdygtighed og de mekaniske egenskaber af bulk glas. Dette kan kombineres med forbedrede fotoluminescens egenskaber af glas dopet med eksempelvis Eu og Yb. Reduktion af Eu^{3+} til Eu^{2+} muliggør, at én ultraviolet-exciteret Eu^{2+} ion kan overføre dens energi til to Yb^{3+} ioner. Yb^{3+} udsender fotoner omkring 1000 nm, hvilket er i det område, hvor krystallinske Si solceller udviser højest energiomdannelseseffektivitet. Derfor kan termisk reduceret Eu-Yb glas potentielt være et interessant solcelle substrat materiale.

Endelig anvender vi temperaturafhængig begrænsningsteori til at forstå og forudsige tre vigtige glasegenskaber (T_g, m, og H). I henhold til denne teori kan glasnetværket betragtes som et netværk af bindingsbegrænsninger, og antallet af disse begrænsninger falder med stigende temperatur. Et centralt element i denne modelleringsmetode er, at den er analytisk, dvs. man undgår de tidskrævende beregninger, der er forbundet med mere grundlæggende beregningsmetoder. Ved brug af teorien påviser vi den universelle rolle, som netværkstopologi spiller for væskers skrøbelighed, og vi forudsiger kvantitativt, hvordan T_g, m, og H ændres som funktion af glassammensætningen. Denne viden giver værdifuld indsigt i den topologiske og mikrostrukturelle baggrund for glasegenskaber. Metoden kan desuden anvendes til kvantitativt at designe nye glasmaterialer med optimerede egenskaber.

Table of Contents

1 Introduction

The glassy state is ubiquitous in nature and technology [Angell 1995]. In fact, glasses have been a part of our everyday life for thousands of years and they have found astonishingly widespread use in our lives ranging from window glass, windshields, container glass, and electric bulbs all the way to liquid crystal displays and optical fibers in telecommunication networks.

Glasses are disordered materials that lack the periodicity of crystals but behave mechanically like solids. Inorganic glasses are most commonly made by cooling a liquid fast enough to avoid crystallization. The resulting rigid material (i.e., glass) has an extremely long time-scale for relaxation to achieve thermal equilibrium in comparison to the observational time-scale. The atomic structure of glass is therefore representative of that of its frozen-in parent liquid at the temperature at which the liquid thermally equilibrated for the last time, i.e., at the so-called fictive temperature. In scientific terms, glass may be defined as a solid having a non-crystalline structure, which continuously converts to a liquid upon heating. Thermodynamically speaking, glass is an unstable state with respect to the supercooled liquid, and the supercooled liquid is itself metastable with respect to the corresponding crystal [Varshneya & Mauro 2010].

Silica (SiO_2), boric oxide (B_2O_3), and soda-lime-silica (Na_2O-CaO-SiO_2) glasses are the traditional materials from which our understanding of the chemistry and physics of the glassy state originated [Tammann 1933]. Specifically, the study of glass structure took off with Zachariasen's classical paper from 1932 [Zachariasen 1932]. He begins the paper by acknowledging that "*It must be frankly admitted that we know practically nothing about the atomic arrangement in glasses*." In the ensuing decades our understanding of the atomic structure of inorganic glasses has advanced substantially, primarily due to huge improvements in experimental methods [Greaves & Sen 2007]. However, even though glass is one of the oldest materials known to civilization, the science of glass is still in its infancy, with the most basic questions remaining largely unanswered [Phillips 1982]. For example, Nobel laureate Philip W. Anderson has regarded the glass transition as "*the deepest and most interesting unsolved problem in solid-state theory*" [Anderson 1995]. The general reason for the many unsolved problems in glass science is that glasses are not in thermal equilibrium, the atomic structure of glass is not periodic, and the glass transition is accompanied by very small structural changes [Phillips 1982]. Hence, many aspects of glass and glass structure remain unsolved mysteries, which make glasses compelling to study. Fundamental scientific breakthroughs can result in new or improved applications of glass.

1.1 Background and Challenges

The development of advanced technologies based on glasses with specific properties requires methods for designing such materials. This becomes especially important since the experimental study of the correlation between composition and properties of any glass-forming system is an expensive and time-consuming task. Hence, the computational design of glasses with specific properties has long been a "holy grail" within the materials chemistry community [Kerner & Phillips 2000; Martin *et al.* 2002; Salmon 2002]. However, there has been no major breakthrough in the quantitative design of glassy materials due to the reasons mentioned in the previous section.

Since the properties of glasses are determined by their structure and topology, understanding and establishing the structural and topological basis of glass properties is of considerable practical significance. Here, structure refers to the spatial arrangements of atoms, whereas topology describes the microscopic connectivity of individual atoms in the glass network [Phillips 1979]. Despite the enormous amount of reliable experimental data on structure and properties of glasses that has been accumulated in the last decades, none of the currently known structural models can be used to determine which type of structural units are responsible for changes in glass properties. One of the aims of the present Ph.D. thesis is to provide insights into the structural and topological basis of selected properties of oxide glasses.

Some of these insights will be gained by using topological constraint theory [Phillips 1979; Thorpe 1983]. This theory has recently shown promise in predicting the temperature and composition dependence of shear viscosity of simple glass-forming systems [Gupta & Mauro 2009; Mauro *et al.* 2009a]. This is important, because accurate knowledge of shear viscosity is of critical importance for all stages of industrial glass production. In this thesis, we therefore investigate whether the theory can be extended to more complicated composition spaces and whether other properties besides shear viscosity can be understood and predicted using this approach.

An important property of glasses is the ionic transport, i.e., the ionic diffusion in glasses. The control of diffusion inside glasses plays an increasingly important role in technology, e.g., for batteries [Varshneya 2006], ion exchanged glasses for enhancing strength [Varshneya 2010], and substrate glass for solar energy conversion [Ishizuka *et al.* 2008]. Furthermore, from a fundamental standpoint, it is crucial to study ionic transport in glasses. This is because the mechanism of ionic diffusion in glass is so poorly understood that a generally accepted model is still missing [Bunde *et al.* 1998; Dyre *et al.* 2009]. Whereas ionic sites in crystalline materials are mostly well defined and diffusion occurs via a hopping process among these sites, ionic diffusion in glassy materials is much more complicated than in crystals and is determined by an interplay among network structure, topology, energetics, and cooperativity. Thus, it is of great scientific and technological interest to understand the structural and topological basis of diffusion in glass. Therefore, another aim of the present Ph.D. thesis is to enhance the understanding of diffusion processes in oxide glasses.

In many cases, the properties of glasses are determined not only by their internal structure and topology, but also by their surface structure and topology. Scientists have therefore been attempting to establish different methods for strengthening glass surfaces. Particularly, the need to improve the fracture strength of glass has attracted attention since industrial glass production began in the late 19^{th} century due to the brittleness of glass [Kurkjian *et al.* 2010]. Physical strengthening (thermal tempering) [Varshneya 2006] and chemical strengthening (ion exchange) [Hale 1968; Varshneya 2010] both create compressive stresses in the glass surface layer that are equilibrated by tensile stresses in the interior. This strengthens the glass surface, because glass products usually break due to excessively applied tension acting on surface flaws. Thin films [Zhao *et al.* 2008] and organic or inorganic coatings [de With *et al.* 1998] have also been applied to improve surface properties.

During the master thesis project of the present author, a novel approach has been established for simultaneously studying diffusion in glass and modifying the surface properties. Namely, the so-called inward cationic diffusion approach [Smedskjaer & Yue 2009; Smedskjaer *et al.*

2009]. The inward diffusion (from surface toward interior) of cations is induced by reduction of a polyvalent element in glass at a temperature around the glass transition temperature T_g (temperature at which equilibrium viscosity is 10^{12} Pa·s). In silicate glasses, the inward diffusion leads to formation of a silica-rich surface layer that is hard and corrosion resistant. However, the detailed diffusion mechanism and kinetics still need to be established. If the details of the approach can be understood, it may used as a simple method to study the composition and structure dependence of diffusion in glass. At the same time, the approach can be used to enhance various surface and bulk properties of glasses due to both the diffusion process and the redox reaction. Hence, the approach is an ideal starting point for investigating the structural and topological basis of diffusion and other glass properties.

1.2 Objectives

Based on the preceding discussion, the objectives of the present Ph.D. thesis are to

1. establish the inward diffusion mechanism and compare the inward diffusion data with diffusion data obtained by other methods,
2. clarify the impact of chemical composition and reduction conditions on the degree of inward diffusion,
3. clarify the impact of glass structure and crystallization on the degree of inward diffusion,
4. determine various surface and bulk properties (mechanical, chemical, thermal, and optical) of glasses modified by redox reactions and diffusion processes, and
5. use and develop topological constraint theory to understand and predict selected dynamical and mechanical properties of glass.

1.3 Thesis Content

The thesis is presented as a plurality, including an introductory overview followed by papers written for publication. The thesis is based on the following publications (in the text these papers will be referred to by roman numerals):

I: M. M. Smedskjaer and Y. Z. Yue, "Redox reactions and inward cationic diffusion in glasses caused by CO and H_2 gases," *Solid State Ionics* **180**, 1121-1124 (2009)

II: M. M. Smedskjaer and Y. Z. Yue, "Surface Modification of Polyvalent Element-Containing Glasses," *Applied Surface Science* **256**, 202-207 (2009).

III: M. M. Smedskjaer, Y. Z. Yue, J. Deubener, and H. P. Gunnlaugsson, "Correlation between Alkaline Earth Diffusion and Fragility of Silicate Glasses," *Journal of Physical Chemistry B* **113**, 11194-11200 (2009).

IV: M. M. Smedskjaer, J. C. Mauro, and Y. Z. Yue, "Ionic Diffusion and the Topological Origin of Fragility in Silicate Glasses," *Journal of Chemical Physics* **131**, 244514 (2009).

V: M. M. Smedskjaer, Y. Z. Yue, J. Deubener, and S. Mørup, "Impact of Cationic Diffusion on Properties of Iron-Bearing Glass Fibers," *Physics and Chemistry of Glasses: European Journal of Glass Science & Technology Part B* **51**, 271-280 (2010).

VI: M. M. Smedskjaer and Y. Z. Yue, "Inward and Outward Diffusion of Modifying Ions and its Impact on the Properties of Glasses and Glass-Ceramics," *International Journal of Applied Glass Science* **2**, 117-128 (2011).

VII: M. M. Smedskjaer, Q. J. Zheng, J. C. Mauro, M. Potuzak, S. Mørup, and Y. Z. Yue, "Sodium Diffusion in Boroaluminosilicate Glasses," *Journal of Non-Crystalline Solids* **357**, 3744-3750 (2011).

VIII: M. M. Smedskjaer, J. C. Mauro, S. Sen, and Y. Z. Yue, "Quantitative Design of Glassy Materials Using Temperature-Dependent Constraint Theory," *Chemistry of Materials* **22**, 5358-5365 (2010).

IX: M. M. Smedskjaer, J. C. Mauro, S. Sen, J. Deubener, and Y. Z. Yue, "Impact of Network Topology on Cationic Diffusion and Hardness of Borate Glass Surfaces," *Journal of Chemical Physics* **133**, 154509 (2010).

X: M. M. Smedskjaer, Y. Z. Yue, and S. Mørup, "Inward Cationic Diffusion and Percolation Transition in Glass-Ceramics," *Journal of the American Ceramic Society* **93**, 2161-2163 (2010).

XI: M. M. Smedskjaer, J. R. Qiu, J. Wang, and Y. Z. Yue, "Near-Infrared Emission from Eu-Yb Doped Silicate Glasses Subjected to Thermal Reduction," *Applied Physics Letters* **98**, 071911 (2011).

XII: M. M. Smedskjaer, J. Wang, and Y. Z. Yue, "Tunable Photoluminescence Induced by Thermal Reduction in Rare Earth Doped Glasses," *Journal of Materials Chemistry* **21**, 6614-6620 (2011).

XIII: M. M. Smedskjaer, M. Solvang, and Y. Z. Yue, "Crystallisation Behaviour and High-Temperature Stability of Stone Wool Fibres," *Journal of the European Ceramic Society* **30**, 1287-1295 (2010).

XIV: M. M. Smedskjaer, J. C. Mauro, and Y. Z. Yue, "Prediction of Glass Hardness Using Temperature-Dependent Constraint Theory," *Physical Review Letters* **105**, 115503 (2010).

2 Diffusion Processes Driven by Redox Reactions

Understanding the fundamentals of diffusion in glasses is important for both scientific exploration and technological applications. In this work, we study diffusion processes driven by redox reactions in oxide glasses at temperatures around T_g. Therefore, we first review the fundamentals of redox reactions in glass and the current understanding of diffusion in glass. Then, inspired by the so-called outward diffusion approach [Cook *et al.* 1990; Cooper *et al.* 1996a; Cooper *et al.* 1996b; Yue *et al.* 2009], we propose the mechanism of the inward diffusion process based on our experimental data from Papers I to VII and our earlier studies [Smedskjaer & Yue 2009; Smedskjaer *et al.* 2009]. We also establish the diffusion and reduction kinetics and compare the inward diffusion data with ion exchange and tracer diffusion data for a series of boroaluminosilicate glasses.

2.1 Redox Reactions in Glass

Polyvalent elements may exist in more than one redox state in glasses. For example, essentially all 3*d* elements (e.g., iron and vanadium) tend to change redox state easily due to their partially filled electron shells. The control of the redox state is important, since the different states possess different structural and topological roles and result in different glass properties, such as color.

The redox state is normally controlled in the glass-forming melt during the preparation of the glass. The redox state depends on several factors: (i) melting temperature and time; (ii) furnace atmosphere; (iii) sample size and cooling rate during quenching; and (iv) composition of the glass-forming melt [Dyar 1985]. Decreasing the partial oxygen pressure in the furnace atmosphere or increasing the melting temperature shifts the oxidation-reduction equilibrium toward the reduced state [Varshneya 2006]. Moreover, the redox ratio can be affected by the melting time, especially in melts of high viscosity where redox kinetics are slow. Optical basicity (Λ_m) describes the negative charge donating ability of oxygen in oxide glasses. The concept allows glasses to be described based on acid-base properties and can be used to predict the impact of host composition on the redox state of a polyvalent element [Duffy & Ingram 1971; Duffy 1993]. Glasses with high values of Λ_m favor the higher charged cations to neutralize the negative charges provided by the oxygen anions.

Instead of controlling the redox state during the melting process in the high temperature liquid, the idea of this work is to perform heat-treatments of the glasses around T_g. This is done in order to cause changes in the redox state of a polyvalent element in the surface layer. As we will see in Section 2.3, this causes surface modifications of the glasses, which can be used to modify various properties. In the glassy state, the permeation of gases into the glass can rate-limit the redox reactions [Shelby 1996; Doremus 2002]. Gases (such as H_2) are able to become dissolved in interstices or atomic-sized holes in glasses. Upon dissolution, the gaseous molecules can diffuse inside the glass and react with polyvalent elements [Paper I]. The kinetics of the interaction between a diffusing gas and the reactive site is controlled by the rates of dissolution, diffusion, and chemical reaction. For redox reactions in glasses, the reaction rate has been found to be very fast. For example, hydrogen gas molecules are consumed as soon as they encounter a reaction site [Shelby 1996]. Therefore, permeability (P) is defined as the product of solubility and diffusivity. For a given molecule, the permeability depends on the openness of the glass structure, because motion of molecular

species in glass occurs by jumping between interstitial positions in the structure [Doremus 2002].

2.2 Diffusion in Glass

In oxide glasses, the chemical components can be divided into different categories according to their role in the structural arrangement of the glass based on the electronegativity of the cation [Stanworth 1971]. The structures of oxide glasses are based on networks created by the so-called network-forming cations (e.g., Si^{4+}). These cations are defined as those that have a fractional ionic bond with oxygen near or below 50%. Network-modifying cations (e.g., Na^{+} and Ca^{2+}) form highly ionic bonds with oxygen, and they serve to modify/interfere with the network structure without becoming a part of the primary network [Shelby 2005]. Hence, they disrupt the connectivity of the oxide network and create non-bridging oxygens (NBOs) that are linked to only one network-forming cation. The motion of the modifying cations has been found to be decoupled from that of the network [Angell 1983]. In other words, network-modifying cations diffuse much faster than network-forming cations, and we therefore consider only the diffusion of modifiers in the following.

The diffusion of network-modifying cations in glasses has been studied extensively in the recent decades, but the fundamentals of diffusion remain relatively poorly understood [Frischat 1975; Greaves & Ngai 1995; Dyre *et al.* 2009]. Ionic diffusivities in glasses result from a complex interplay of structural parameters: (i) strength of the cation-anion Columbic attraction; (ii) mechanical strain energy imposed by ionic diffusion upon the glass network (i.e., porosity of network); (iii) number of nearby well-matched target sites; and (iv) average jump distance. These factors are affected by the glass composition and studying the composition dependence of diffusion therefore becomes important. For example, it is well known that an increase of the modifier content in binary modifier-former glasses (e.g., Na_2O-SiO_2) increases the ionic conductivity [Bunde *et al.* 1998]. This is because the number of target sites increases, the average jump distance decreases, and often the mechanical strain effect diminishes with increasing network-modifier concentration. The relationship between glass microstructure and network-modifier diffusion has also been addressed [Greaves & Ngai 1995]. However, it is a difficult task to establish such relationships due to the complicated nature of the glass structure.

Diffusion coefficients of network-modifier ions in glasses are often determined by tracer diffusion experiments. The tracer, which may be radioactive or an enriched stable isotope, is made come into contact with the glass. Following a heat-treatment for a given duration and temperature, the glass is sectioned or etched layer by layer. Afterwards, radioactivity counting or mass spectrometry is used to determine the distribution of the tracer inside the glass. The self-diffusion coefficient is then obtained by fitting the measured distribution to a solution of Fick's second law with the appropriate initial and boundary conditions [Varshenya 2006].

Ion exchange experiments can be employed to determine alkali diffusivities in glasses [Varshneya 2010]. During these experiments, large alkali ions (e.g., K^{+}) from a molten salt bath diffuse into a host glass containing smaller alkali ions (e.g., Na^{+}) that diffuse out into the salt bath. An interdiffusion coefficient ($\bar{D}$) is used to describe the diffusion process, since the small and large alkali ions diffuse at different rates. $\bar{D}$ is calculated based on the diffusion depths of the alkali ions combined with the ion exchange time and temperature. In

the classical description of mutual diffusivity, $\bar{D}_{i-j}$ between alkali ions *i* and *j* is given by the Nernst-Planck equation [Varshneya 2010],

$$\bar{D}_{i-j} = \frac{D_i D_j}{D_i N_i + D_j N_j}, \tag{2.1}$$

where *N* and *D* are the fractional concentration and self-diffusion coefficient of an alkali ion, respectively. In the following, we consider alternative methods for studying diffusion in glasses, viz., diffusion processes driven by redox reactions in the surface region.

2.3 Mechanisms of Outward and Inward Diffusion

2.3.1 Oxidation Induced Outward Diffusion

If a glass containing polyvalent ions is placed in an oxygen chemical potential gradient, different chemical reactions and internal transport processes will take place in the attempt of the glass to equilibrate with the environment. Two approaches have been used to study what happens during heat-treatment of iron-containing silicate glasses in oxidizing atmospheres [Cooper *et al.* 1996a]:

- Tracer experiments where the glass is placed in a gaseous environment enriched in ^{18}O [Dunn 1982; Canil & Muehlenbachs 1990]. Isotope exchange between the glass and the environment occurs by diffusion. Two diffusion processes are acting in parallel: (i) molecular diffusion involving exchange of ^{18}O from the enriched ^{18}O environment with the dissolved O_2 in the glass; and (ii) ionic diffusion involving incorporation of ^{18}O into the glass as O^{2-} which then diffuses.

- Chemical diffusion experiments where the glass is exposed to environments with different oxygen partial pressure resulting in changes of the valence state of iron [Dunn 1983; Wendlandt 1991; Schreiber *et al.* 1986]. These experiments are analyzed based on the assumption that the redox kinetics is dominated by the diffusion of an oxygen species.

A discrepancy exists between the results of the oxygen tracer experiments and those of the redox chemical diffusion experiments. For structurally similar glasses, the ^{18}O tracer diffusion data predict redox kinetics 10 to 10^3 times slower than that determined in the chemical diffusion experiments [Cook *et al.* 1990]. The discrepancy can be explained if the dissipation of the redox potential does not involve the motion of an oxygen species at all, i.e., the two procedures are measuring different processes. This is possible because iron as a polyvalent element makes the glass an electronic conductor (polaron-type semiconductor) [Jurado-Egea *et al.* 1987; Zarzycki 1991; Cook & Cooper 2000]. Such a solid contains highly mobile electronic species (electrons or electron holes) that may serve to decouple the ionic fluxes, i.e., charge can transfer between Fe^{2+} and Fe^{3+}. In fact, the electronic mobility is many, many orders of magnitude larger than ionic diffusivities in glasses [Kingery *et al.* 1976].

The dynamic process that dissipates the driving force most rapidly dominates the overall response to the oxygen potential gradient. During oxidation of a Fe^{2+}-containing glass, it has been found that the most rapid dissipation of the driving force involves the diffusion of fast

moving network-modifying cations and faster moving electron species (electron holes, $h^{\bullet}$) [Cook *et al.* 1990; Cooper *et al.* 1996a]. Thus, no diffusion of oxygen species is involved in the oxidation. Instead, it is the electron holes that dissipate the driving force, i.e., the oxidation front moves from the surface toward the interior by charge transfer from Fe^{3+} to Fe^{2+}. The electron holes are created at the glass surface due to reaction of molecular oxygen with Fe^{2+}. To maintain charge neutrality, the inward motion of electron holes is charge-coupled with the motion of network-modifying cations in the opposite direction (i.e., so-called outward diffusion from interior toward surface). The migration of an electron hole can be schematically illustrated by following the motion of the distortion accompanying the migration of the positive, mobile charge (Fig. 2.1). The distortion moves with the electron hole, whereas the network-modifying cation migrates in the opposite direction.

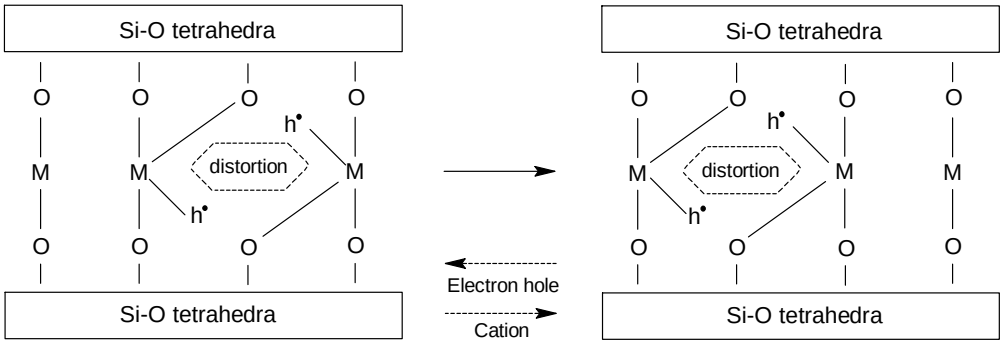

Figure 2.1. Schematic illustration of the migration of an electron hole ($h^{\bullet}$) and the motion of a divalent network-modifying cation (M) in the opposite direction in a silicate glass. The structural distortion follows the migration of the electron hole. Adapted from [Cook & Cooper 2000].

Divalent alkaline earth ions are generally smaller than monovalent alkali ions (e.g., both K^+ and Na^+ are larger than Ca^{2+}), but it is widely accepted that network-modifying alkali ions are much more mobile than alkaline earth ions. The higher ionic charge of the latter tends to keep these ions in place by electrostatic attraction of the oxygen anions [Varshneya 2006]. However, it has been found that primarily the divalent cations diffuse during oxidation of a Fe^{2+}-containing glass. The reason for this discrepancy has still not been clarified [Magnien *et al.* 2008].

The oxidation mechanism presented above is supported by studies that show that tracer diffusion coefficients of divalent cations match well with the diffusion coefficients determined in the chemical diffusion experiments described above [Watson 1981; Cook *et al.* 1990]. Two important consequences of the suggested mechanism are: (i) oxidation of a Fe^{2+}-containing glass does not require diffusion of an oxygen species; and (ii) the driving force for the diffusion of divalent cations towards the surface is the oxidation of Fe^{2+}. It must be noted that at temperatures above the melting temperature, the oxidation of a Fe^{2+}-containing silicate composition is controlled by diffusion of oxygen either as molecular O^2 or as O^{2-} ions due to differences in diffusion activation energies between network-modifying cations and oxygen species [Schreiber *et al.* 1986; Wendlandt 1991; Magnien *et al.* 2008]. The results presented above deal with experiments in the glassy state at temperature around T_g, where oxygen diffusion is not involved in the oxidation.

In Paper II, we have shown that the oxidation mechanism presented above not only applies to iron, but also to other polyvalent elements. We have studied the oxidation of a series of soda-lime-silicate glasses containing different polyvalent elements (Ti, V, Fe, Cu, Cr, Ce, and Mn). The glasses were heat-treated in air at their respective T_g and the elemental concentration profiles in the surface layer were determined by secondary neutral mass spectroscopy (SNMS). The results show that besides the vanadium-containing glass, all glasses reveal an outward diffusion of Ca^{2+} ions. This indicates that the proposed oxidation mechanism of polyvalent elements in glasses is universal. Furthermore, we have shown that the degree of Ca^{2+} outward diffusion is intimately linked with the degree of oxidation of the polyvalent element (Fig. 2.2). This confirms that the outward diffusion is driven by the oxidation reaction.

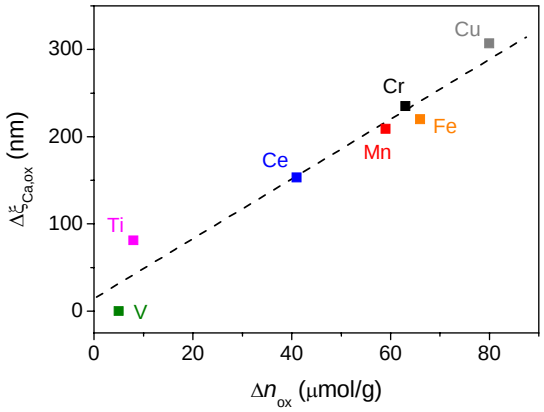

Figure 2.2. Correlation between degree of outward diffusion and degree of oxidation for $68SiO_2$-$23CaO$-$8Na_2O$-$1X_2O_y$ glasses, where X is Ti, V, Fe, Cu, Cr, Ce, or Mn. $\Delta\xi_{Ca,ox}$ is the outward diffusion depth of Ca^{2+}. Δn_{ox} is the oxidized number moles of the polyvalent element per grams of glass. The glasses were heat-treated at their respective T_g for 6 h in air. The line is drawn as a guide for the eye. Data taken from Paper II.

Heat-treatment of polyvalent element-containing glasses under oxidizing conditions can be used to modify the surface chemistry due to the outward diffusion process. In detail, nano-crystalline alkaline earth oxides (e.g., CaO and MgO) are formed at the surface due to the reaction of O^{2-} with alkaline earth ions [Cooper *et al.* 1996a; Yue *et al.* 2009]. O^{2-} is created due to the electron transfer from Fe^{2+} to atmospheric O_2. In Section 5.3, we will see how the surface modification changes the properties of iron-containing glass fibers.

2.3.2 Reduction Induced Inward Diffusion

Now the question arises: what happens during reduction of a polyvalent element-containing glass? For the oxidation mechanism in air, the oxygen permeation into the glass has been found to be negligible and the oxidation kinetics are dominated by outward cationic diffusion. In the following, we consider the reduction mechanism of Fe^{3+} during heat-treatment in a H_2/N_2 (1/99 v/v) atmosphere [Papers I to VII]. In this case, the permeation of the gas into the glass may become important, since the molecular size of H_2 (1.2 Å) is smaller than that of O_2 (2.6 Å) [Cordero *et al.* 2008]. In Sections 3.3 and 3.4, we will investigate the universality of the reduction mechanism as a function of the type of the

polyvalent element and the type and partial pressure of the reducing gas, respectively. We have illustrated three potential reduction mechanisms in Figure 2.3.

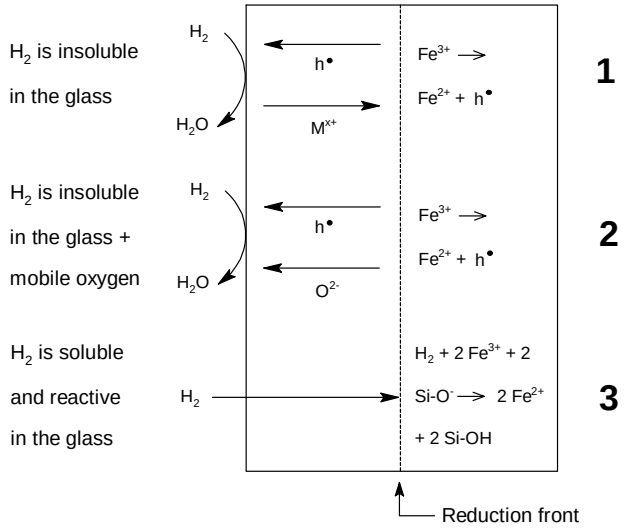

Figure 2.3. Schematic representation of the possible mechanisms for Fe^{3+} reduction in a silicate glass heated in H_2-containing atmosphere. (1) Molecular H_2 is insoluble in the glass and the reduction proceeds through outward migration of electron holes ($h^{\bullet}$) charge-balanced by inward migration of network-modifying cations (M^{x+}); this mechanism is a mirror-image of the oxidation mechanism presented in Section 2.3.1. (2) Molecular H_2 is insoluble in the glass and the outward migration of electron holes is charge-balanced by a flow of oxygen anions towards the free surface. (3) Permeation of molecular H_2 in the glass is rate-limiting.

Mechanism #1 is a mirror-image of the oxidation mechanism described in Section 2.3.1, whereas mechanism #2 involves outward motion of oxygen anions to charge-balance the outward flux of electron holes. For these mechanisms, the polyvalent ions are reduced at the internal reduction front, which generates electron holes. Simultaneously, at the surface, ionic oxygen is released to the atmosphere as molecular water (i.e., the conversion of H_2 to H_2O) by surrendering electrons to fill the electron holes. In the zone between the two reaction sites, electron holes move toward the glass surface. This motion is charge-balanced by a counter flux of mobile cations (#1) or a parallel flux of oxygen anions (#2). Mechanism #3 is the permeation of gaseous H_2 into the glass, which does not involve ionic diffusion processes.

To determine which mechanism is dominant, we have heat-treated various iron-containing glasses in H_2/N_2 (1/99) at temperatures around T_g. Then we have determined the changes in the surface chemistry and the redox state of iron. For example, Figure 2.4 shows the SNMS surface concentration profiles of an iron-containing glass heat-treated in H_2/N_2 (1/99). Prior to the heat-treatment, the concentration profiles show no fluctuations as a function of depth. However, the thermal reduction (heat-treatment in reducing atmosphere) has caused a depletion of primarily the alkaline earth ions near the surface, which creates a silica-rich surface layer, since the Si^{4+} ions are virtually immobile. The inset of Figure 2.4 shows that the change in surface chemistry is accompanied by a reduction of Fe^{3+} to Fe^{2+}, since the intensity of the broad Fe^{2+} absorption band near 1050 nm increases due to the heat-treatment in H_2/N_2 (1/99).

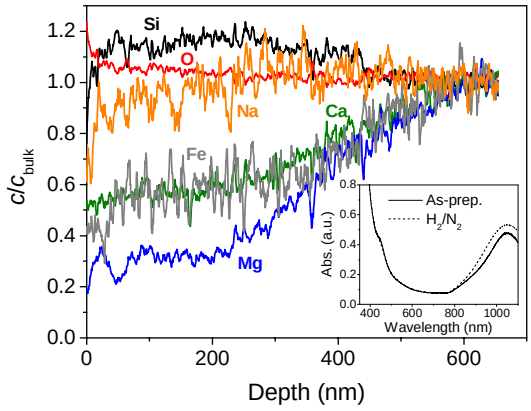

Figure 2.4. Surface concentration profiles of iron-containing MgO-CaO-Na_2O-SiO_2 glass heat-treated at its T_g = 926 K for 16 h in H_2/N_2 (1/99). The curves are determined by SNMS and are plotted as concentration of the element at a given depth divided by the concentration of the same element in the bulk of the glass (c/c_{bulk}). Inset: corresponding UV-VIS-NIR (ultraviolet-visible-near infrared) absorption spectra of 0.20 mm thick as-prepared (solid curve) and heat-treated (dashed curve) samples. The band near 1050 nm is due to a *d*-*d* transition of Fe^{2+}. Data taken from Paper I.

The results presented in Figure 2.4 indicate that mechanism #1 is dominant. However, Figure 3 in Paper I shows that hydroxyl groups are incorporated into the glass structure when the glass has been heat-treated in H_2/N_2 (1/99). This indicates that hydrogen permeation also occurs. Thus, it seems that a combination of mechanisms #1 and #3 occurs. However, to provide direct evidence, we need to address the following issues: (i) provide evidence that the glasses possess semiconductor behavior to allow mechanism #1 to occur; (ii) provide evidence that hydrogen exists and diffuses as molecular H_2 to allow mechanism #3 to occur; (iii) exclude that other processes besides mechanism #1 can be responsible for the depletion of network-modifiers in the surface layer; and (iv) show that both the inward diffusion and reduction processes are diffusion limited processes. We discuss points (i)-(iii) in the following, whereas point (iv) is considered separately in Section 2.3.3.

(i): Literature studies have shown that even for a total iron content less than 0.05 at%, iron-containing glasses are a p-type semiconductor, i.e., the product of concentration and mobility of $h^{\bullet}$ exceeds that of any ionic species in the glass [Cook & Cooper 2000]. All the glasses studied in this work therefore possess semiconductor behavior. The electronic species move through the glass network by thermal "hopping" between localized electronic states (e.g., Fe^{2+} and Fe^{3+}). This transfer happens within the valence band of the material, i.e., by electron holes instead of by conduction electrons [Hirsch *et al.* 1993].

(ii): The diffusion of hydrogen in glass has been attributed to either motion of molecular H_2 or hydroxyl ions. However, various experimental results support the motion of hydrogen as molecular species in oxide glasses. For example, the evidence comes from the pressure dependence of the diffusion coefficients and the strong dependence of the diffusion on the openness of the glass structure [Doremus 2002]. In addition, various reduction reactions (such as reduction of silver ions to atomic silver) controlled by the permeation of H_2 have been reported in the glass literature [Shelby 1996].

(iii): To investigate whether inward diffusion of network-modifying cations is the responsible mechanism behind the surface depletion of those ions, we heat-treat both iron-free and iron-containing soda-lime-silicate glasses in H_2/N_2 (1/99). No surface depletion of cations occurs when the iron-free glass is heat-treated (Fig. 2.5a), i.e., the cations do not evaporate from the surface during the heat-treatment. When the iron-containing glass is heat-treated (Fig. 2.5b), a surface depletion of Na^+ and Ca^{2+} occurs, and these cations are found in higher concentrations in the interior of the samples. We have calculated the amounts of depleted and enriched Na^+ and Ca^{2+} ions and there is mass balance. Hence, mechanism #1 does indeed contribute to the reduction process.

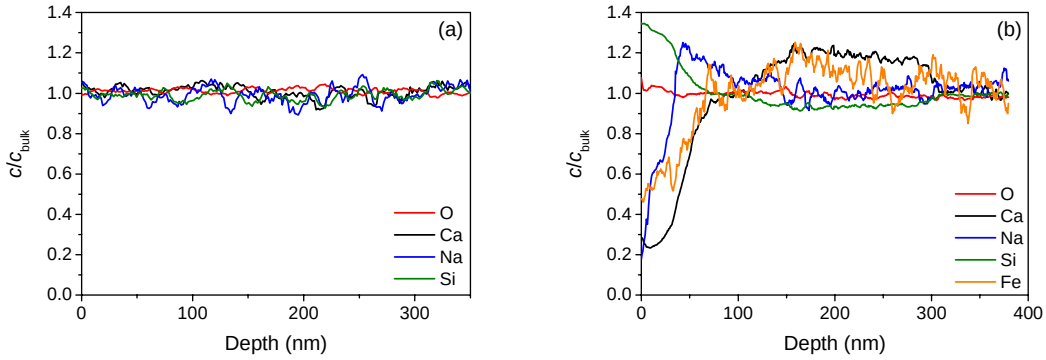

Figure 2.5. Surface concentration profiles of (a) iron-free and (b) iron-containing $CaO\text{-}Na_2O\text{-}SiO_2$ glasses heat-treated at 892 K for 2 h in H_2/N_2 (1/99).

It should be mentioned that most of the SNMS surface concentration profiles shown in this thesis and in the supporting papers have not been measured to sufficiently large depths to observe the "real bulk", i.e., to observe the enrichment of the network-modifying cations in the interior (see, e.g., Fig. 2.4). This has not been done, because we are mainly interested in the diffusion depth of the cations. In these cases, "bulk" refers to the concentration at the end of the measurement, i.e., at the end of the SNMS sputtering process.

2.3.3 Diffusion and Reduction Kinetics

First, we consider the kinetics of the inward diffusion process (i.e., mechanism #1). In Paper VI, we have studied the kinetics of the Mg^{2+} inward diffusion in a $79SiO_2\text{-}15MgO\text{-}5Na_2O\text{-}1Fe_2O_3$ glass (all iron reported as Fe_2O_3) with T_g = 950 K. As shown in Figure 3b in Paper VI, the inward diffusion carries a parabolic kinetic signature, i.e., diffusion-limited kinetics. Now, we seek to calculate the Mg^{2+} diffusion coefficient ($D_{Mg^{2+}}$) in order to compare it with literature values of diffusion coefficients for divalent cations in similarly polymerized glasses. We calculate $D_{Mg^{2+}}$ from the parabolic rate constant (k'), which is determined from the relation [Schmalzried 1984]

$$\Delta\xi^2 = 2k't\,, \qquad (2.2)$$

where $\Delta\xi$ is the diffusion depth and t is time. We can calculate k' from the slope of the plot of the squared Mg^{2+} diffusion depth vs. diffusion time (Fig. 3b in Paper VI).

To calculate $D_{Mg^{2+}}$ from *k*', we first consider Fick's first law written for ionic materials. It is used to describe the flux of magnesium ions and electron holes between the reduction front ($\xi = \xi'$) and the surface ($\xi = 0$) [Schmalzried 1984; Cooper *et al.* 1996a]:

$$j_{Mg^{2+}} = \frac{-c_{Mg^{2+}} D_{Mg^{2+}}}{RT} \frac{d\eta_{Mg^{2+}}}{d\xi} = \frac{-c_{Mg^{2+}} D_{Mg^{2+}}}{RT} \left(\frac{d\mu_{Mg^{2+}}}{d\xi} + 2F \frac{d\varphi}{d\xi} \right) \tag{2.3}$$

and

$$j_{h^\bullet} = \frac{-c_{h^\bullet} D_{h^\bullet}}{RT} \frac{d\eta_{h^\bullet}}{d\xi} = \frac{-c_{h^\bullet} D_{h^\bullet}}{RT} \left(\frac{d\mu_{h^\bullet}}{d\xi} + F \frac{d\varphi}{d\xi} \right), \tag{2.4}$$

where j_i is flux, c_i is concentration, D_i is diffusion coefficient, η_i is electrochemical potential, and μ_i is chemical potential of species *i*. *R* is the universal gas constant, *T* is temperature, *F* is the Faraday constant, and φ is the electrical potential. To maintain charge neutrality, the following condition must be valid

$$\sum_i z_i j_i = 0 = 2 j_{Mg^{2+}} + j_{h^\bullet} \Leftrightarrow 2 j_{Mg^{2+}} = - j_{h^\bullet} , \tag{2.5}$$

where z_i is valence. Applying Eq. (2.5) to Eqs. (2.3) and (2.4) gives

$$\begin{aligned} &\frac{-2c_{Mg^{2+}} D_{Mg^{2+}}}{RT} \left(\frac{d\mu_{Mg^{2+}}}{d\xi} + 2F \frac{d\varphi}{d\xi} \right) = \frac{c_{h^\bullet} D_{h^\bullet}}{RT} \left(\frac{d\mu_{h^\bullet}}{d\xi} + F \frac{d\varphi}{d\xi} \right) \Leftrightarrow \\ &-2c_{Mg^{2+}} D_{Mg^{2+}} d\mu_{Mg^{2+}} - 4c_{Mg^{2+}} D_{Mg^{2+}} F d\varphi = c_{h^\bullet} D_{h^\bullet} d\mu_{h^\bullet} + c_{h^\bullet} D_{h^\bullet} F d\varphi \Leftrightarrow \\ &-F d\varphi (4c_{Mg^{2+}} D_{Mg^{2+}} + c_{h^\bullet} D_{h^\bullet}) = c_{h^\bullet} D_{h^\bullet} d\mu_{h^\bullet} + 2c_{Mg^{2+}} D_{Mg^{2+}} d\mu_{Mg^{2+}} \end{aligned} \tag{2.6}$$

Iron-containing glasses are electronically conducting, i.e., $c_{Mg^{2+}} D_{Mg^{2+}} << c_{h^\bullet} D_{h^\bullet}$ ("semiconductor condition"). Therefore, Eq. (2.6) reduces to

$$\begin{aligned} &-F d\varphi (c_{h^\bullet} D_{h^\bullet}) = c_{h^\bullet} D_{h^\bullet} d\mu_{h^\bullet} \Leftrightarrow \\ &F d\varphi = -d\mu_{h^\bullet} \text{ or } d\eta_{h^\bullet} = 0 \end{aligned} \tag{2.7}$$

Eq. (2.7) is now substituted into the flux equation for Mg^{2+} (Eq. (2.3)):

$$j_{Mg^{2+}} = \frac{-c_{Mg^{2+}} D_{Mg^{2+}}}{RT} \left(\frac{d\mu_{Mg^{2+}}}{d\xi} - 2 \frac{d\mu_{h^\bullet}}{d\xi} \right). \tag{2.8}$$

The ionization of the metallic Mg is now considered,

$$Mg + 2h^\bullet \rightarrow Mg^{2+} , \tag{2.9}$$

which results in the following equation for the chemical potentials:

$$d\mu_{Mg^{2+}} - 2d\mu_{h^{\bullet}} = d\mu_{Mg}. \tag{2.10}$$

Eq. (2.8) now becomes

$$j_{Mg^{2+}} = \frac{-c_{Mg^{2+}} D_{Mg^{2+}}}{RT} \frac{d\mu_{Mg}}{d\xi}. \tag{2.11}$$

Similarly, the oxidation of metallic Mg can be described by

$$Mg + 1/2O_2 \rightarrow MgO, \tag{2.12}$$

which results in the following equation for the chemical potentials:

$$d\mu_{Mg} + ½ d\mu_{O_2} = d\mu_{MgO}. \tag{2.13}$$

The activity of MgO in the reduced glass is only slightly affected by the chemical diffusion process [Everman & Cooper 2003]. Thus, $d\mu_{MgO} \approx 0$, which reduces Eq. (2.11) to

$$j_{Mg^{2+}} = \frac{c_{Mg^{2+}} D_{Mg^{2+}}}{2RT} \frac{d\mu_{O_2}}{d\xi}. \tag{2.14}$$

Eq. (2.14) states that a cation flux is generated by a chemical potential gradient in oxygen, even though there is no diffusion of oxygen species. The equation can be integrated from $\xi = 0$ to $\xi = \xi'$ by separating the chemical potential and distance variables:

$$\int_{\xi=0}^{\xi=\xi'} j_{Mg^{2+}} d\xi = \int_{\mu_{O_2}^{\xi=0}}^{\mu_{O_2}^{\xi=\xi'}} \frac{X_{Mg^{2+}} D_{Mg^{2+}}}{2V_m RT} d\mu_{O_2}. \tag{2.15}$$

$c_{Mg^{2+}}$ has been replaced by $X_{Mg^{2+}} / V_m$, where $X_{Mg^{2+}}$ is the cation mole fraction of Mg^{2+} and V_m is the molar volume of the glass. To perform the integration, we assume that $j_{Mg^{2+}}$ is constant, i.e., all Mg^{2+} ions released at the surface are incorporated at the reduction front [Everman & Cooper 2003]. Eq. (2.15) now becomes,

$$j_{Mg^{2+}} \cdot \Delta\xi = \frac{X_{Mg^{2+}}}{2V_m RT} \int_{\mu_{O_2}^{\xi=0}}^{\mu_{O_2}^{\xi=\xi'}} D_{Mg^{2+}} d\mu_{O_2}. \tag{2.16}$$

$D_{Mg^{2+}}$ is a function of oxygen activity in Eq. (2.16) as it is the product of the concentration of point defects (by which the diffusion occurs) and the intrinsic mobility of the defects [Gersten & Smith 2001]. This is the case, because a physical manifestation of an oxygen activity gradient in a glass is a gradient in the concentration of structural distortions [Dickenson & Hess 1986]. Therefore, an average diffusion coefficient for magnesium ions ($\bar{D}_{Mg^{2+}}$) is defined as

$$\bar{D}_{Mg^{2+}} = \frac{1}{\Delta\mu_{O_2}} \int_{\mu_{O_2}^{\xi=0}}^{\mu_{O_2}^{\xi=\xi'}} D_{Mg^{2+}} d\mu_{O_2}, \tag{2.17}$$

where

$$\Delta\mu_{O_2} = RT \ln \frac{a_{O_2}^{\xi=\xi'}}{a_{O_2}^{\xi=0}}, \tag{2.18}$$

a_{O_2} is the oxygen activity, and $\Delta\mu_{O_2}$ is the difference in oxygen activity between the surface and the reduction front. Application of Eqs. (2.17) and (2.18) to Eq. (2.16) gives

$$j_{Mg^{2+}} \Delta\xi = \frac{X_{Mg^{2+}} \bar{D}_{Mg^{2+}}}{2V_m} \ln \frac{a_{O_2}^{\xi=\xi'}}{a_{O_2}^{\xi=0}}. \tag{2.19}$$

The rate of the reaction that is moving through the sample is $d\Delta\xi / dt$ and it equals the product of the cation flux and molar volume of the glass. It now follows from Eq. (2.19) that

$$\frac{d\Delta\xi}{dt} = j_{Mg^{2+}} V_m = \frac{X_{Mg^{2+}} \bar{D}_{Mg^{2+}}}{2\Delta\xi} \ln \frac{a_{O_2}^{\xi=\xi'}}{a_{O_2}^{\xi=0}}. \tag{2.20}$$

Integration of Eq. (2.20) yields

$$(\Delta\xi)^2 = X_{Mg^{2+}} \bar{D}_{Mg^{2+}} \ln \frac{a_{O_2}^{\xi=\xi'}}{a_{O_2}^{\xi=0}} \cdot \Delta t, \tag{2.21}$$

or

$$\bar{D}_{Mg^{2+}} = \frac{(\Delta\xi)^2}{X_{Mg^{2+}} \ln \frac{a_{O_2}^{\xi=\xi'}}{a_{O_2}^{\xi=0}} \cdot \Delta t} = \frac{2k'}{X_{Mg^{2+}} \ln \frac{a_{O_2}^{\xi=\xi'}}{a_{O_2}^{\xi=0}}}. \tag{2.22}$$

$\bar{D}_{Mg^{2+}}$ can then be calculated using Eq. (2.22) following the procedure described in Papers I and VI. $\bar{D}_{Mg^{2+}}$ is calculated for each heat-treatment temperature and plotted in Arrhenian coordinates in Figure 2.6. The Arrhenius equation for describing the temperature dependence of diffusion is

$$D = D_0 \cdot \exp\left(\frac{-E_{diff}}{RT}\right), \tag{2.23}$$

where E_{diff} is the diffusion activation energy and D_0 is the pre-exponential factor.

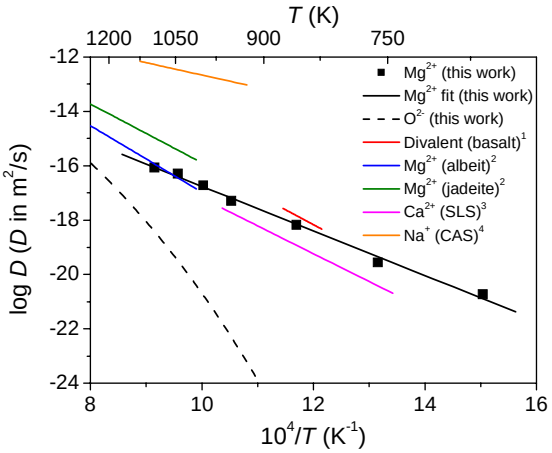

Figure 2.6. Comparison of ionic diffusion coefficients obtained in this work and tracer diffusion coefficients from literature. The numbers 1, 2, 3, and 4 refer to the references [Cooper *et al.* 1996a], [Roselieb & Jambon 2002], [Natrup *et al.* 2005], and [Lu & Dieckmann 2007], respectively. Reproduced from Paper VI.

Figure 2.6 reveals good agreement between the diffusion coefficient of Mg^{2+} obtained in this work and tracer diffusion coefficients found in literature for divalent cations. This provides evidence for the occurrence of mechanism #1 in Figure 2.3. Furthermore, Figure 2.6 shows that at temperatures near and below the glass transition, the dominating diffusion mechanism is clearly related to inward diffusion of magnesium cations, and hence, not the outward diffusion of oxygen anions (mechanism #2). This finding is in agreement with several previous studies concerning iron oxidation [Cook *et al.* 1990; Cooper *et al.* 1996a; Magnien *et al.* 2008]. We notice that with increasing temperature, the diffusivities of the divalent cations become closer to that of ionic oxygen due to differences in activation energy. Hence, at sufficiently high temperatures, mechanism #2 will become dominant [Magnien *et al.* 2008]. Furthermore, the cationic diffusion exhibits an Arrhenius temperature dependence, whereas the ionic oxygen diffusion exhibits a super-Arrhenius behavior. This is because the diffusion of ionic oxygen is controlled by the viscosity [Dunn 1982], which itself exhibits super-Arrhenius behavior [Mauro *et al.* 2009b].

In Papers I and IV, we show that the reduction reaction of Fe^{3+} to Fe^{2+} in H_2/N_2 (1/99) also reveals diffusion-limited kinetics, i.e., the squared concentration of Fe^{2+} increases linearly with the reduction time. This confirms that diffusion-limited processes are responsible for the reduction of Fe^{3+}. However, the observed change in Fe^{2+} concentration is too large to be caused solely by the inward diffusion mechanism. This conclusion can drawn by comparing the inward diffusion depths with the degree of reduction as determined from optical spectroscopy in Papers I and IV. Hence, all of the results presented in the above suggest that a combination of mechanisms #1 and #3 is responsible for the reduction of Fe^{3+} to Fe^{2+} in a H_2/N_2 (1/99) atmosphere at temperatures around T_g.

2.4 Comparison of Inward Diffusion with Ion Exchange and Tracer Diffusion

In the previous sections, we have clarified the inward diffusion mechanism in glasses. We have shown that the inward diffusion coefficients of alkaline earth ions compare well with tracer diffusion coefficients from literature. In Paper VII, we have directly compared the composition dependence of sodium inward diffusion with that of sodium tracer diffusion and sodium-potassium interdiffusion in $(79\text{-}x)SiO_2\text{-}xAl_2O_3\text{-}5B_2O_3\text{-}15Na_2O\text{-}1Fe_2O_3$ glasses with x equal to 2.5, 5, 7.5, 10, 12.5, and 15. In Section 4.2, we will discuss the composition dependence of diffusion and its relation with the glass structure. Here, we focus on the comparison of the three methods.

Both the ^{22}Na tracer diffusion coefficient (D^*_{Na}) and the K^+-for-Na^+ interdiffusion coefficient ($\bar{D}_{Na-K}$) decrease with increasing $[SiO_2]/[Al_2O_3]$ ratio (Fig. 2.7a). Even though D^*_{Na} has been determined at a lower temperature (300 °C) than $\bar{D}_{Na-K}$ (410 °C), the value of the former is larger than that of the latter. This is because the interdiffusion process is rate-limited by the diffusion of the larger (i.e., slower) K^+ ions. Figure 2.7b shows that the sodium inward diffusivity also decreases with increasing $[SiO_2]/[Al_2O_3]$ ratio. However, the absolute value of the sodium diffusivity is five orders of magnitude lower for inward diffusion in comparison to tracer diffusion, even though the diffusion experiments were carried out at 575 and 300 °C, respectively. We discuss this in Section 3.1.

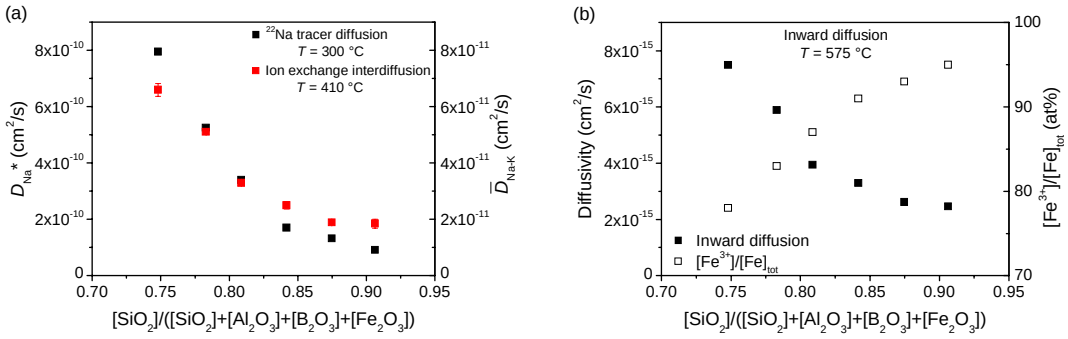

Figure 2.7. Composition dependence of isothermal alkali diffusivity in the $(79\text{-}x)SiO_2\text{-}xAl_2O_3\text{-}5B_2O_3\text{-}15Na_2O\text{-}1Fe_2O_3$ glasses with x = 2.5, 5, 7.5, 10, 12.5, and 15. (a) K^+-for-Na^+ interdiffusion coefficient ($\bar{D}_{Na-K}$) as determined by ion exchange experiments at 410 °C and ^{22}Na tracer diffusion coefficient (D^*_{Na}) at 300 °C. (b) Sodium diffusivity as determined by inward diffusion experiments at 575 °C. The secondary axis depicts the composition dependence of the iron redox ratio ($[Fe^{3+}]/[Fe]_{tot}$) of the as-prepared glasses as determined by ^{57}Fe Mössbauer spectroscopy. Data taken from Paper VII.

The results presented in Figure 2.7 suggest that the inward diffusion approach may be used as a simple alternative method to assess compositional trends of diffusivity, since the alkali diffusivity reveals the same composition dependence for all three methods. However, the extent of sodium inward diffusion depends on the iron redox ratio [Smedskjaer & Yue 2009]. Thus, if the iron redox ratio varies significantly in a studied series of glasses, it may be difficult to extract the true composition dependence of the diffusion. Figure 2.7b shows that the iron redox ratio does indeed depend on the $[SiO_2]/[Al_2O_3]$ ratio, but the differences are

too small to cause changes in the composition dependence of diffusion, as discussed in Paper VII.

2.5 Summary

We have established the reduction mechanism of iron-containing glasses in H_2/N_2 (1/99). Both H_2 permeation and inward cationic diffusion contribute to the reduction process. The kinetics of the inward diffusion process has been clarified by calculating the diffusion coefficients of alkaline earth ions. These coefficients are in good agreement with tracer diffusion coefficients from literature. Direct comparison of the sodium inward diffusion with sodium tracer diffusion and sodium-potassium interdiffusion reveals that the inward diffusion approach may be used as an alternative method for studying the composition and structure dependence of ionic diffusion in glass, provided that the impact of the polyvalent element redox state on diffusion is accounted for. However, the absolute value of the sodium inward diffusivity is several orders of magnitude lower than the sodium tracer diffusion coefficient.

3 Impact of Chemical Composition, Gas, and Liquid Fragility on Inward Diffusion

The inward cationic diffusion is a complicated process, which depends on several factors. In the following sections, we discuss the influences of chemical composition (charge and size of diffusing ions and type and concentration of polyvalent element), gas (reduction conditions), and liquid fragility index on the spatial extent of the inward diffusion process. These studies serve two purposes: (i) understand the fundamentals of ionic diffusion in oxide glasses; and (ii) optimize the conditions for obtaining the largest inward diffusion depth.

3.1 Alkali versus Alkaline Earth Ionic Diffusion

The inward diffusion of alkali ions is slower than that of alkaline earth ions (see, e.g., Fig. 2.5b). However, the monovalent alkali ions are generally much more mobile than the divalent alkaline earth ions in glasses due to the charge difference. In addition, Figure 2.7 shows that the inward diffusivity of sodium ions is in fact several orders of magnitude lower than the tracer diffusion coefficient of sodium. On the other hand, there is a good agreement between inward diffusion coefficients and tracer diffusion coefficients of alkaline earth ions (Fig. 2.6). We have also found that alkali ions can lower the inward diffusivity of the alkaline earth ions [Paper IV]. This implies that the relatively slow alkali ions might block the diffusion of the faster alkaline earth ions in the interconnected channels, i.e., the slow alkali ions occupy interstices and hereby increase the packing density.

In the following, we put forward five scenarios to explain the slow inward diffusivity of alkali ions during reduction in H_2/N_2 (1/99). We argue why four of those can be ruled out, and this leaves us with only one possibility. Of course, other possible explanations can exist and further studies are needed to completely clarify the origin of the slow alkali diffusivity.

First, the alkali ions diffuse so fast that their inward diffusion is not observed in the measured SNMS depth profiles, i.e., the alkali ions diffuse to larger depths than those examined during the SNMS measurement. To examine this hypothesis, we have performed heat-treatments of a SiO_2-CaO-Na_2O-Fe_2O_3 glass for very short durations (0.2 and 1 h). Figure 3.1 shows that in the beginning of the process, the Na^+ ions have not yet started to diffuse to any significant extent and the diffusion of Ca^{2+} and Fe^{2+} completely dominates. The high concentration of sodium in the surface layer of the glass heat-treated for 0.2 h is caused by the inward diffusion of calcium and iron, whereas there is no inward diffusion of sodium (inset of Fig. 3.1). Hence, this hypothesis can be disproved.

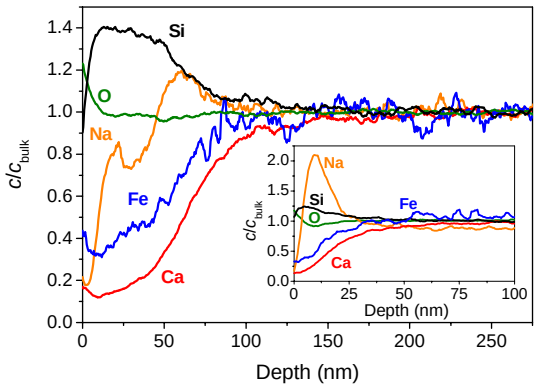

Figure 3.1. Surface concentration profiles of a $68SiO_2$-$23CaO$-$8Na_2O$-$1Fe_2O_3$ glass heat-treated in H_2/N_2 (1/99) for 1 h at its T_g = 892 K. Inset: the same glass heat-treated at 892 K for 0.2 h. Reproduced from Paper IV.

Second, the "semiconductor condition" ($c_{M^{x+}} D_{M^{x+}} << c_{h^\bullet} D_{h^\bullet}$, where M^{x+} is an arbitrary cation and $h^\bullet$ is an electron hole) is not fulfilled. The assumption is generally reasonable since $D_{h^\bullet} >> D_{M^{x+}}$, but if $c_{h^\bullet}$ is small enough, the assumption no longer holds. This can occur, if another reduction mechanism besides inward diffusion (such as #3 in Fig. 2.3) consumes too many electron holes. In this case, the effective inward diffusivity is no longer that of the alkali or alkaline earth cation, but a convolution of the concentration and diffusion coefficients of the electron holes and cations [Cooper *et al.* 2010]. Consequently, the electronic conductivity effectively slows down the inward diffusivity. The inward diffusion process may still occur, just with a slower effective diffusion coefficient. This could explain the slow alkali diffusivity. However, the hypothesis can be ruled out, because it cannot explain why the alkali ions diffuse slower than the alkaline earth ions.

Third, the delivery of electrons at the surface by the hydrogen gas is rate-limiting for the overall process. This will slow down the inward diffusion of alkali ions, because they diffuse in order to charge-balance the flow of electron holes in the opposite direction. However, this hypothesis can also not explain why the alkali ions diffuse slower than the alkaline earth ions.

Fourth, the redox reaction of the polyvalent element is rate-limiting for the overall process. However, according to literature studies, such redox reactions are very fast in comparison to cationic diffusion processes [Shelby 1996]. In addition, this hypothesis is also not able to account for the faster diffusion of the alkaline earth ions.

Fifth, alkali ions diffuse slow since they are only capable of neutralizing one $h^\bullet$, compared to two $h^\bullet$ for alkaline earth ions. The electron hole motion is much faster than that of both alkali and alkaline earth ions in glasses, i.e., the rate of the inward diffusion depends on the degree of the ease of the joint motion of the cations with the electron holes. The alkaline earth ions should diffuse faster than alkali ions, because the former ones are able to carry more positive charges than the latter ones to charge-balance the flux of electron holes. To charge-balance the same amount of electron holes, half the number of alkaline earth ions is demanded in comparison to the alkali ions. Thus, the alkali ions are more crowded and hence more easily block each other during transport. This argument would then lead to the assumption that

trivalent modifier ions (e.g., Al^{3+}) should diffuse faster than the alkaline earth ions. But this is not the case [Paper VII], since the former ones are more strongly bound to the oxygen anions. For the case of the alkaline earth ions, the charge-balancing capability turns out to be a predominant effect in comparison to the effect of cation-oxygen bond strength that hinders the divalent cationic diffusion. This implies that for alkali inward diffusion, the charge-compensation is the rate-limiting process and hence, a governing factor for determining the absolute value of its diffusivity. We believe that this is the main source of the slow inward diffusivity of alkali ions.

3.2 Size Effect of Diffusing Cations

In Paper III, we have investigated the impact of the size of the alkaline earth ion on its inward diffusivity. Specifically, we have investigated the alkaline earth inward diffusion in the $68SiO_2$-$23RO$-$8Na_2O$-$1Fe_2O_3$ (R = Mg, Ca, Sr, or Ba) glass series. We have then determined the rate constant *k'* (Eq. (2.2)) of the alkaline earth diffusion. According to Section 2.3.3, *k'* is proportional to the product of the diffusion coefficient of the rate-limiting species and a thermodynamic driving force (gradient in oxygen activity). Thus, from the temperature sensitivity of *k'* and gradient in oxygen activity, the activation energy of alkaline earth diffusion (E_{diff}) can be obtained by plotting the data in Arrhenian coordinates (see Fig. 7 in Paper III). The diffusion data for each glass reveal an Arrhenius dependence on temperature in the studied temperature range. E_{diff} is calculated from the slope of each line and is plotted as a function of the ionic radius of the alkaline earth ion (*r*) in Figure 3.2.

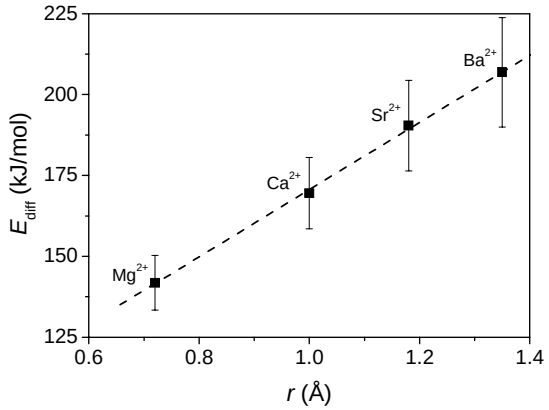

Figure 3.2. Activation energy of alkaline earth inward diffusion (E_{diff}) as a function of ionic radius of the alkaline earth ion (*r*) for the glasses SiO_2-RO-Na_2O-Fe_2O_3 with R = Mg, Ca, Sr, Ba. The line is drawn as a guide for the eye. Data taken from Paper III.

Figure 3.2 shows that E_{diff} increases with increasing *r*. Similarly, Martiny *et al.* have reported that the activation energy of alkaline earth diffusion increases approximately linearly with the ionic radius in $Li_2O{\cdot}2RO{\cdot}4SiO_2$ glasses with R = Mg, Ca, Sr, Ba [Martiny *et al.* 2002]. To explain the correlation between E_{diff} and *r*, we consider the modified random network (MRN) model for glasses proposed by Greaves [Greaves 1985]. The model has been confirmed by molecular dynamics simulations [Huang & Cormack 1990]. According to the MRN model, the network-modifying oxides form interconnected channels (i.e., a percolative network) at sufficiently high concentration. The threshold for percolation occurs at 16 vol% of modifying oxides [Zallen 1998]. Employing a partial molar volumes model [Lange &

Carmichael 1987], we find that the modifying oxides make up more than 16 vol% in the studied glass series. Thus, these glasses contain interconnected channels. The walls of the channels are constituted by [SiO_4] tetrahedra, and the required displacement of oxygen is relatively small for a small alkaline earth ion. Hence, the alkaline earth ions should diffuse fastest through the channels when their size is smallest, which explains the results in Figure 3.2.

3.3 Polyvalent Ions

It is expected that the type and concentration of the polyvalent element will influence the extent of the inward diffusion, since the reduction of the polyvalent ions drives the diffusion process. To study this, we have performed thermal reduction of SiO_2-Na_2O-CaO glasses doped with different types of polyvalent elements (Fe, Mn, Cu, Ce, Ti, V, and Cr) [Paper II]. In Table 3.1, the polyvalent elements are listed in order of increasing ease of reduction in a SiO_2-Na_2O-CaO melt at 1400 °C [Schreiber *et al.* 1999].

Table 3.1. Polyvalent elements listed in order of increasing ease of reduction. The corresponding inward diffusion depth of calcium ($\Delta\xi_{Ca}$) in the glasses heat-treated at their T_g for 6 h in H_2/N_2 (1/99) is also shown. Data taken from Paper II.

Polyvalent element	Reduction reaction	*E*'(V)[a]	$\Delta\xi_{Ca}$ (nm)
Titanium	$Ti^{4+} \rightarrow Ti^{3+}$	-4.0	93
Vanadium	$V^{5+} \rightarrow V^{4+}$	-1.3	249
Iron	$Fe^{3+} \rightarrow Fe^{2+}$	-1.0	264
Copper	$Cu^{2+} \rightarrow Cu^{+}$	-0.2	315
Chromium	$Cr^{6+} \rightarrow Cr^{3+}$	0.4	202
Cerium	$Ce^{4+} \rightarrow Ce^{3+}$	0.5	173
Manganese	$Mn^{3+} \rightarrow Mn^{2+}$	1.2	83

[a] *E*' is defined as the relative reduction potential of the $A^{m+}/A^{(m-n)+}$ couple at 1400 °C in soda-lime-silicate melts [Schreiber *et al.* 1999].

Following heat-treatment in H_2/N_2 (1/99), we have determined the surface concentration profile of Ca^{2+} in the seven glasses. We find that reduction of Cu^{2+} to Cu^{+} results in the largest spatial extent of inward diffusion in comparison to that of the other types of polyvalent ions under the same reduction conditions (Table 3.1). The lowest extent of inward diffusion is observed in the glasses containing polyvalent ions with either the highest or lowest valence state, when these glasses undergo the reduction treatments. If an element is almost completely reduced before heat-treatment in H_2/N_2 (1/99) (such as Mn), the concentration of ions that may be reduced is low, and hence, the diffusion depth will be small. If the element is almost completely oxidized (such as Ti), the concentration of reducible ions is high, but the reduction reaction is thermodynamically unfavorable, which will also result in a small diffusion depth.

From our previous study [Smedskjaer & Yue 2009] and Paper I we know that the concentration of the polyvalent ions also influences the inward diffusion depth. The depth increases with increasing Fe_2O_3 content for identical reduction conditions. When more Fe^{3+} ions are available for reduction, more electron holes are created, i.e., the inward diffusion depth increases. However, too high Fe_2O_3 content can result in cluster formation [Liu *et al.* 2011] and a decrease of the glass-forming ability [Richet *et al.* 2006].

3.4 Type and Partial Pressure of Reducing Gas

We have previously found that no inward diffusion occurs when a $69SiO_2$-14MgO-11CaO-$4Na_2O$-$2Fe_2O_3$ glass is heat-treated in H_2/N_2 (10/90) [Smedskjaer & Yue 2009]. However, when the same glass is heat-treated in H_2/N_2 (1/99), the inward diffusion does occur. Therefore, in this thesis, we have mainly studied the inward diffusion as a result of heat-treatment in H_2/N_2 (1/99). The lack of inward diffusion under the H_2/N_2 (10/90) atmosphere is due to the fact that the hydrogen pressure is so high that all Fe^{3+} ions are reduced entirely by H_2 molecules before the mobile cations start to diffuse. At low pressure, the concentration of dissolved H_2 molecules in the glass is proportional to the H_2 partial pressure in the H_2/N_2 gas [Doremus 2002]. Hence, by lowering the H_2 partial pressure, the rate of the gaseous permeation is decreased, and hence, the inward diffusion mechanism can contribute to the reduction process. The critical H_2 pressure for inward diffusion to occur should depend on the glass composition, since the H_2 permeability depends strongly on the glass porosity (i.e., composition and structure).

Furthermore, the rate of gaseous permeation depends on the size of the gaseous element or molecule [Shelby 1996]. To reveal whether a gas with larger reducing molecules than H_2 at a higher pressure can induce the inward diffusion, we apply a CO/CO_2 (98/2 v/v) atmosphere as a reducing agent for heat-treatment of the silicate glass mentioned above [Paper I]. Both H_2 and CO are capable of permeating the glass as shown in the infrared (IR) absorption spectra of the heat-treated glasses (Fig. 3.3). Bands at 3550 and 2850 cm^{-1} are caused by O–H stretching vibrations of weakly and strongly hydrogen-bonded OH species, respectively [Scholze 1959], whereas the bands positioned at 1510 and 1425 cm^{-1} (see inset of Fig. 3.3) are assigned to vibrations of chemically dissolved carbonate species [Brooker *et al.* 2001].

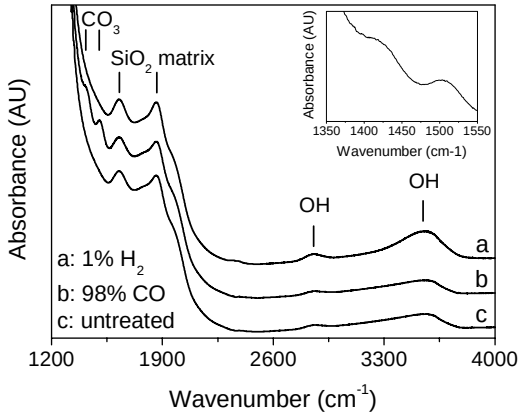

Figure 3.3. Fourier transform infrared (FT-IR) absorption spectra of 0.20 mm thick $69SiO_2$-14MgO-11CaO-$4Na_2O$-$2Fe_2O_3$ glass samples: untreated and heat-treated in H_2/N_2 (1/99) and CO/CO_2 (98/2) at T_g = 926 K for 16 h. Inset: curve of the CO-treated glass in the region with the bands of the chemically dissolved carbonate species. Data taken from Paper I.

SNMS analyses in Paper I show that inward diffusion occurs due to heat-treatment in CO/CO_2 (98/2). Thus, both CO permeation (Fig. 3.3) and outward flux of electron holes (Fig. 4 in Paper I) contribute to the reduction of Fe^{3+} in CO/CO_2 (98/2), i.e., inward diffusion occurs even though the CO partial pressure is much higher than that of H_2. This is explained by the slower permeation rate of CO in comparison to H_2 due to the size difference.

3.5 Link between Liquid Fragility and Diffusion

In this section, we apply the inward cationic diffusion approach to study the possible correlation between liquid fragility and diffusion. But what is liquid fragility? Glass-forming liquids become increasingly viscous upon cooling, until the viscosity inevitable becomes so large that they fail to flow on experimental timescales. In the famous Angell plot (Fig. 3.4), the logarithmic viscosity (log η) is plotted against the T_g-scaled inverse temperature (T_g/T) [Angell 1985].

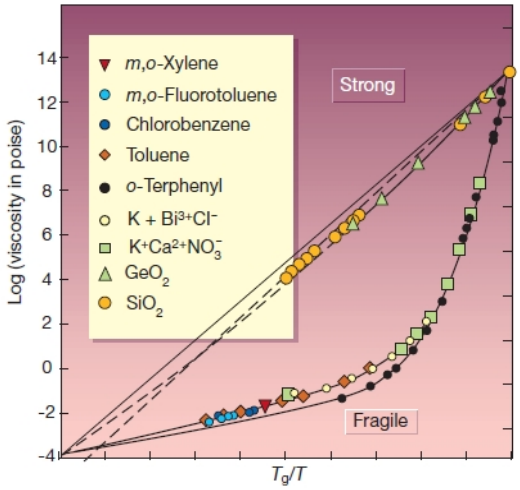

Figure 3.4. Angell plot showing the logarithm of viscosity as a function of the T_g-scaled inverse temperature for various organic and inorganic glass-forming liquids. "Strong" liquids exhibit approximately linear behavior (Arrhenius behavior), whereas "fragile" liquids exhibit non-linear behavior (super-Arrhenius behavior). Reproduced from [Debenedetti & Stillinger 2001].

The slope of the Angell curve at T_g defines the liquid fragility index *m*,

$$m \equiv \left. \frac{d \log_{10} \eta(T)}{d\left(T_g/T\right)} \right|_{T=T_g} . \tag{3.1}$$

m is a common measure of the slowing down of liquid dynamics upon cooling through the glass transition. Liquids can be classified as either "strong" or "fragile" depending on whether they exhibit an Arrhenius or super-Arrhenius scaling of viscosity with temperature, respectively [Angell 1985; Angell 1995]. The degree of non-Arrhenius scaling depends on the composition and structure of the glass-forming liquid (Fig. 3.4) and reflects the second derivative of the viscosity curve with respect to inverse temperature. However, since there exists a universal high temperature limit of viscosity (η_∞) [Zheng *et al.* 2011a], the non-Arrhenius character is directly connected to *m*.

To study the possible correlation between fragility and diffusion, we have prepared two silicate glass series: SiO_2-CaO-Fe_2O_3-A_2O (A = Na, K, Rb, Cs) and SiO_2-RO-Fe_2O_3-Na_2O (R = Mg, Ca, Sr, Ba) [Paper III; Paper IV]. From the temperature dependence of the inward diffusion of the alkaline earth ions, we have calculated the activation energy of diffusion (E_{diff}). We determine *m* by fitting measured viscosity values as a function of temperature to

the recent Mauro-Yue-Ellison-Gupta-Allan (MYEGA) model of viscosity [Mauro *et al.* 2009b],

$$\log_{10}\eta(T) = \log_{10}\eta_\infty + (12 - \log_{10}\eta_\infty)\frac{T_g}{T}\exp\left[\left(\frac{m}{12-\log_{10}\eta_\infty} - 1\right)\left(\frac{T_g}{T} - 1\right)\right]. \qquad (3.2)$$

The equation has been derived from an energy landscape analysis and topological constraint theory. We use this model, since it is the physically most realistic and accurate model of liquid dynamics. It is the only model of viscosity that accounts for a realistic extrapolation of configurational entropy (S_c) in both the high and low temperature limits [Mauro *et al.* 2009b].

We find that E_{diff} increases with increasing m for both series of glasses (Fig. 3.5). The remarkable linear relationship implies that the diffusion of alkaline earth ions in glasses is indeed related to the liquid fragility. We know that m is proportional to the activation energy of viscous flow at T_g [Yue 2009]. However, the mobile ions use the transportation pathways with the lowest activation energy. Therefore, they bypass the slow cooperative rearrangements of the structural silica units, i.e., the diffusion of the alkaline earth ions is decoupled from the network change [Paper III].

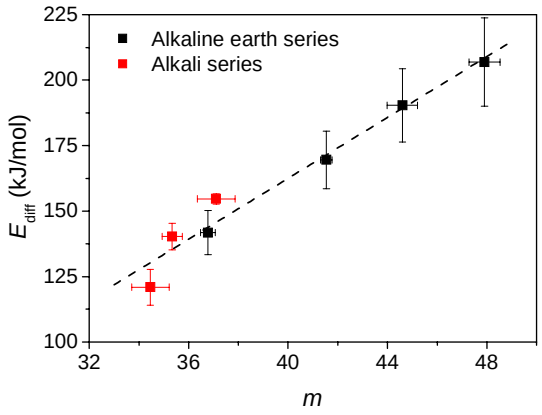

Figure 3.5. Activation energy of alkaline earth diffusion around T_g (E_{diff}) versus the liquid fragility index (m) for the glasses SiO_2-CaO-Fe_2O_3-A_2O with A = Na, K, Rb, Cs and SiO_2-RO-Fe_2O_3-Na_2O with R = Mg, Ca, Sr, Ba. The line is drawn as a guide for the eye. Reproduced from Paper VI.

Instead, the link between E_{diff} and m could be attributed to the fact that the liquid fragility is linked to S_c of the system. It is known that strong glass systems have a smaller S_c than fragile glass systems at the same T/T_g if the thermal history is the same [Yue 2009]. S_c is the part of the entropy of a pure liquid that is determined by the abundance of possible packing states obtainable at the temperature T [Martinez & Angell 2001]. Therefore, fragility depends on the multiplicity of states (local potential energy minima in energy landscape) for systems with identical T/T_g values [Speedy 1999; Sastry 2001]. The strong systems have lower activation barriers for viscous flow, and hence, the strong systems will have correspondingly fewer of the local potential energy minima, i.e., lower transition state entropy. Consequently, the non-equilibrium viscosity is lower for strong compared to fragile systems [Mauro *et al.* 2009c]. Similarly, alkaline earth ions should therefore diffuse faster in strong systems than in

fragile systems due to the simpler diffusion paths in the former ones. This provides a possible explanation for the observed trend in Figure 3.5.

3.6 Summary

We have revealed how various factors impact the spatial extent of the inward diffusion process. The type and partial pressure of the reducing gas are important factors governing the reduction mechanism. Interestingly, the inward diffusion of alkaline earth ions is faster than that of alkali ions and this might be attributed to the fact that for alkali inward diffusion, the charge-compensation of electron holes is a rather slow process, which slows down the rate of diffusion. Among the alkaline earth ions, Mg^{2+} has the lowest activation energy of inward diffusion, whereas copper is the polyvalent element that causes the most intense inward diffusion. Finally, we have shown that the activation energy of alkaline earth inward diffusion is lower in “strong” compared to “fragile” glass systems.

4 Impact of Glass Structure and Crystallization on Inward Diffusion

An adequate understanding of the composition and temperature dependence of ionic diffusion in glass requires microscopic information on the glass structure. Here, we discuss the impact of glass structure on diffusion by clarifying the composition dependence of inward diffusion in borate and boroaluminosilicate glasses. We also reveal how crystallization affects the inward diffusion in partially crystallized glasses (i.e., glass-ceramics).

4.1 Boron Anomaly Effect

Borate glasses have been important materials for both industry and daily life, particularly when mixed with silica to form borosilicates, e.g., as fiberglass and heat-resistant glass. Alkali and alkaline earth borate glasses are characterized by nonmonotonic variations of physical properties with metal oxide content, a phenomenon known as the "boron anomaly" effect. As described in the following section, these variations are caused by nonmonotonic variations in boron speciation. This makes borate glasses interesting model materials for studying the influence of glass structure on ionic transport.

4.1.1 Structure of Borate Glasses

Boron atoms, unlike silicon in silicate glasses, can assume both 3-fold and 4-fold coordination, forming BO_3 triangles and BO_4 tetrahedra. However, like silicate glasses, oxygen atoms can adopt both bridging (BO) and non-bridging (NBO) configurations. Consequently, borate glasses offer a wider variety of configurations amongst network-former and network-modifier atoms than silicates. In detail, when alkali or alkaline earth oxides are added to B_2O_3, there are two possible scenarios: (a) creation of a NBO, rupturing the linkage between two trigonally coordinated BO_3 groups; or (b) conversion of boron from a three-coordinated (B^3) to a four-coordinated (B^4) state without the creation of NBO [Paper VIII]. Moreover, the random pair model of Gupta [Gupta 1986] establishes three rules for network formation: (i) BO_4 tetrahedra occur in corner-sharing pairs, where the B-O-B angle within a pair is random; (ii) pairs of BO_4 tetrahedra cannot be bound to each other; and (iii) NBOs occur in BO_3 groups only.

Here, we investigate the sodium and calcium inward diffusion in the $(89\text{-}x)B_2O_3\text{-}xNa_2O\text{-}10CaO\text{-}1Fe_2O_3$ system with x = 5, 10, 15, 20, 25, 30, and 35 [Paper IX]. For $x < 23\%$, BO_3 units are converted into BO_4 unit as the Na_2O content increases. For $x > 23\%$, NBOs start to form [Paper VIII].

4.1.2 Diffusion versus Boron Speciation

The composition dependence of sodium and calcium inward diffusion is illustrated in Figure 4.1a. The Ca^{2+} inward diffusivity decreases with increasing Na_2O content for $x \leq 25$. We attribute this to the increase in atomic packing density as BO_3 units are converted into BO_4 groups (Fig. 4.1b), i.e., the steric hindrance for ionic motion increases with increasing x for $x \leq 25$. As discussed in Paper IX, this result is contrary to findings in the literature, where it is reported that the ionic mobility increases with increasing BO_4 concentration in binary alkali borate glasses [Berkemeier *et al.* 2005].

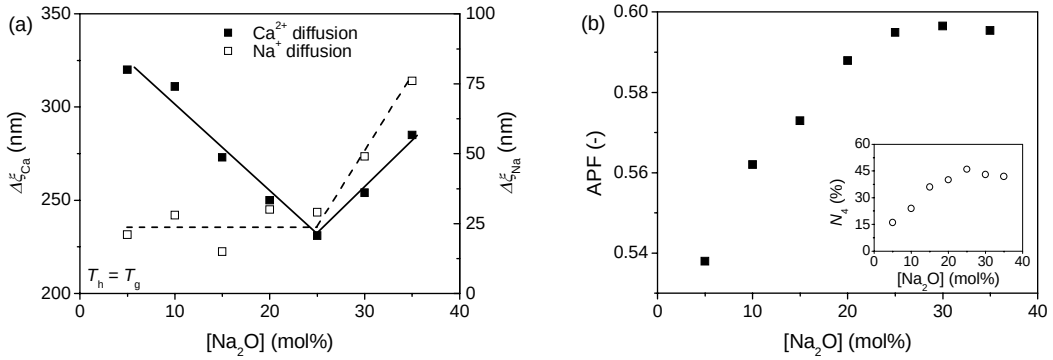

Figure 4.1. (a) Composition dependence of the extent of calcium ($\Delta\xi_{Ca}$) and sodium ($\Delta\xi_{Na}$) diffusion in the (89-x)B_2O_3-$x$$Na_2O$-10CaO-1$Fe_2O_3$ glasses. The glasses were heat-treated for 8 h in H_2/N_2 (1/99) at their respective T_g. (b) Composition dependence of atomic packing factor (APF) for the same glasses. APF is the ratio between the minimum theoretical volume occupied by the ions and the corresponding effective volume of the glass. Inset: composition dependence of boron speciation expressed as the fraction of tetrahedral to total boron (N_4). Data taken from Papers VIII and IX.

Both Na^+ and Ca^{2+} diffusion become faster as soon as NBOs start to form, and the diffusivity of Ca^{2+} is generally larger than that of Na^+ (Fig. 4.1a). To understand these results, we consider far-IR spectroscopic studies of alkali borates [Duffy & Ingram 1971] and alkaline earth borates [Duffy *et al.* 1997]. These studies show that network-modifying ions can occupy two types of sites in borate glasses, one of higher optical basicity (negative charge donating ability of oxygen) and one of lower. The sites of higher basicity provide a lower residual electronic charge on the cation, i.e., the cations in these sites are more mobile [Duffy *et al.* 1993; Kamitsos *et al.* 1996]. For x < 23%, there are no NBOs and the cations occupy sites of low optical basicity and hence of relatively low mobility. A higher field strength cation such as Ca^{2+} with its stronger affinity for oxygen should be able to be get charge-neutralized more easily than Na^+ and will move faster. Once NBOs are formed, both Na^+ and Ca^{2+} will be charge-neutralized more easily and move faster compared to the situation in the absence of NBOs for glasses with similar atomic packing density.

These results provide information on the impact of network structure on ionic transport in borate glasses. We have shown that both atomic packing and electrostatic environments of mobile cations play important roles in controlling the transport properties.

4.2 Network Polymerization Effect

Boroaluminosilicate (BAS) glasses are widely applied in technologies such as active matrix liquid crystal display substrates [Ellison & Cornejo 2010], photochromic glass [Armistead & Stookey 1964], fiber glass [Varshneya 2006], and radioactive waste glass [Jantzen *et al.* 2010]. These glasses are also interesting model materials for investigating the impact of glass structure on ionic diffusion, since the network-modifying ions can play different roles in the mixed network-former glasses. Here, we investigate the sodium inward diffusion in the (79-x)SiO_2-$x$$Al_2O_3-5B_2O_3-15Na_2O-1Fe_2O_3$ system with x = 2.5, 5, 7.5, 10, 12.5, and 15. The details are presented in Paper VII.

4.2.1 Structure of Boroaluminosilicate Glasses

The structural role of sodium in the BAS glasses depends on the ratio between the network-formers (B_2O_3, Al_2O_3, and SiO_2). There are three different possibilities of sodium behavior: (i) Na^+ to stabilize aluminum in tetrahedral configuration; (ii) Na^+ to convert boron from trigonal to tetrahedral coordination; and (iii) Na^+ to form NBOs on tetrahedral silicon and/or trigonal boron. Aluminum is predominantly present in tetrahedral configuration (AlO_4^-) provided that sufficient Na^+ is available for charge-balancing, since there is preference in the formation of tetrahedral Al^{3+} over that of tetrahedral B^{3+} [Bertmer *et al.* 2000; Chan *et al.* 1999]. Since all of the glasses under study are peralkaline, there is sufficient Na^+ available to stabilize all aluminum in 4-fold coordination in all of the glasses. Hence, aluminum speciation is unaffected by glass composition (x) as evidenced by ^{27}Al MAS (magic angle spinning) NMR (nuclear magnetic resonance) spectra of corresponding iron-free glasses (Fig. 4.2a) [Zheng *et al.* 2011b].

The additional Na^+ ions not used for stabilizing aluminum in tetrahedral configuration are either used for changing the boron coordination or for forming NBOs on tetrahedral silicon or trigonal boron. By using ^{11}B MAS NMR spectroscopy, we have found that the fraction of tetrahedral to total boron (N_4) depends on the $[SiO_2]/[Al_2O_3]$ ratio [Zheng *et al.* 2011b]. In the low Al_2O_3 region, most of the boron is present in 4-fold coordination, and N_4 then gradually decreases with increasing x (Fig. 4.2b).

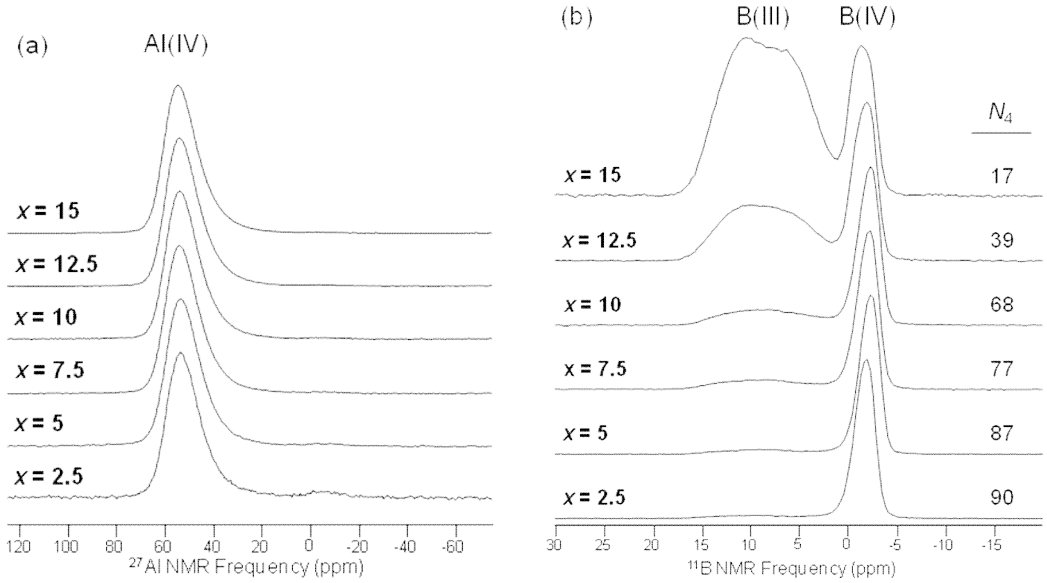

Figure 4.2. MAS NMR spectroscopy on $(80\text{-}x)SiO_2\text{-}xAl_2O_3\text{-}5B_2O_3\text{-}15Na_2O$ glasses with x = 2.5, 5, 7.5, 10, 12.5, and 15 [Zheng *et al.* 2011b]. (a) ^{27}Al MAS NMR spectra collected at 11.7 T referenced to aqueous aluminum nitrate. Aluminum is four-coordinated in all glasses. (b) ^{11}B MAS NMR spectra collected at 11.7 T referenced to $BF_3{\cdot}(C_2H_5)_2O$. The fraction of 4-fold coordinated boron (N_4) decreases with increasing x.

4.2.2 Diffusion versus $[SiO_2]/[Al_2O_3]$ Ratio

As shown in Figure 2.7b, the sodium inward diffusivity decreases with increasing $[SiO_2]/[Al_2O_3]$ ratio, i.e., with decreasing x. This may be due to the following two factors. First, the structural role of sodium differs depending on the $[SiO_2]/[Al_2O_3]$ ratio. In the high

Al_2O_3 region, Na^+ is used for charge-compensation of AlO_4^- and BO_4^-. In the low Al_2O_3 region, some of the sodium ions create NBOs bonded with Si-O and these sodium ions could be less mobile, as they are a more rigid part of the network. Second, the differences in boron speciation and chemical composition lead to differences in atomic packing of the glass networks. The BAS network becomes more densely packed with increasing $[SiO_2]/[Al_2O_3]$ ratio [Paper VII], and this contributes to the lowering of the sodium diffusivity.

Our results demonstrate that the impact of glass structure on diffusion is a complicate matter. The presence of NBOs increases the sodium diffusivity in borate glasses (Fig. 4.1a), whereas it lowers the sodium diffusivity in BAS glasses (Fig. 2.7b). Such dependences of diffusivity on glass structure are important to elucidate for various high-tech applications of glasses. For example, our results on sodium diffusivity in BAS glasses could be useful for optimizing basic compositions of BAS glasses concerning the efficiency of ion exchange strengthening [Varshneya 2010].

4.3 Crystallization Effect

Glass-ceramics are produced by controlled crystallization of a glass, generally induced by adding nucleating agents. The materials contain a residual glassy phase and one or more embedded crystalline phases. The controlled crystallization of glasses gives an array of materials with an interesting combination of properties. This enables various technical applications of glass-ceramics. For example, some crystalline phases have a negative coefficient of thermal expansion (CTE) that can be combined with the positive CTE of the residual glass. This is applied, e.g., in glass-ceramic cooktops [Bach & Krause 2005].

The diffusion of mobile ions in glass-ceramics occurs in a more complicated manner than in glasses, since the extent and manner of diffusion differ in the two phases [Chen *et al.* 1984; Kanert *et al.* 2000]. In the following, we investigate the impact of the crystallization degree (α) on the inward diffusion in iron-containing diopside ($CaMgSi_2O_6$) glass ceramics [Paper X].

4.3.1 Diopside Glass-Ceramics

We chose diopside as the object of this study, because diopside glass crystallizes congruently, i.e., the resulting crystalline phase will have the same composition as the residual glass phase. This allows us to compare the diffusion extent in glass-ceramics with different degrees of crystallization. If the crystalline phase removes certain ions from the residual glass, the ionic diffusion in the glass will be affected [Shelby 2005]. Experimentally, we first crystallize the $CaMgSi_2O_6$ glass doped with 1 mol% Fe_2O_3 to various extents by heat-treatment in argon and then determine α. Afterwards we induce the inward diffusion by heat-treatment at 995 K ($\sim T_g$) for 2 h in H_2/N_2 (1/99) and determine the diffusion depth by SNMS analysis.

We have used x-ray diffraction (XRD) and differential scanning calorimetry (DSC) analyses to study the crystallization process. The inset of Figure 4.3a shows that the as-prepared glass is completely amorphous, since the XRD spectrum only contains the broad amorphous peak. When the glass is heat-treated at 1223 K for 30 min in argon, it becomes fully crystallized due to formation of augite crystals ($Ca(Mg,Fe)(Si,Fe)_2O_6$), i.e., iron-containing diopside crystals. Figure 4.3a shows the DSC crystallization peaks of the samples that have been crystallized at various temperatures (T_h) for 30 min prior to the DSC scan. The crystallization enthalpy (ΔH) decreases with increasing T_h. A small value of ΔH means that

the sample has crystallized to a large extent prior to the DSC scan [Moesgaard *et al.* 2007]. Hence, α increases with increasing T_h.

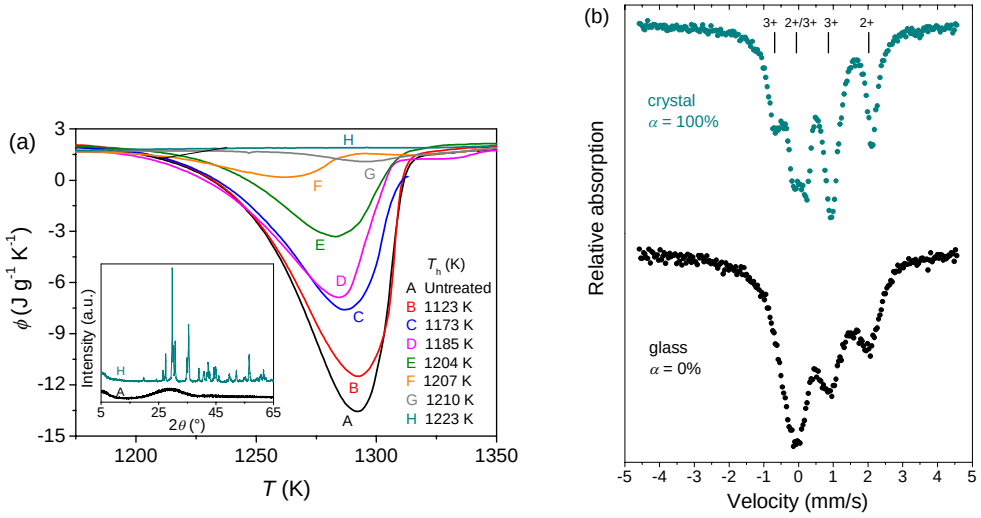

Figure 4.3. (a) DSC scans of the iron-containing diopside glasses in the temperature range of crystallization. Samples were crystallized for 30 min in argon at various temperatures (T_h) prior to the DSC scan. Inset: XRD patterns for two samples: untreated (A) and heat-treated at 1223 K for 30 min in argon (H). All peaks can be assigned to augite. (b) ^{57}Fe Mössbauer spectra of the iron-containing diopside glass (α = 0%) and crystal (α = 100%). Data taken from Paper X.

We have also performed ^{57}Fe Mössbauer spectroscopy analyses of the samples, since it is important to elucidate whether the crystallization changes the iron redox state. Figure 4.3b shows that the $[Fe^{2+}]/[Fe_{tot}]$ ratios, where $[Fe_{tot}] = [Fe^{2+}] + [Fe^{3+}]$, of the samples with α = 0 and 100 vol% are 34±3% and 31±3%, respectively. Hence, the crystallization of the glass does not change the redox state of iron within the error range of the data. However, the crystallization does change the iron coordination, but we do not expect that this will affect the inward diffusion depths.

4.3.2 Texture and Percolation Threshold

Figure 4.4 illustrates the correlation between the degree of crystallization and the extent of inward diffusion. The extent of diffusion is quantified by the diffusion depth of the Mg^{2+} ions ($\Delta\xi_{Mg}$), but similar results are obtained for the diffusion of calcium and iron ions. $\Delta\xi_{Mg}$ decreases with increasing α and no diffusion is observed in the fully crystalline sample. As shown by the linear fits (dashed lines) in Figure 4.4, the decrease of $\Delta\xi_{Mg}$ is especially pronounced in the range of α from 80 to 100 vol%. A similar behavior has been reported for the lithium ion conductivity in $LiAlSiO_4$ glass-ceramics [Biefeld *et al.* 1997].

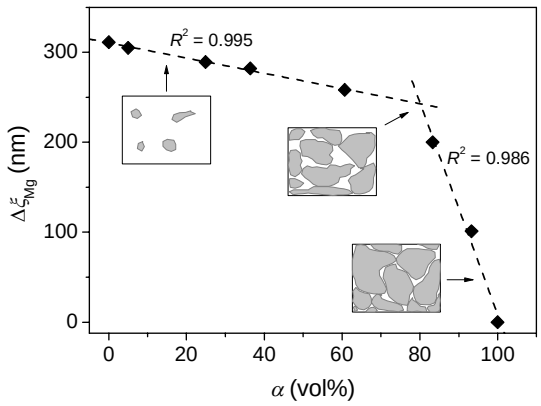

Figure 4.4. Inward diffusion depth of Mg^{2+} ions ($\Delta\xi_{Mg}$) as a function of the degree of crystallization (α) in the diopside ($CaMgSi_2O_6$) system doped with 1 mol% Fe_2O_3. Schematic two dimensional illustrations of the expected glass-ceramic structures are shown to illustrate the occurrence of the proposed percolation transition (white areas = glass; gray areas = crystal). Reproduced from Paper VI.

The existence of a critical value (α ~ 80 vol%), above which $\Delta\xi_{Mg}$ drastically drops to zero with α, indicates that a sudden drop in the degree of interconnection of the glass phase occurs. We describe the existence of the critical value in terms of a percolation transition [Frary & Schuh 2007; Nagler *et al.* 2011], since there are both easy and difficult paths through which the cations diffuse. At low degrees of crystallization, the glassy phase might consist of interconnected channels allowing a relatively fast cationic diffusion. At a certain degree of crystallization, the glassy phase starts to be disconnected, gradually becomes isolated domains, and finally disappears. Hence, as long as the glass phase domains are interconnected (or percolated), the inward diffusion occurs. Nevertheless, the diffusion does not stop until the sample is fully crystallized. This implies that a limited number of the interconnected paths still remain. The critical value may therefore be associated with a percolation threshold value at which the interruption of the diffusion pathways begins. We have drawn schematic two dimensional images in Figure 4.4 to illustrate the expected glass-ceramic structures as a function of the degree of crystallization. However, these texture scenarios in the glass-ceramics still need to be experimentally verified, e.g., by transmission electron microscopy.

4.4 Summary

We have used the inward cationic diffusion approach to study the impacts of glass structure and crystallization on diffusion. Both in borate and BAS glasses, the mobility of the network-modifying cations depends on their structural role in the network, i.e., whether they create non-bridging oxygens or act as charge compensators to stabilize network-formers. We also find that the inward diffusion occurs only in glass and not in crystals. The percolation transition in glass-ceramics from an interconnected to a disconnected glass phase has a strong impact on the diffusion extent.

5 Consequences of Surface Redox Reactions and Diffusion to Properties of Glass

In modern glass technology, it is often economically advantageous to perform post-treatment of glass surfaces in comparison to modifying the bulk composition of the glass to obtain a desired set of properties. Therefore, a wide range of post-treatment techniques exists, such as ion exchange, thermal tempering, coating, firepolishing, and surface crystallization [Varshneya 2006]. Here, we apply surface redox reactions and diffusion processes (i.e., the inward and outward diffusion approaches) to modify the properties of glasses. We reveal (i) the impact of inward diffusion on the hardness, elastic modulus, and chemical durability of silicate glasses, (ii) the consequences of surface reduction reactions to the optical properties of rare earth doped glasses, and (iii) the modification of the thermal properties of glass fibers due to both inward and outward diffusion.

5.1 Formation of Silica-Rich Surface Layer

When polyvalent element-containing silicate glasses are subjected to thermal reduction for sufficiently low partial pressure of the reducing gas, SNMS analyses have shown that a silica-rich surface layer is formed due to the inward diffusion process (see, e.g., Fig. 2.4). To investigate whether this causes an increase in the bridging oxygen (BO) content at the surface, we consider the FT-IR (Fourier transform infrared) reflection spectroscopy and XPS (x-ray photoelectron spectroscopy) measurements in Figure 5.1. Figure 5.1a shows that the wavenumber and intensity of the Si-O-Si antisymmetric stretching peak increase due to the thermal reduction, which is ascribed to an increase in the BO content [Lynch *et al.* 2007]. Figure 5.1b directly reveals that the thermal reduction increases the BO content, since the BO and NBO atoms appear as separate components in the XPS O1*s* spectrum and the BO-to-NBO ratio increases upon reduction [Paper XI].

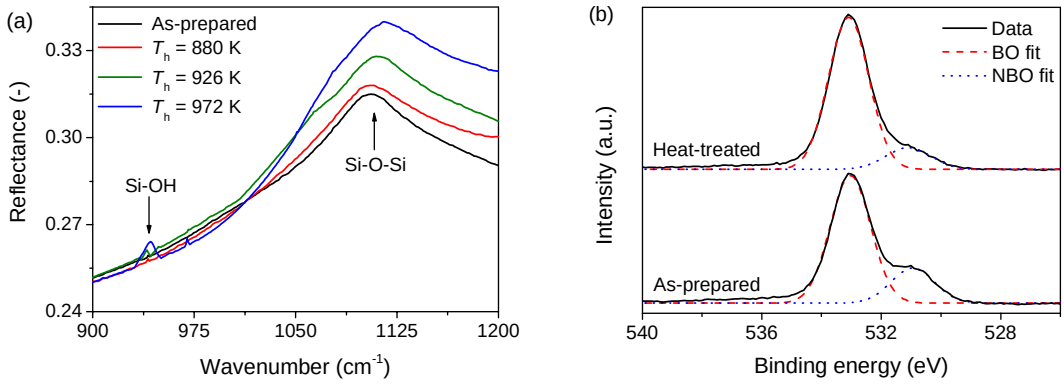

Figure 5.1. (a) FT-IR reflection spectra of a SiO_2-MgO-CaO-Na_2O-Fe_2O_3 glass heat-treated at various temperatures (T_h) for 2 h in H_2/N_2 (1/99). The peaks near 940 and 1100 cm^{-1} are assigned to vibration of Si-OH and antisymmetric stretching of Si-O-Si, respectively. (b) XPS spectra of O1*s* from a SiO_2-CaO-Na_2O-Eu_2O_3-Yb_2O_3 glass heat-treated at 773 K for 8 h in H_2/N_2 (5/95). The solid lines are the experimental data, whereas the dashed and dotted lines are the fit to the BO and NBO components, respectively. Reproduced from Paper XI.

Pure silica glass possesses excellent chemical, thermal, and mechanical properties. Based on the results in Figure 5.1, we therefore believe that the formation of the silica-rich surface

layer should enhance various surface properties. In the following, we investigate the impact of inward diffusion on hardness, elastic modulus, and chemical durability of silicate glasses.

5.1.1 Micro- and Nanoindentation

Hardness is an important mechanical property of materials that is defined as the resistance of a solid object to permanent deformation under pressure. Using microindentation with a diamond pyramid indenter, we have determined Vickers hardness (H_V). Results from our previous studies [Smedskjaer *et al.* 2009; Smedskjaer & Yue 2009] and Papers I and XI show that H_V increases as a consequence of the formation of the silica-rich surface layer. In fact, we have shown a positive correlation between the increase in H_V and the degree of inward diffusion [Paper XI]. H_V of a pure SiO_2 glass (OH content: 150 ppm) has been measured to be 11.3±0.3 GPa at a load of 0.25 N. However, the thermally reduced glasses do not become as hard as pure SiO_2 glass due to the following reasons. First, the modified surface layer is not solely composed of SiO_2. Second, in most experiments, the indenter penetrates the silica-rich layer and reaches into the interior of the glass. Third, the increased network connectivity caused by the inward diffusion of the network-modifying cations is to some extent counteracted by the partial permeation of H_2 into the glass, since this permeation results in the breaking of some Si-O-Si bonds. Fourth, the reduction reaction typically converts network-forming ions (e.g., Fe^{3+}) into network-modifying ions (e.g., Fe^{2+}).

We have also used nanoindentation to determine hardness (H) and elastic modulus (E) in the near-surface region of the thermally reduced glasses. This method measures both depth and load during the indentation process. The nanoindentation analysis is based on the Oliver-Pharr method that relies on an accurate knowledge of the indenter geometry and uses the unloading portion of the load-depth curve [Oliver & Pharr 1992]. Hardness is generally defined as

$$H = \frac{P_{max}}{A_c}, \tag{5.1}$$

where P_{max} is the maximum load and A_c is the contact area of the indenter. We use a Berkovich tip, which gives $A_c = 24.56h_c^2$, where h_c is the contact depth. h_c is the depth at which the surface and indenter profiles diverge, and it is obtained by subtracting the surface deflection from the maximum depth of penetration (h_{max}): $h_c = h_{max} - \varepsilon P_{max}/S$. S is the stiffness obtained from the unloading curve slope ($S = dP/dH$) and ε is an indenter geometry constant (0.75 for Berkovich [Pharr & Bolshakov 2002]). The unloading stiffness defines the reduced elastic modulus (E_r) as

$$E_r = \frac{\sqrt{\pi}}{2}\frac{S}{\sqrt{A_c}}. \tag{5.2}$$

The calculated elastic properties are a composite of the sample and the indenter tip. The relation is given by

$$\frac{1}{E_r} = \frac{1-\nu_s^2}{E_s} + \frac{1-\nu_i^2}{E_i}, \tag{5.3}$$

where the subscripts i and s refer to indenter and sample, respectively, and ν is Poisson's ratio. Poisson's ratio is the negative of the ratio of transverse contraction strain to longitudinal extension strain in the direction of elastic loading and reflects the resistance of a material to volume change with respect to shape change. For the diamond indenter, E_i = 1140 GPa and ν_i = 0.17 [Klein 1992; Zouboulis *et al.* 1998].

Here, we have performed nanoindentation analyses on as-prepared and heat-treated $64SiO_2$-$15Al_2O_3$-$5B_2O_3$-$15Na_2O$-$1Fe_2O_3$ glasses. The heat-treatment has been performed in H_2/N_2 (1/99) at 575 °C for 16 h, which causes an inward diffusion of sodium (depth ~210 nm), as described in Section 4.2 and Paper VII. Ten load-depth curves (P_{max} = 1 mN) have been recorded for each sample and representative examples are shown in Figure 5.2. The unloading curves are fitted to an empirical power-law equation [Oliver & Pharr 1992], and this gives average hardness values of 8.4±0.2 and 8.8±0.2 GPa for as-prepared and heat-treated samples, respectively. Using the measured Poisson's ratio of 0.22 for this glass [Zheng *et al.* 2011b], we obtain elastic moduli of 81±2 and 86±1 GPa for as-prepared and heat-treated samples, respectively. Hence, the formation of the silica-rich surface layer improves various mechanical properties.

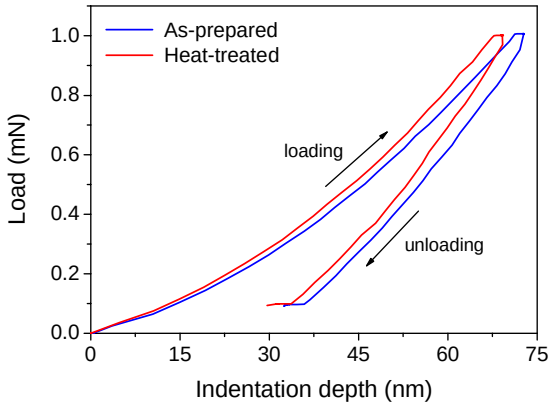

Figure 5.2. Representative load-depth curves for as-prepared and heat-treated $64SiO_2$-$15Al_2O_3$-$5B_2O_3$-$15Na_2O$-$1Fe_2O_3$ glasses. The heat-treatment was performed in H_2/N_2 (1/99) at 575 °C for 16 h. The loading and unloading rate was 200 µN/s and the hold time at the maximum load was 3 s. Measurements were performed on a Agilent Nano Indenter XP by Shen Lu at National University of Singapore.

5.1.2 Chemical Durability

The chemical durability of a glass can be defined as the resistance of the glass towards attack of water, acidic, and basic solutions. The corrosion of silicate glasses arises from several coupled mechanisms. The dominant mechanism depends on the acidity of the solution. In water or acidic solutions, primarily the monovalent alkali ions (M^+) will leave the glass and be replaced by H^+ and/or H_3O^+ by an ion exchange process [Conradt 2007]:

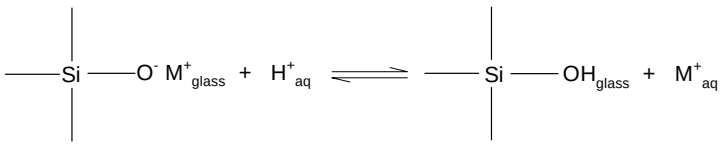

The alkali concentration in the surrounding solution increases with the square root of time as it is characteristic for diffusion controlled processes [Doremus 1975]. In basic solutions, the liquid directly attacks the network bonds as hydroxyl ions can break the Si-O-Si bonds leading to the formation of silanol-groups (Si-OH) [Frischat, 1975]:

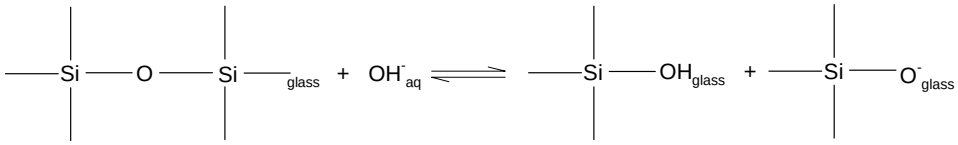

A continuous dissolution of the glass from the surface is the result of this mechanism, and the dissolved components in the liquid have approximately the same chemical composition as in the original glass. Various factors influence the acidic and basic dissolution rates, such as pH, temperature, and the ratio between solution volume and sample surface area. Thus, we keep these factors constant when determining the chemical durability.

In Papers I, II, and V, we have found that the formation of the silica-rich surface layer (i.e., the depletion of network-modifying cations at the surface) enhances the chemical durability in both acidic and basic solutions. For identical dissolution conditions, the chemical durability increases with increasing thickness of the silica-rich surface layer. The increase of acid resistance is easily explained by the reduced surface concentrations of alkali and alkaline earth ions. The increase of resistance against basic solution is explained by the high surface concentration of silica. The OH^- ions directly attack the Si-O-Si network bonds to continuously dissolve the glass. The thermal reduction increases the concentration of Si-O-Si bonds, i.e., more Si-O-Si bonds need to be broken in order to dissolve a relatively large amount of alkali and alkaline earth ions in the thermally reduced samples.

5.2 Photoluminescence and Quantum Cutting Induced by Reducing Gas

The use of rare earth ions to convert photons to different, more useful wavelengths is well-known from a wide range of applications, e.g., display technology, fluorescent tubes, lasers, and white light phosphors [van der Ende *et al.* 2009]. Oxide glasses are good host materials for rare earth ions owing to their optical properties, chemical durability, mechanical stability, manufacturability, and relatively low price. Among the various rare earth elements, europium is of particular interest, because both Eu^{2+} and Eu^{3+} show strong luminescence [Herrmann *et al.* 2009; Bünzli 2010]. Europium is usually incorporated into the glassy matrix in its trivalent state, but controlling the redox state of europium is important in tailoring the optical performances. There have been different strategies for obtaining Eu^{2+} doped materials [Peng *et al.* 2003; Wang *et al.* 2007; Qiu *et al.* 1999; Nogami *et al.* 2010; Gao *et al.* 2011]. Here, the idea is to induce reduction reactions in the surface layer of Eu doped glasses, since it may be an economically competitive option. This is because a synergy effect might occur: reduction of Eu^{3+} to Eu^{2+} and formation of silica-rich surface layer leading to better surface performances.

In Section 5.2.1, we investigate the static and dynamic luminescence properties of thermally reduced Eu doped glasses [Paper XII]. In Section 5.2.2, we perform thermal reduction of Eu-Yb co-doped glasses that may potentially be applied in solar cells [Paper XI].

5.2.1 Eu Doped Glasses

The electronic configuration of Eu is [Xe]$4f^7 5d^0 6s^2$. Photoluminescence (PL) of Eu^{3+} occurs in the red spectral region and is dominated by a series of sharp emissions bands originating from *f-f* transitions ($^5D_0 \rightarrow {}^7F_J$ with J = 0, 1, 2, 3, and 4). The emission wavelengths and intensities are nearly independent of ligand field strength due to the shielding by the $5s^2p^6$ electron cloud. PL of Eu^{2+} is found in the blue region and is due to the $4f^6 5d^1 \rightarrow 4f^7 (^8S_{7/2})$ transition. The transition is dipole allowed and therefore gives intense emission, but the emission band is broad due to the large spatial extension of the 5*d* wave function. Consequently, the intensity and position of the Eu^{2+} emission are strongly dependent on the host composition [Herrmann *et al.* 2009], because the 5*d*-electrons are not shielded from their surroundings.

We investigate the europium luminescence properties of a series of silicate, aluminosilicate, borosilicate, and boroaluminosilicate glasses (see compositions in Paper XII). Figure 5.3a shows emission spectra of the as-prepared glasses under excitation with 325 nm light. In all of the glasses, sharp peaks are detected in the region of 575-725 nm due to Eu^{3+} transitions from $^5D_0$ to the indicated states. The Eu^{3+} emission wavelengths are hardly influenced by host composition, whereas emission intensities of both Eu^{3+} and Eu^{2+} depend on the host composition (see inset of Fig. 5.3a). Most of the as-prepared glasses do not contain Eu^{2+} in any amount influencing the luminescence.

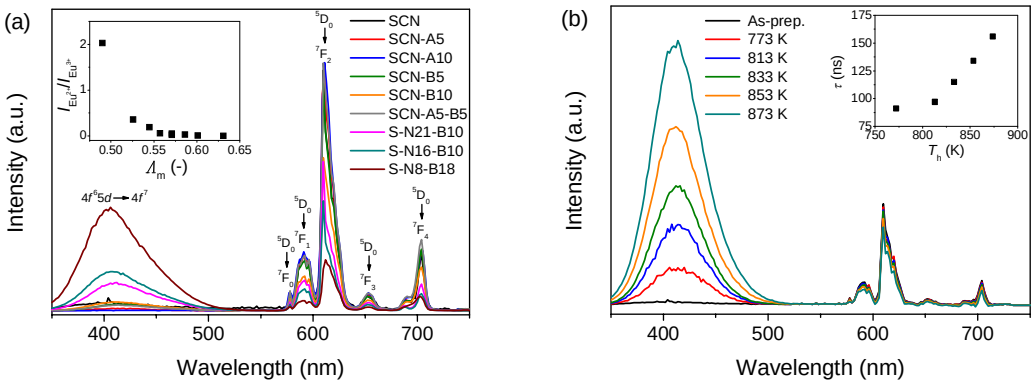

Figure 5.3. Emission spectra of Eu doped glasses under 325 nm excitation. The broad peak around 425 nm is ascribed to Eu^{2+}, whereas the sharp peaks from 575 to 725 nm are ascribed to Eu^{3+}. (a) Spectra of various as-prepared glasses (names of glasses are explained in Paper XII). Inset: ratio of the maximum intensity of the broad Eu^{2+} peak around 425 nm to that of the Eu^{3+} peak at 610 nm ($I_{Eu^{2+}} / I_{Eu^{3+}}$) against the optical basicity (Λ_m) of the host composition. (b) Spectra of as-prepared SCN glass and SCN glasses heat-treated in H_2/N_2 (5/95) for 8 h at various temperatures (T_h). Inset: luminescence lifetime (τ) of Eu^{2+} as a function of T_h. Reproduced from Papers XI and XII.

Heat-treatment of the glasses in H_2/N_2 (5/95) causes a reduction of Eu^{3+} to Eu^{2+}, as shown in Figure 5.3b for a SiO_2-CaO-Na_2O (SCN) glass. The degree of reduction increases with increasing heat-treatment temperature (T_h) and the luminescence intensities can also be tuned by adjusting the host composition (see details in Paper XII). Furthermore, the lifetime of the Eu^{2+} luminescence increases with increasing T_h (inset of Fig. 5.3b). This is because the excited Eu^{2+} ions can nonradiatively transfer their energy to Eu^{3+}, and this cross relaxation

from Eu^{2+} to Eu^{3+} diminishes with increasing T_h, as the concentration of remaining Eu^{3+} ions decreases with increasing T_h [Paper XII].

As shown in Figure 5.3, dual-mode photoemission from Eu^{2+} and Eu^{3+} is possible. By changing the temperature of the thermal reduction and/or adjusting the host composition, the $I_{Eu^{2+}} / I_{Eu^{3+}}$ ratio can be varied almost continuously. Consequently, the color of the luminescence can be finely tuned [Gao *et al.* 2011]. In addition, the heat-treatment in H_2/N_2 (5/95) has the simultaneous effect that it increases the glass hardness due to the formation of a silica-rich surface layer [Paper XI]. This could make these glasses interesting for various applications as phosphor materials.

5.2.2 Eu-Yb Doped Glasses

A new potential application of rare earth doped glasses has recently emerged, viz., the use of rare earth ions for spectral conversion in solar cells. The main energy loss in the conversion of solar energy to electricity is related to the so-called spectral mismatch (Fig. 5.4). Namely, low energy photons are not absorbed by the solar cell, while high energy photons are not used efficiently. To reduce the spectral mismatch losses, different approaches have been attempted [Richards 2006]. Here, we focus on quantum cutting (QC). This is a down-conversion process, during which one high energy photon is "cut" into two lower energy photons that can both be absorbed by the solar cell.

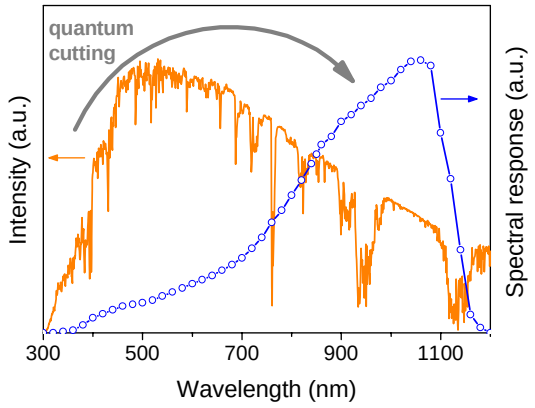

Figure 5.4. Solar spectrum (orange curve) and spectral response of crystalline Si solar cells (blue curve). Adapted from [Zhou *et al.* 2010].

We may detect the QC in glasses containing both Eu^{2+} and Yb^{3+} (Fig. 5.5a). This is possible because we know that the energy of the $4f^6 5d \rightarrow 4f^7$ transition of Eu^{2+} is approximately twice the energy of the $^2F_{5/2} \rightarrow {}^2F_{7/2}$ transition of Yb^{3+} [Zhou *et al.* 2010]. Yb^{3+} emits photons around 1000 nm, which matches the greatest spectral response of crystalline Si solar cells (Fig. 5.4). The main problem with the Eu-Yb system is the requirement of europium to be in the 2+ state. Therefore, we adopt the same strategy as that described in the preceding section, i.e., we perform thermal reduction of the Eu-Yb doped glasses. Figure 5.5b indicates that this approach is successful. With increasing heat-treatment temperature in H_2/N_2 (5/95), the emission band of Eu^{2+} around 425 nm increases simultaneously with the emission bands of Yb^{3+} near 1000 nm.

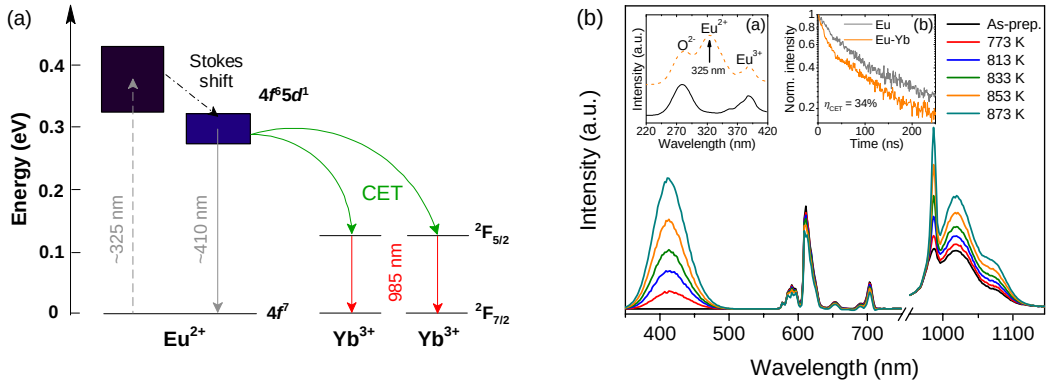

Figure 5.5. (a) Schematic energy level diagram of Eu^{2+} and Yb^{3+} showing the mechanism for the cooperative energy transfer (CET) from a UV-excited Eu^{2+} ion to two Yb^{3+} ions that relax by NIR (near infrared) emission. (b) Emission spectra of the co-doped Eu-Yb SCN glasses under 325 nm excitation. The peaks in the NIR region are due to Yb^{3+}. Inset (a): excitation spectrum monitored at 985 nm of the as-prepared co-doped Eu-Yb SCN glass (solid curve) and the same glass heat-treated at 853 K (dashed curve). Inset (b): luminescence decay curves of Eu^{2+} emission under 325 nm excitation of Eu and Eu-Yb doped SCN glasses heat-treated at 853 K. Reproduced from Paper XI.

We provide three evidences for the existence of cooperative energy transfer (CET) from Eu^{2+} to Yb^{3+}. First, as shown in inset (a) of Fig. 5.5b, one of the excitation peaks for 985 nm emission of Yb^{3+} is due to Eu^{2+}. In the as-prepared glass, the excitation peaks are located near 280 and 370-410 nm due to the charge transfer state absorption of Yb^{3+} and various transitions of Eu^{3+}, respectively [Paper XI]. However, the glass heat-treated at 853 K contains an additional peak near 325 nm ascribed to the $4f^{6}5d \rightarrow 4f^{7}$ transition of Eu^{2+}. Second, the relative intensity of the Eu^{2+} peak to that of the Eu^{3+} peaks is lower in the co-doped Eu-Yb glasses than in the corresponding singly Eu doped glasses (compare Fig. 5.5b with 5.3b). This is due to the additional relaxation mechanism for Eu^{2+} being available in the Eu-Yb glass. Third, as shown in inset (b) of Fig. 5.5b, the lifetime of Eu^{2+} emission is shorter in the heat-treated Eu-Yb glass (88 ns) than in the heat-treated Eu glass (134 ns).

We estimate the CET efficiency (η_{CET}) from the PL decay curves in inset (b) of Fig. 5.5b. η_{CET} is defined as the ratio of Eu^{2+} ions that depopulate by energy transfer to Yb^{3+} over the total number of Eu^{2+} ions excited. To determine η_{CET}, we therefore calculate the integrated luminescence intensity of the Eu^{2+} donor ion in both the absence and presence of Yb^{3+}. η_{CET} is then given by [Vergeer *et al.* 2005]

$$\eta_{CET} = 1 - \frac{\int I_{Eu^{2+}-Yb^{3+}}\, dt}{\int I_{Eu^{2+}}\, dt}. \qquad (5.4)$$

This gives η_{CET} = 34% for the glass heat-treated at T_h = 853 K. The total quantum efficiency (η_{TQ}) is defined as the ratio of the number photons emitted to the number of photons absorbed and is given by

$$\eta_{TQ} = \eta_{Q,Eu}\left(1-\eta_{CET}\right) + 2\eta_{CET}, \qquad (5.5)$$

where the quantum efficiency for the Eu^{2+} ions ($\eta_{Q,Eu}$) is set to 1 [Vergeer *et al.* 2005]. This gives η_{TQ} = 134%, which means that depopulation of the Eu^{2+} $4f^6 5d$ level proceeds 34 out of 100 times by excitation of two Yb^{3+} to the $^2F_{5/2}$ level. This value is similar to values reported elsewhere for the Eu-Yb system [Zhou *et al.* 2010]. However, the actual NIR quantum efficiency will be always be lower, since the method assumes that all Yb^{3+} ions decay radiatively, i.e., it does not account for concentration quenching of the Yb^{3+} emission. It is expected that a higher concentration of Yb_2O_3 will increase η_{TQ}. Nonetheless, the QC approach enables silicon-based solar cells to more efficiently utilize the solar energy. When the approach is combined with improved properties of the glass surface, such glasses may potentially act as interesting solar cell substrate materials.

5.3 Modification of Glass Fiber Properties

Man made glass wool fibers (GWFs) are typical hyperquenched (rapidly cooled) glasses produced from iron-rich alkaline earth aluminosilicate compositions. GWFs are widely used for thermal and sound insulation and as a fire barrier [Širok *et al.* 2008]. The wide range of applications of the glass fibers is due to their particular chemical and mechanical properties and high temperature stability (HTS).

Glass fibers have much larger surface-to-volume ratio than bulk glasses. Therefore, the inward and outward diffusion approaches are expected to considerably influence glass fiber properties. Hence, it is interesting to investigate the impact of the oxidation and reduction processes on the fiber properties, especially since many glass fibers are of basaltic composition, i.e., they contain the polyvalent iron.

5.3.1 Glass Transition Temperature

Oxidation (i.e., heat-treatment in air) of iron-containing aluminosilicate GWFs results in an increase of T_g [Paper XIII], whereas reduction (i.e., heat-treatment in H_2/N_2) results in a decrease of T_g [Paper V]. The increase of T_g is due to the conversion of network-modifying Fe^{2+} ions into network-forming Fe^{3+} ions. Furthermore, some alkali ions will change role, i.e., instead of being network-modifiers they will act as charge balancers (Fe^{3+} in tetrahedral coordination), which should contribute to the increase of T_g. The opposite arguments can explain the decrease of T_g during reduction.

5.3.2 Crystallization Behavior and High Temperature Stability

Oxidation of the GWFs in air has a strong impact on their bulk crystallization behavior, because different chemical conditions for nucleation and crystal growth are created. During oxidation, a nano-crystalline surface layer is created due to outward diffusion of cations such as Mg^{2+} and Ca^{2+}. The formation of the nano-crystalline surface layer shifts the onset temperature of crystallization (T_c) in argon to a lower value [Paper XIII; Yue *et al.* 2009]. In Paper XIII, we show that this occurs because the crystals lower the energy barrier of surface nucleation, i.e., nucleation in the interface between the nano-crystalline layer and the glassy bulk part of the fibers. In addition, the formation of the nano-crystalline surface layer enhances the HTS of the fibers in argon, i.e., the fibers are able to maintain their original geometric shape in a high temperature environment. This enhancement of HTS may be ascribed to the relatively high melting points of MgO and CaO crystals [Paper XIII].

Reduction of the GWFs in H_2/N_2 (1/99) also influences their crystallization behavior and HTS [Paper V]. The glass transition temperature decreases and the crystallization onset

temperature increases when the glass fibers are reduced and subsequently heated in argon (left panel in Fig. 5.6). However, the type of crystalline phases that form is not affected by the reduction process (middle panel in Fig. 5.6). The reduction deteriorates the HTS of the fibers in argon, as the fibers lose their original geometry and sinter together (right panel in Fig. 5.6). This may be due to the decrease of T_g and increase of T_c, since the fibers become viscous in the temperature range between T_g and T_c. Thus, the viscous softening takes place in a broader temperature range for the reduced fibers than for the as-prepared fibers.

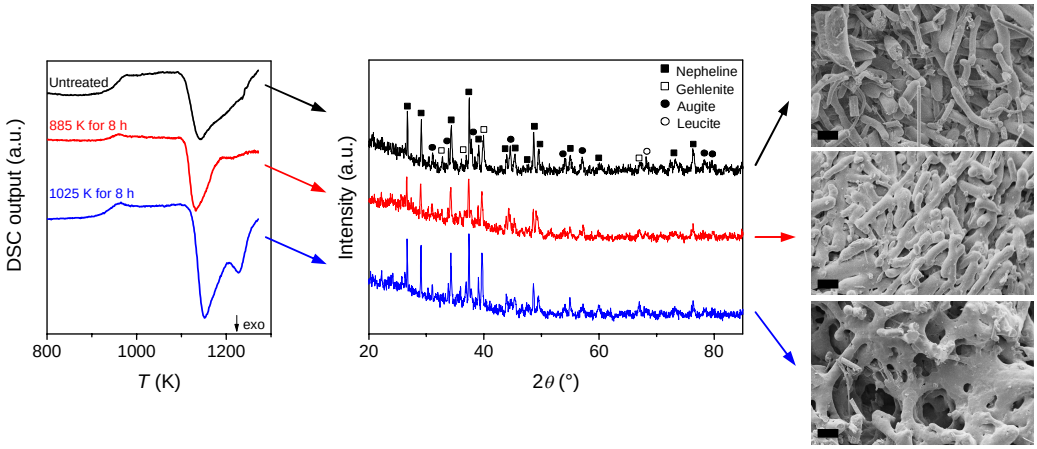

Figure 5.6. Impact of thermal reduction of iron-containing GWFs on their calorimetric response (left panel), crystallization behavior (middle panel), and high temperature stability (right panel) in argon. Left panel: DSC output as a function of temperature at a rate of 10 K/min. Middle panel: XRD patterns of the samples that have been subjected to the dynamic heating process during the DSC measurement. Right panel: scanning electron microscopy images of the dynamically heated samples to illustrate the high temperature stability (scale bar corresponds to 20 µm). Reproduced from Paper VI.

In Paper XIII, we have also studied the influence of chemical composition and heat-treatment atmosphere on the crystallization behavior and HTS of the GWFs. In general, the HTS is lower in argon and H_2/N_2 than in atmospheric air for as-prepared fibers. This is because the fibers heated in argon and H_2/N_2 lack the nano-crystalline surface layer that develops during heating in air and protects the fibers from sintering. The chemical composition of the fibers also influences the HTS, e.g., a high content of MgO seems to be beneficial for the HTS due to the high field strength (i.e., high charge-to-radius ratio) of Mg^{2+}.

5.4 Summary

Surface redox reactions and diffusion processes may be effective methods for modifying the properties of glasses. The formation of a silica-rich surface layer due to inward diffusion benefits the mechanical and chemical performances. For example, this approach may used to strengthen substrate or cover glass for solar cells, since the reduction reactions can simultaneously induce quantum cutting effects in Eu-Yb doped glasses. Finally, the crystallization behavior and HTS of glass fibers can be tuned according to the specific application by varying the post-treatment conditions.

6 Topological Understanding and Prediction of Glass Properties

The previous four chapters have dealt with the use of the inward and outward diffusion approaches to (i) understand the composition and structure dependence of diffusion and (ii) modify various surface and bulk properties of glasses. In this chapter, a different approach is taken to understand the origins of glass properties. This is done by using topological constraint theory.

6.1 Temperature-Dependent Constraint Theory

The Phillips-Thorpe constraint theory [Phillips 1979; Thorpe 1983] originally addresses the glass-forming ability of non-oxide covalent systems (i.e., chalcogenide glasses). In their view, glass-forming ability is determined by comparing the number of atomic degrees of freedom with the number of interatomic force field constraints. Each atom has three translational degrees of freedom in the three-dimensional space. However, these degrees of freedom are removed through the presence of rigid bond constraints. The network is considered to be underconstrained or "floppy", if the number of constraints is less than the available degrees of freedom. If the number of constraints is greater than the available degrees of freedom, the network becomes overconstrained.

In the floppy regime, the atoms may easily arrange themselves into the minimum energy configuration of the crystalline state. In the overconstrained regime, rigid structures easily percolate throughout the system, resulting in crystallization. Hence, according to Phillips and Thorpe, the tendency for glass formation is maximized when the number of constraints exactly equals the degrees of freedom, in which case the glass network is isostatic. The Phillips-Thorpe approach has been successfully applied to predict changes in various properties of chalcogenide glasses [Swiler *et al.* 1990; Senapati *et al.* 1997], but it has also been extended to oxide glasses [Kerner & Phillips 2000; Phillips & Kerner 2008].

While the original Phillips-Thorpe theory is formulated for zero temperature conditions, Gupta and Mauro [Gupta & Mauro 2009; Mauro *et al.* 2009a] conjectured that incorporation of temperature-dependent constraints would make it possible to calculate properties depending on temperature (T), such as the composition (x) dependence of shear viscosity ($\eta(T,x)$). The idea is that the rigidity of a given constraint depends on the available thermal energy (i.e., temperature) compared to the energy required to break that constraint. Hence, for a given composition x at high temperatures, the number of constraints is low and the network is floppy, whereas more constraints become rigid ("frozen-in") with decreasing temperature of the system. ^{77}Se NMR spectroscopy studies on germanium selenide liquids have recently provided direct experimental evidence for the temperature dependence of network constraints [Gjersing *et al.* 2010].

By accounting quantitatively for the effect of temperature, the Gupta-Mauro approach can be used to predict various properties of glasses. In the following, we apply and extend the temperature-dependent constraint theory in order to (i) understand the topological basis of glass properties and (ii) predict dynamical and mechanical properties of glasses.

6.2 Topological Origin of Liquid Fragility

As discussed in Section 3.5, the liquid fragility index m is a first-derivative property of the viscosity curve at T_g and it is one of the two (together with T_g) independent parameters for describing the complete temperature dependence of liquid and supercooled liquid viscosity [Mauro *et al.* 2009b; Zheng *et al.* 2011a]. Therefore, there has been intensive research in understanding the microstructural and topological origin of liquid fragility [Vilgis 1993; Angell *et al.* 2000; Novikov & Sokolov 2004; Dudowicz *et al.* 2005], yet key questions remain unanswered. In Paper IV, we have investigated the problem by considering two series of glasses with the same molar ratio between the different components, but the type of alkali and alkaline earth ions varies (in mol%):

- Alkali series: 68 SiO_2 – 23 CaO – 1 Fe_2O_3 – 8 A_2O (A = Na, K, Rb, Cs)
- Alkaline earth series: 68 SiO_2 – 8 Na_2O – 1 Fe_2O_3 – 23 MO (M = Mg, Ca, Sr, Ba)

We seek to investigate whether the alkali and alkaline earth ions play the same topological role in the glass networks and how they affect m. As we will see in the following, we can determine whether the network-modifying cations play the same topological role from the correlation between T_g and m. Therefore, we first determine the values of m and T_g of the glasses by using viscosity and DSC measurements, respectively. m and T_g are plotted as a function of the ionic radius of the alkali or alkaline earth ion in Figure 6.1. m and T_g vary as a function of the ionic radius, as discussed in Papers III and IV.

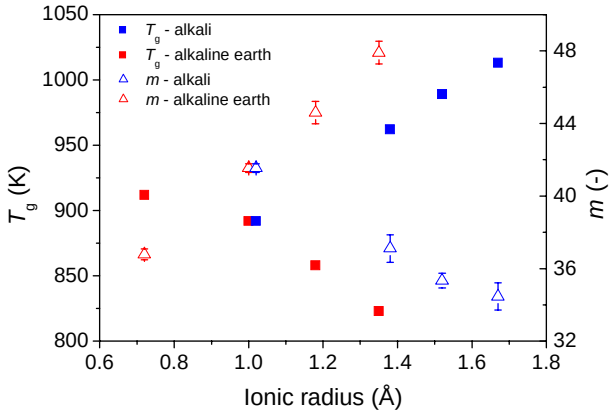

Figure 6.1. Dependence of glass transition temperature (T_g) and liquid fragility index (m) on the ionic radius of alkali and alkaline earth ions in the two glass series: SiO_2-CaO-Fe_2O_3-A_2O with A = Na, K, Rb, Cs and SiO_2-MO-Fe_2O_3-Na_2O with R = Mg, Ca, Sr, Ba. Notice that the same glass corresponds to A = Na and M = Ca. Data taken from Papers III and IV.

We then consider the MYEGA model of viscosity, which may be written in a simplified form as [Mauro *et al.* 2009b]

$$\log\eta = \log\eta_\infty + \frac{K}{T}\exp\left(\frac{C}{T}\right), \tag{6.1}$$

where K is a normalized activation barrier for structural rearrangements and C is the temperature at which a topological floppy-to-rigid transition occurs during cooling (i.e., the

constraint onset temperature). For deriving a simple analytical relation between T_g and m, we need to use an approximate form of MYEGA. To do so, we consider the high temperature limit, in which the exponential of Eq. (6.1) can be expanded as a Taylor series,

$$\log\eta = \log\eta_\infty + \frac{K}{T\exp\left(-C/T\right)} \approx \log\eta_\infty + \frac{K}{T\left(1-C/T\right)} = \log\eta_\infty + \frac{K}{T-C}. \qquad (6.2)$$

This expression is exactly the empirical Vogel-Fulcher-Tammann (VFT) form of viscosity that has been successfully applied for a variety of liquids [Vogel 1921; Fulcher 1925; Tammann & Hess 1926], even though it seems to break down at low temperatures [Laughlin & Uhlmann 1972; Mauro *et al.* 2009b]. Most importantly, our deviation of the VFT equation as an approximation to the MYEGA equation shows that the Vogel temperature T_0 corresponds to the floppy-to-rigid transition temperature C. VFT predicts a divergence of viscosity at T_0. Following the Adam-Gibbs model [Adam & Gibbs 1965], such divergence corresponds to a vanishing of the configurational entropy at T_0. However, according to the energy landscape view, a liquid cannot be confined in a single microstate at a finite temperature, and so the entropy cannot truly vanish unless the system is cooled completely to absolute zero [Stillinger 1988]. Therefore, based on the recent work of Gupta and Mauro [Gupta & Mauro 2009; Mauro *et al.* 2009a], it seems more appropriate to associate T_0 with the floppy-to-rigid transition temperature at which the system becomes optimally constrained, i.e., the number of constraints equals the number of degrees of freedom.

If the alkali and alkaline earth ions play the same topological role in the glass networks, the glasses should become isostatic and percolation break down at approximately the same temperature upon cooling. According to the preceding analysis, this then corresponds to T_0 being a constant. To test whether this is the case, we first set $D_0 = K/T_0$ in Eq. (6.2),

$$\log\eta = \log\eta_\infty + \frac{1}{T}\frac{D_0T_0}{\left(1-T_0/T\right)}. \qquad (6.3)$$

Then, we set the viscosity at T_g and infinite temperature equal to 10^{12} Pa·s [Yue 2009] and 10^{-3} Pa·s [Zheng *et al.* 2011a], respectively, which gives

$$D_0 = \frac{15\left(T_g - T_0\right)}{T_0}. \qquad (6.4)$$

This expression for D_0 is substituted back into Eq. (6.3), and from the definition of fragility m (Eq. (3.1)), we have

$$m = 15\left(1+\frac{T_0}{T_g - T_0}\right). \qquad (6.5)$$

Thus, this equation is useful for studying the topological role of the alkali and alkaline earth ions, because it contains the parameters m, T_g, and T_0. Using the glass with A = Na (i.e., M = Ca) as a reference gives T_0 = 570 K based on its values of T_g and m. Inserting this value of T_0 into Eq. (6.5) gives the solid line in Figure 6.2, in which m is plotted as a function of T_g.

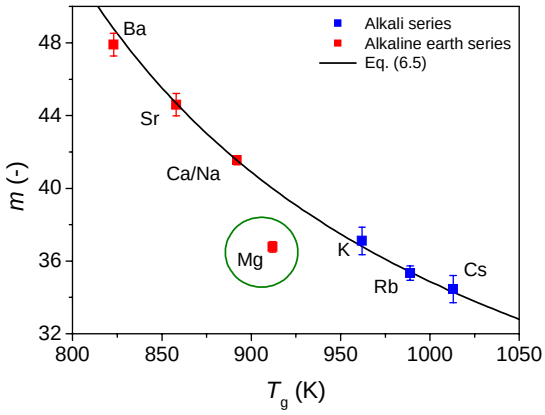

Figure 6.2. Correlation between fragility index m and glass transition temperature T_g in the alkali and alkaline earth series. The solid lines corresponds to Eq. (6.5) with T_0 = 570 K. The Mg-containing glass is the only glass that does not reveal good agreement between experimental data and model. Data taken from Papers III and IV.

The agreement of the experimental data with the model is nearly perfect. As discussed in Paper IV, only the Mg data point falls off the curve, which may be due to its special structural and topological role in silicate glasses. Hence, all of the alkali and alkaline earth ions (except Mg^{2+}) do indeed play the same topological role in the glass networks, as T_0 is a constant. This provides good verification of the temperature-dependent constraint approach of Gupta and Mauro, since the model is based on the existence of a floppy-to-rigid transition temperature. The result also demonstrates the universal role of network topology in governing liquid fragility, since m depends on T_0 (Eq. (6.5)) and T_0 corresponds to the floppy-to-rigid transition temperature (i.e., rigidity percolation temperature).

6.3 Prediction of Dynamical Properties

The temperature-dependent constraint theory of Gupta and Mauro can be used to calculate the composition dependence of T_g and m, i.e., the composition dependence of shear viscosity. Their calculations build on the analysis of Naumis [Naumis 2005; Naumis 2006]. Naumis found that the major contribution to configurational entropy ($S_c(T,x)$) in glass-forming systems is the presence of floppy modes. With decreasing temperature, the number of floppy modes decreases (i.e., they become rigid), and consequently the configurational entropy also decreases. Adam-Gibbs theory [Adam & Gibbs 1965] is then applied to describe $\eta(T,x)$ in terms of $S_c(T,x)$, i.e., the major composition dependence of T_g and m is due to variations in the configurational entropy. This allows T_g and m to be calculated as a function of the number of constraints, i.e., as a function of composition. The approach is described in more detail elsewhere [Gupta & Mauro 2009; Mauro *et al.* 2009a].

In the following sections, we extend the Gupta-Mauro topological model for the first time to a ternary composition space (soda-lime-borate glass system) and the theory is further developed to take structural heterogeneities into consideration during the prediction of T_g and m. We also demonstrate how the approach can be applied to the quantitative design of new glass compositions. These results are described in detail in Paper VIII.

6.3.1 Model Glass System

We choose the soda-lime-borate ternary ((1-*x*-*y*)B_2O_3-*x*Na_2O-*y*CaO) as the object of this study for the following three reasons. First, borate glasses contain an abundance of interesting structural and topological features, e.g., boron anomaly effect and heterogeneous distribution of network-modifiers [Greaves & Sen 2007]. Second, borate glasses have posed a particular challenge for traditional molecular dynamics simulations, because of the change in boron coordination that occurs in the presence of network-modifiers [Inoue *et al.* 1987]. Third, the particular soda-lime-borate system has received little previous attention [Donohoe & Shelby 2006]. It should be noticed that some of the glasses under study contain 1 mol% Fe_2O_3, since they have also been used for investigating the impact of boron speciation on inward diffusion (cf. Section 4.1).

The structure of borate glasses depends on the molar ratio between B_2O_3 and alkali and alkaline earth oxides (cf. Section 4.1.1). In our model, we assume that the effect of CaO on boron speciation is the same as adding Na_2O [Greenblatt & Bray 1967]. The first steps of the topological modeling approach are then to (i) identify and count the number of distinct network-forming species as a function of composition, (ii) identify and count the number of constraints associated with each species, and (iii) rank the different constraints in terms of their relative bond strengths (i.e., constraint onset temperatures).

We have identified four distinct network-forming species: (i) four-coordinated boron bonded to four bridging oxygens (B^4); (ii) three-coordinated boron bonded to three or two bridging oxygens (B^3); (iii) oxygen (O), including both bridging and non-bridging varieties; and (iv) network-modifiers (Na and Ca) that create NBOs (M^{NB}). As explained in Paper VIII, we then describe the boron speciation in terms of the random pair model of Gupta [Gupta 1986]. Using Gupta's rules for network formation, we calculate the fractions of network-forming species as a function of composition (see Supporting Information of Paper VIII). Figure 6.3 shows that there is good agreement between these calculated fractions and those determined experimentally using ^{11}B MAS NMR spectroscopy.

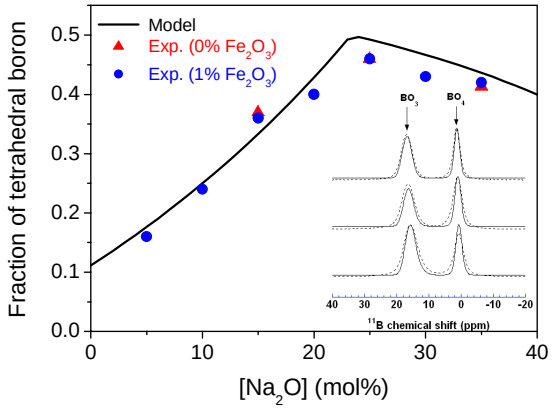

Figure 6.3. Fraction of tetrahedral to total boron in (90-*x*)B_2O_3-*x*Na_2O-10CaO glasses with and without 1 mol% Fe_2O_3 calculated using the random pair model of Gupta or determined experimentally using ^{11}B MAS NMR spectroscopy. Inset: corresponding ^{11}B MAS NMR spectra with (dashed lines) and without (solid lines) 1 mol% Fe_2O_3. The spectra from top to bottom correspond to glasses with 35, 25, and 15 mol% Na_2O. Data taken from Paper VIII.

We then consider the following types of bond constraints [Paper VIII]:

- α: B-O and M^{NB}-O linear constraints. There are two α constraints at each oxygen.
- β: O-B-O angular constraints. There are five β constraints per B^4 to form a rigid BO_4 tetrahedron and three β constraints per B^3 to keep the BO_3 unit planar.
- γ: B-O-B angular constraints. There is one γ constraints at each oxygen.
- μ: additional modifier rigidity due to clustering effects. Based on the ensuing discussion in Section 6.3.2, we consider two μ constraints per NBO-forming sodium, whereas there are zero constraints for calcium.

Based on the above, there are two types of network-modifying cations to consider: (i) those which convert boron to tetrahedral coordination; and (ii) those which create NBOs. These two types have been dealt with separately in our model. In the first case, the effects of both the sodium and calcium on the network topology are accounted for in the additional linear and angular constraints on the boron. However, it should be noticed that the modifier ion itself is not actually a part of the network, since it is just serving in a charge-compensating role for the tetrahedral boron. In the second case, the modifiers are a part of the glass network and hence each contributes three degrees of freedom to the network. Both have linear constraints which are counted on the NBOs, i.e., two constraints for Ca^{2+} and one for Na^{+}. The difference between sodium and calcium is that only sodium has the additional clustering μ constraint.

As discussed in Paper VIII, the constraint onset temperatures are ordered such that

$$T_\gamma < T_g(0,0) < T_\beta(0,0) < T_\mu < T_\alpha . \tag{6.6}$$

Now we are able to count the constraints n as a function of composition (x,y) and temperature, which allows us to calculate T_g and m as a function of composition.

6.3.2 Glass Transition Temperature

The composition dependence of the glass transition temperature can be calculated using the following equation [Paper VIII]

$$T_g(x,y) = \min\left[T_\beta(x,y), \frac{f(0,0)}{f(x,y)} T_g(0,0) \right], \tag{6.7}$$

where f is the number of atomic degrees of freedom and $f(x,y) = 3 - n(x,y)$. The calculated values of $T_g(x,y)$ using Eq. (6.7) are compared with experimental values of $T_g(x,y)$ for the $(90\text{-}x)B_2O_3$-xNa_2O-10CaO system in Figure 6.4a, and the agreement is excellent. The modeled results are given under two different assumptions: no modifier rigidity (dashed curve) and two rigid μ constraints per NBO-forming Na atom and zero for Ca (solid curve). There are other possible assignments of modifier rigidity (Na and Ca can each have 0, 1, 2, or 3 constraints per atom), but the assumption of two rigid μ constraints per NBO-forming Na provides the best prediction of the experimental values.

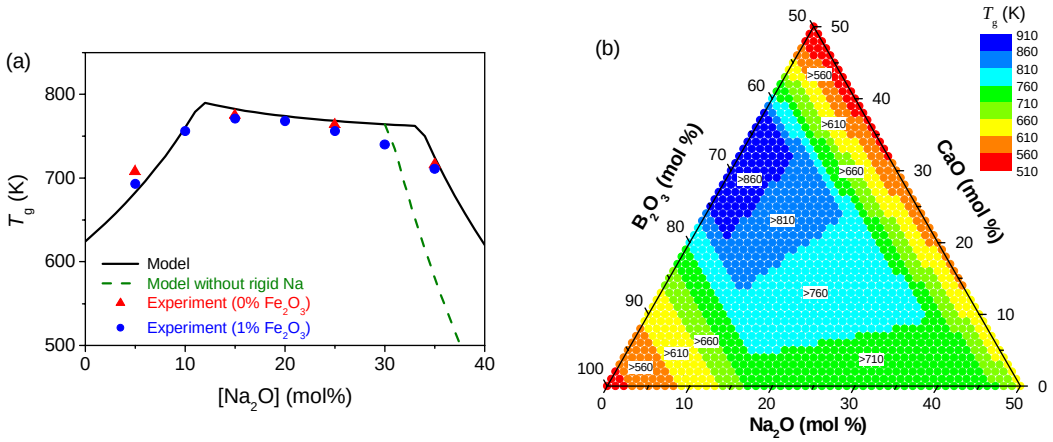

Figure 6.4. (a) Dependence of glass transition temperature on composition for (90-x)B_2O_3-$x$$Na_2O$-10CaO glasses with and without 1 mol% Fe_2O_3. The experimental data points were obtained by DSC measurements. The lines show the computed $T_g(x,y)$ values using Eq. (6.7) assuming two rigid μ constraints per NBO-forming sodium (solid) or zero modifier rigidity constraints (dashed). (b) Model calculations of $T_g(x,y)$ for the (1-x-y)B_2O_3-$x$$Na_2O$-$y$CaO system using Eq. (6.7). Reproduced from Paper VIII.

Figure 6.4b shows a complete ternary diagram for $T_g(x,y)$. Hence, the temperature-dependent constraint theory is proving to be useful for efficiently exploring uncharted regions of composition space. Calculations like those shown in Figure 6.4b may be used for the quantitative design of new glassy materials with optimized functionalities.

6.3.3 Liquid Fragility

The composition dependence of the fragility index m can be calculated from the temperature derivative of $f(T,x,y)$ [Paper VIII],

$$m(x,y) = m_0\left(1+\left.\frac{\partial \ln f(T,x,y)}{\partial \ln T}\right|_{T=T_g(x,y)}\right), \qquad (6.8)$$

where $m_0 \approx 17$ is the fragility of a strong liquid. As discussed in Paper VIII, we need a fitting parameter to calculate $m(x,y)$. The parameter is the product of ν (vibrational attempt frequency) and t_{obs} (observation time), which is required for calculating the rigidity of the constraints as a function of temperature. We consider a constant value of νt_{obs} and we obtain the value by fitting to the experimentally determined values of fragility. We determine m using both DSC (as described in Paper VIII) and viscosity measurements. Zheng *et al.* have measured the temperature dependence of viscosity by employing the concentric cylinder and micropenetration techniques, and fragility values were obtained by fitting the viscosity vs. temperature data to the MYEGA equation (Eq. (3.2)) [Zheng *et al.* 2011b]. Figure 6.5a shows the composition dependence of fragility using both methods.

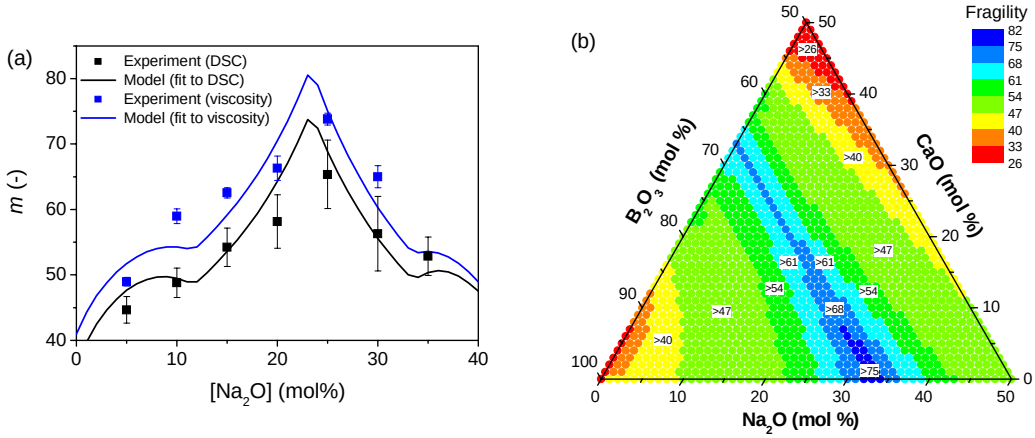

Figure 6.5. (a) Dependence of liquid fragility index on composition for (90-x)B_2O_3-$x$$Na_2O$-10CaO glasses with and without 1 mol% Fe_2O_3. The experimental data points were obtained by DSC and viscosity measurements. The lines show the computed $m(x,y)$ values using Eq. (6.8) with vt_{obs} = 60 (DSC) and vt_{obs} = 120 (viscosity). (b) Model calculations of $m(x,y)$ for the (1-x-y)B_2O_3-$x$$Na_2O$-$y$CaO system using Eq. (6.8) with vt_{obs} = 60. Reproduced from Paper VIII.

The fragility values using both methods follow the same qualitative compositional trend. The main feature is that fragility peaks around $x + y = 1/3$, i.e., at the onset of NBO formation (cf. Fig. 6.3). The fragility values are fit to our topological model, and we obtain vt_{obs} equal to 60 (DSC) and 120 (viscosity). The computed $m(x,y)$ values are also shown in Figure 6.5a and the experimental $m(x,y)$ values are in remarkably good agreement with the calculated $m(x,y)$ values. Figure 6.5b shows a complete ternary diagram for $m(x,y)$.

The topological modeling approach can also be used to elucidate the microstructural and topological origins of the calculated glass properties. Specifically, the microscopic origin of fragility of our borate glasses is the scaling of the concentration of O-B-O angles with composition (see detailed discussion in Paper VIII). Thus, the nonmonotonic scaling of fragility with composition is yet another consequence of the boron anomaly in these systems.

6.4 Prediction of Mechanical Properties

The topological modeling approach presented in Section 6.3 has the advantage that it can isolate the key physics governing macroscopic properties with all unnecessary details filtered out. Indeed, the success of predicting the composition dependence of T_g and m suggests that other thermal, mechanical, and rheological properties of glass may also be accurately predicted using constraint theory. This should be possible, since these properties are also strongly linked to the network topology.

We focus on predicting mechanical properties, in particular the composition dependence of glass hardness. High-strength, high-hardness glasses are currently one of the most important research areas in the glass community. The next wave of growth in high-tech glasses will most likely be through achievement of previously unthinkable values of strength and hardness. For example, hardness is a critical property when glass is used as scratch-resistant cover glass for personal electronic devices, such as iPhones. Hence, understanding the composition dependence of glass hardness is of critical importance.

Direct calculation of hardness from first principles has shown to be too complex. Therefore, scientists have attempted to correlate the hardness of oxide glasses with (i) the properties of its individual constituents [Georoff & Babcock 1973; Yamane & Mackenzie 1974], (ii) structural parameters such as the number of non-bridging oxygens [Deriano *et al.* 2004], and (iii) the glass transition temperature T_g [Deriano *et al.* 2004; Sehgal & Ito 1999]. However, more detailed information about the glass network is required for accurate prediction of hardness [Deriano *et al.* 2004]. In Paper XIV, we have developed an alternative topological approach for predicting the hardness of glass. In the following, we present this novel approach and show how it can be applied to predict changes in hardness of borate glass surfaces modified by inward diffusion.

6.4.1 Hardness of Glass

We investigate the composition dependence of Vickers hardness (H_V) for the soda-lime-borate system, for which we have already identified and counted the constraints as a function of composition and temperature (cf. Section 6.3.1). Figure 6.6 shows the composition dependence of the experimentally determined H_V values of the (89-x)B_2O_3-$x$$Na_2O$-10CaO-1$Fe_2O_3$ glasses. H_V increases with increasing Na_2O content up to around 25 mol% and then decreases.

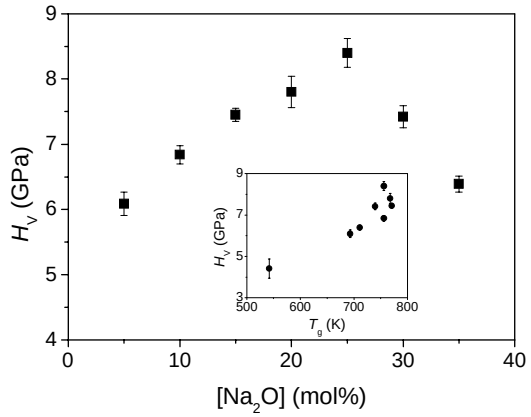

Figure 6.6. Composition dependence of Vickers hardness (H_V) for the (89-x)B_2O_3-$x$$Na_2O$-10CaO-1$Fe_2O_3$ glasses. H_V was measured at a load of 0.25 N. Inset: correlation between H_V and T_g, including data of a B_2O_3 glass. Data taken from Paper XIV.

Interestingly, we notice that H_V displays a distinct peak around the composition where the fraction of four-coordinated boron achieves a maximum, whereas there is a smaller change in T_g in the same region (Fig. 6.4a). Hence, there is not a direct correlation between T_g and H_V (inset of Fig. 6.6). This points to the importance of including the temperature dependence of network constraints when calculating properties such as $T_g(x,y)$ and $H_V(x,y)$. Since hardness is measured in the glassy state at room temperature, additional low temperature constraints are important (viz., the B−O−B angular γ constraints) and must be considered in the model.

To predict the composition dependence of glass hardness, we start from the idea that a certain critical number of constraints (n_{crit}) must be present for the material to display mechanical resistance, i.e., for hardness to become nonzero. When the average number of

atomic constraints is less than this critical value ($n < n_{crit}$), the mechanical response is liquid-like, i.e., there is no resistance to an incoming indenter, and hence no hardness. When $n > n_{crit}$ there are enough constraints to make a rigid network that produces a solid-like mechanical response. A value of $n = 2$ gives a network that is rigid along one dimension (i.e., rigid chains, as in Se), whereas $n = 3$ gives a network that is rigid in three dimensions (fully isostatic). We propose that in order for a network to display mechanical resistance, it must be rigid in at least two dimensions. Thus, we set $n_{crit} = 2.5$ since this gives a network that is exactly rigid in two dimensions of the three-dimensional space. Finite values of hardness are a result of the additional constraints to form a three-dimensional network. We then assume that hardness is directly proportional to the number of these additional constraints, i.e., the constraints in excess of n_{crit}. Hence, we obtain the following equation for calculating glass hardness

$$H_V(x,y) = \left(\frac{dH_V}{dn}\right)\left[n(x,y) - n_{crit}\right] = \left(\frac{dH_V}{dn}\right)\left[n(x,y) - 2.5\right], \qquad (6.9)$$

where $n(x,y)$ is the average number of atomic constraints at room temperature, which can be calculated as described in Papers VIII and XIV. The proportionality constant (dH_V/dn) is determined empirically and found to be dependent on the load of the indenter. With this model, we find excellent agreement between the predicted and measured values of hardness, as shown in Figure 6.7a. This allows us to calculate $H_V(x,y)$ in the complete ternary diagram (Fig. 6.7b). Notice the difference in the composition dependence of T_g (Fig. 6.4b) and H_V (Fig. 6.7b). This difference demonstrates the importance of considering the additional low temperature constraints when evaluating glass properties measured at room temperature.

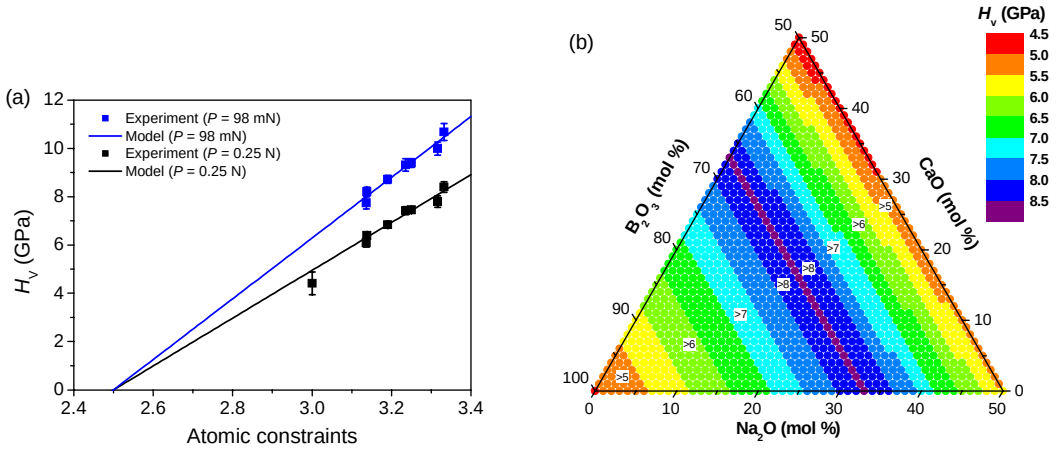

Figure 6.7. (a) Measured H_V at loads (P) of 98 mN and 0.25 N as a function of the average number of atomic constraints at room temperature. The solid lines represent model predictions using Eq. (6.9) with dH_V/dn equal to 12.6 and 9.9 GPa for loads of 98 mN and 0.25 N, respectively. (b) Model calculations of $H_V(x,y)$ at a load of 0.25 N for the (1-x-y)B_2O_3-$x$$Na_2O$-$y$CaO system using Eq. (6.9). Reproduced from Paper XIV.

The success of our model implies that the hardness of a glass can be quantitatively predicted from a basic knowledge about its network topology, with only an unknown proportionality

constant (dH_V/dn) that depends on the load of the indenter. We expect that other mechanical properties (such as elastic modulus) should have similar connections to the glass topology.

6.4.2 Hardness of Glass Modified by Inward Diffusion

The aim of this section is to test the validity of our hardness model. To do so, we modify the surface compositions of the soda-lime-borate glasses and then calculate the hardness using Eq. (6.9) and compare it with the experimental value. We perform the surface modification by using the inward diffusion approach. The results are described in detail in Paper IX.

As discussed in Section 4.1.2, the degree of inward diffusion of Ca^{2+} and Na^{+} (i.e., the degree of surface modification) in the soda-lime-borate glasses depends on the glass composition. Therefore, the change in hardness of the borate glasses due to the heat-treatment in H_2/N_2 (1/99) also depends on the glass composition (Fig. 6.8). H_V is lower for the heat-treated compared to the untreated samples for $x \leq 25$. This may be due to the removal of network modifiers from the surface layer, which should result in a decrease of the surface concentration of BO_4. The heat-treatment increases the hardness of the glasses for $x > 25$ (i.e., in the NBO regime). Since the modifying ions associated with NBOs are more mobile than those associated with four-coordinated boron as charge compensators (cf. Section 4.1.2), heat-treatment of glasses with $x > 25$ could cause a decrease in the surface concentration of NBOs [Paper IX].

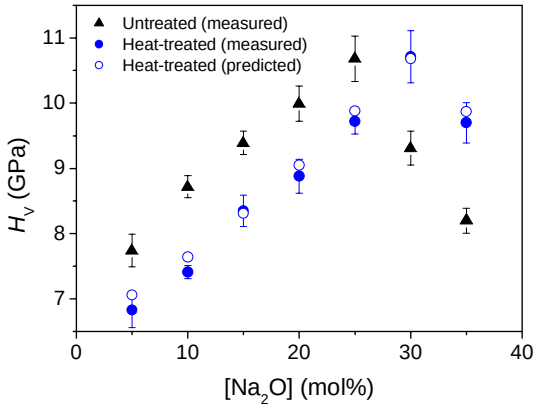

Figure 6.8. Composition dependence of the measured H_V for the untreated (89-x)B_2O_3-$x$$Na_2O$-10CaO-1$Fe_2O_3$ glasses and the measured and predicted H_V for the same glasses heat-treated for 8 h in H_2/N_2 (1/99) at 1.1 times their respective T_g. H_V was measured at a load of 98 mN. Reproduced from Paper IX.

Now we use the measured surface compositions of the heat-treated samples to calculate the number of room temperature constraints in the depth range that the indenter penetrates in order to calculate the hardness of that layer. As a consequence of the Vickers indenter geometry, the penetration depth is calculated as 1/7 of the impression diagonal length. Based on the number of room temperature constraints in the indented surface layer, we can then calculate H_V from the correlation in Figure 6.7a for the utilized load of 98 mN (see details in Paper IX). Figure 6.8 shows that the agreement between calculated and measured values of Vickers hardness is excellent. This is strong support for the validity of our hardness model.

6.5 Summary

Using temperature-dependent constraint theory, we have investigated the topological origin of liquid fragility in silicate glasses and predicted the composition dependence of dynamical and mechanical properties of borate glasses. A key feature of this modeling approach is that it is analytical, and hence, avoids the costly computations associated with first principles calculations. Constraint theory thus offers an efficient tool for the design of new glass compositions with desired values of properties. The success of the approach also points to the importance of accounting for the temperature dependence of the glass network constraints, which becomes evident by comparing the composition dependence of a room temperature glassy-state property (such as hardness) with a high temperature liquid-state property (such as the glass transition temperature). This difference in compositional scaling is attributed to the glass having additional rigid constraints at room temperature compared to the liquid.

7 General Discussion and Perspectives

Scientists have attempted to computationally design glassy materials for specific applications for several decades. Despite some progress, computational restrictions often render impossible the accurate quantitative design of glassy materials. The properties of glassy materials are particularly challenging to predict owing to the existence of structural and dynamical heterogeneities. Particularly, the ionic transport mechanisms in glass remain relatively poorly understood due to the complicated nature of glass structure. In this thesis, we have applied novel approaches for investigating the structural and topological basis of various glass properties, with focus on the transport properties.

The study of the transport properties of glasses and glass-forming melts is a crucial subject of glass science due to the importance of these properties in glass technology. The tracer and ion exchange diffusion processes in glass have been extensively investigated for decades, i.e., considerable progress has been achieved in understanding these diffusion phenomena in glass. In this work, we have investigated the inward and outward diffusion in glass, which are caused by surface reduction and oxidation, respectively. Despite the progress reported in this thesis, these two types of diffusion processes are still not completely understood and several challenging problems need to be explored in the future, as discussed in the following.

Most importantly, the questions of why the alkali ions diffuse much slower than alkaline earth ions and why the alkali inward diffusivity is several orders of magnitude lower than the alkali tracer diffusivity should be further clarified. This should be done by: (i) looking into the medium-range structure; (ii) using the constraint theory; (iii) studying the interaction between the diffusing species in the diffusing channels; and (iv) considering the charge-compensation of the electron holes. Furthermore, it would be interesting to investigate the reversibility of the outward and inward diffusion processes, i.e., perform thermal reduction of an initially oxidized glass and vice versa. For example, the creation of the nano-crystalline surface layer during oxidation might inhibit the subsequent inward diffusion during thermal reduction. In addition, the microstructures of both the modifying oxide surface layer and the silica-rich surface layer should directly be probed by means of advanced imaging techniques, e.g., high resolution transmission electron microscopy (HR-TEM). Finally, investigating the inward diffusion in mixed-alkali glasses would also be interesting. The mixed-alkali effect is a well known phenomenon in glasses. In a glass with two types of alkali ions, the ionic conductivity goes through a deep minimum as the ratio of the alkali ions is varied [Varshneya 2006]. The effect is one of the longstanding unresolved problems in the glass science community, because a widely accepted explanation for the effect does not exist.

In this work, we have demonstrated that the inward diffusion can occur in various silicate, borate, and boroaluminosilicate glass systems. To further understand the diffusion mechanism, the diffusion could also be studied in, e.g., phosphate and germanate glasses. For example, in germanate glasses, initial addition of alkali oxide results in a coordination change of Ge from 4-fold to 5- or 6-fold with no formation of NBO, while further alkali addition at some point results in conversion back to 4-fold coordinated Ge with concomitant formation of NBOs [Henderson 2007]. Hence, it could be investigated whether the impact of germanimum speciation on inward diffusion is similar to the impact of boron speciation. Moreover, it would also be interesting to investigate the oxidation mechanism of non-oxide glass systems, e.g., chalcogenide, chalcohalide, or metallic glasses. Thus, the question of whether surface diffusion processes occur during heat-treatment in air should be clarified.

The application of these types of glasses is limited to some extent by their uncontrolled drift in properties over time due to aging processes [Ratushnyak & Gonchukova 2007; Delaizir *et al.* 2009; Lucas *et al.* 2009]. Even though these glasses are already commercially available, the origin and consequences of physical and chemical aging have not yet been fully understood. Clarifying the origin of chemical aging (i.e., oxidation) could help to optimize the glass compositions and preparation conditions to make the glasses suitable for additional high-tech applications. Furthermore, it is expected that a thorough understanding of these diffusion processes will lead to more insights into the nature of the glassy state in general, because diffusion is linked with the glass structure and dynamics.

In Chapter 5, we have shown how various properties of glasses can be modified by the inward and outward diffusion approaches. To apply these approaches in glass technology, the conditions for creating the silica-rich and nano-crystalline surface layers should be optimized in terms of heat-treatment conditions and glass composition and structure. The results presented in this thesis provide such information. For example, we have found that copper is the ideal polyvalent element for creating the thickest silica-rich surface layer. Of course, other properties such as the glass-forming ability and optical transparency (affected by polyvalent element) should also be considered. Regarding the formation of the silica-rich surface layer in glass-ceramics, more compositions should be tested to see whether the percolative phenomenon reported for the diopside system is universal. It would be useful for such a study if the percolation degree can be quantified and the percolation pathways can be detected (e.g., by HR-TEM). The impact of the percolation phenomena on the surface performances of the glass-ceramics should also be studied in order to find applications. We believe that determining the percolation threshold value for the inward diffusion in glass-ceramics is crucial for tailoring the physical and chemical performances of glass-ceramics. Since the inward diffusion can take place even in glass-ceramics with high content of crystals up to 80 vol%, it indicates that the surface properties of glass-ceramics with a large range of crystals can be improved by inward diffusion. In commercial glass-ceramic products, the degree of crystallization varies most frequently between 30 and 70% [Zanotto 2010], i.e., below the percolation threshold value in the case of diopside glass-ceramics.

Besides using the inward and outward diffusion approaches to gain insights into the transport properties of oxide glasses, we have applied temperature-dependent constraint theory to enhance the understanding of the structural and topological basis of selected dynamical and mechanical properties of glasses. Glassy materials have proved to be especially challenging for first principles modeling, owing to their non-crystalline structure and the long time scales involved in the glass transition process. However, the topological modeling approach presented in Chapter 6 exhibits the remarkable ability to map new composition spaces of glassy materials with straightforward analytical derivations based on the topology of the glass network. This is currently not possible using any other approach. The approach is also proving to be a powerful tool for revealing the microscopic origin of properties such as liquid fragility, a longstanding unsolved problem in condensed matter science.

The topological modeling approach represents an intermediate level of approach between traditional atomistic simulation techniques such as molecular dynamics (MD) and other more empirical macroscopic modeling techniques. The disadvantages of MD simulations are the requirements of accurate knowledge of interatomic potentials and the small integration time steps. The advantage of applying constraint theory is that the key physics governing glass properties can be treated analytically without the need for MD or other complicated

numerical solutions. Hence, a main feature of the modeling approach is that it is analytical. Consequently, it enables calculation of properties across a wide range of composition space with minimal level of calculation. This work suggests that with additional research, other thermal, mechanical, and rheological properties of glass may also be accurately predicted using constraint theory. Indeed, we believe that the approach opens a new vista for prediction of inorganic glass properties in general. It would also be worthy to try to apply the constraint theory to predict the composition dependence of ionic diffusion in glass.

In this thesis, we have applied the approach to a series of soda-lime-borate glasses, because this glass series contains an abundance of interesting structural and topological features and has shown to be particularly challenging for traditional techniques such as MD. In future work, it would be interesting to investigate the network topology of more complicated glass systems that are commercially utilized, such as borosilicate or boroaluminosilicate glasses. To do so, one should notice that the implicit assumption of constraint theory is that the network-forming structural units and their associated constraints can be identified. Such information can often be obtained from structural characterization using experimental techniques such as NMR and Raman spectroscopy. However, when direct experimental measurements are not available, structural information and the energies associated with the different types of constraints may in some cases be obtained from MD simulations [Mauro & Varshneya 2007; Micoulaut *et al.* 2010; Mauro 2011].

A complete chemical and physical description of the glassy state has hitherto been impossible due to the complicated non-crystalline nature of glass structure. In the past few decades, new insights have followed from tremendous improvements both in experimental (such as NMR and neutron spectroscopy) and computational methods. The combined experimental and theoretical studies represented in this thesis can provide insights into some of the mysteries of the glassy state. However, there is certainly still much work to be done in the future.

8 Conclusions

We have clarified the dependences of selected glass properties on the network structure and topology, with focus on ionic diffusion that plays an important role in glass technology. In detail, we have investigated the so-called inward and outward diffusion processes. These processes have not yet been fully understood. They are also a potential way to tailor various physical and chemical performances of both surface and bulk of glasses. Moreover, we have used topological constraint theory to understand and predict dynamical and mechanical properties of glasses.

The inward and outward diffusion of network-modifying cations occur during thermal reduction and oxidation of polyvalent element-containing oxide glasses, respectively. For sufficiently low partial pressures of the reducing and oxidizing gases, it is chemical diffusion of the network-modifying cations that dissipates the driving force for the redox reaction. The cations diffuse in order to charge-compensate the flux of electron holes in the opposite direction. While the mechanism and kinetics of the outward diffusion process have already been thoroughly studied in the glass literature, this has not been the case for the inward diffusion process. Therefore, we have focused on the inward diffusion process.

We have shown that the inward diffusion can occur in various glass-forming systems and can be driven by reduction of various polyvalent ions, i.e., it appears to be a universal phenomenon in oxide glasses. We have also found that the inward diffusion approach may be used as an alternative method for studying the composition and structure dependence of ionic diffusion in glass. The kinetics and temperature dependence of the diffusion have been established by calculating the diffusion coefficients, and we have found good agreement between inward diffusivity and tracer diffusivity of alkaline earth ions. In contrast, the alkali inward diffusivity is several orders of magnitude lower than the alkali tracer diffusivity. The origin of this discrepancy still needs to be further clarified, but it might be attributed to the fact that for alkali inward diffusion, the charge-compensation of electron holes is a rather slow process, which rate-limits the diffusion.

The inward diffusion approach has been applied to study the composition and structure dependence of diffusion in order to understand how glass structure and topology influences the motion of cations. The activation energy of the alkaline earth diffusion increases linearly with the ionic radius of the alkaline earth ion. The type and concentration of the polyvalent element influences the extent of inward diffusion. The lowest diffusion extent is observed in glasses with high concentration of a polyvalent element in either the highest or lowest valence state. Both in borate and boroaluminosilicate glasses, we have found that the mobility of the network-modifying cations depends on their structural role in the network, i.e., whether they create non-bridging oxygens (NBOs) or act as charge compensators to stabilize network-formers. The presence of NBOs enhances the sodium diffusivity in borate glasses, whereas it lowers the sodium diffusivity in BAS glasses. The inward diffusion approach may also be applied to understand glassy dynamics, as a correlation has been found between the liquid fragility index (m) and the diffusion activation energy (E_{diff}), viz., E_{diff} increases with increasing m. We have ascribed this to the existence of more simple diffusion pathways in “strong” compared to “fragile” glass systems.

We have also explored how the crystallization of a diopside glass (i.e., the percolation of the glassy and crystalline phases) influences the mobility of cations. The inward diffusion occurs

only in glass and not in crystals, i.e., the diffusion degree decreases with increasing crystallization degree. The decrease is especially pronounced above a critical value of crystallinity, which we have attributed to the occurrence of a percolation transition from an interconnected to a disconnected glass phase.

The surface redox reactions and diffusion processes modify the surface and bulk chemistry and structure of glasses. The silica-rich surface layer created as a result of inward diffusion in silicate glasses enhances the chemical durability and mechanical properties. This can be combined with improved photoluminescence properties of, e.g., Eu-Yb doped glasses and such materials may potentially act as interesting solar cell substrate materials. In detail, thermal reduction of Eu-Yb doped glasses induces a quantum cutting effect in the surface layer by reduction of Eu^{3+} to Eu^{2+}. Consequently, energy can be transferred from one UV-excited Eu^{2+} ion to two Yb^{3+} ions that relax by NIR emission around 1000 nm, which matches the greatest spectral response of crystalline Si solar cells.

Due to the high surface-to-volume ratio of glass fibers, the properties of these materials are strongly affected by the redox reactions and surface diffusion processes. Thermal oxidation causes an increase of T_g and enhances the high temperature stability (HTS), which is an important property when the fibers are applied as insulation materials. The increase in HTS might be due to the formation of a nano-crystalline surface layer with relatively high melting point. On the other hand, thermal reduction causes a decrease of T_g and an increase of the crystallization temperature. Consequently, the thermal reduction deteriorates the HTS of the glass fibers.

In the last part of this work, we have applied topological constraint theory to understand and predict three important glass properties: glass transition temperature T_g, liquid fragility index m, and Vickers hardness H_V. According to this approach, the glass network can be considered as a network of bond constraints and the number of these constraints decreases with increasing temperature. We have demonstrated the universal role of network topology in governing liquid fragility of silicate glasses and have found that a series of alkali and alkaline earth ions (except Mg^{2+}) play the same topological role in the glass networks. In addition, we have quantitatively predicted the composition dependence of T_g, m, and H_V for a soda-lime-borate glass system. The observed difference in composition dependence of T_g (high temperature property) and H_V (room temperature property) provides evidence for the importance of accounting for the temperature dependence of the network constraints. Moreover, we have found that the change in hardness due to inward diffusion can be predicted quantitatively based on the measured change in surface composition. The success of the approach in predicting T_g, m, and H_V of the borate glasses suggests that it can be applied for the quantitative design of new glassy materials with optimized properties. Furthermore, it can be used to elucidate the microstructural and topological origins of the calculated glass properties.

9 Bibliography

G. Adam and J. H. Gibbs, "On the temperature dependence of cooperative relaxation properties in glass-forming liquids," *J. Chem. Phys.* **43**, 139-146 (1965).

P. W. Anderson, "Through the Glass Lightly," *Science* **267**, 1615-1616 (1995).

C. A. Angell, "Fast ion motion in glassy and amorphous materials," *Solid State Ionics* **9-10**, 3-16 (1983).

C. A. Angell, "Spectroscopy simulation and scattering, and the medium range order problem in glass," *J. Non-Cryst. Solids* **73**, 1-17 (1985).

C. A. Angell, "Formation of glasses from liquids and biopolymers," *Science* **267**, 1924-1935 (1995).

C. A. Angell, K. L. Ngai, G. B. McKenna, P. F. McMillan, and S. W. Martin, "Relaxation in glassforming liquids and amorphous solids," *J. Appl. Phys.* **88**, 3113-3157 (2000).

W. H. Armistead and S. D. Stookey, "Photochromic Silicate Glasses Sensitized by Siliver Halides," *Science* **144**, 150-154 (1964).

H. Bach and D. Krause, *Low Thermal Expansion Glass Ceramics*, Springer, Berlin, (2005).

F. Berkemeier, S. Voss, Á. W. Imre, and H. Mehrer, "Molar volume, glass-transition temperature, and ionic conductivity of Na- and Rb-borate glasses in comparison with mixed Na-Rb borate glasses," *J. Non-Cryst. Solids* **351**, 3816-3825 (2005).

M. Bertmer, L. Züchner, J. C. C. Chan, and H. Eckert, "Short and Medium Range Order in Sodium Aluminoborate Glasses. 2. Site Connectivities and Cation Distributions Studied by Rotational Echo Double Resonance NMR Spectroscopy," *J. Phys. Chem. B* **104**, 6541-6553 (2000).

R. M. Biefeld, G. E. Pike, and R. T. Johnson Jr., "Percolative ionic conduction in the $LiAlSiO_4$ glass-ceramic system," *Phys. Rev. B* **15**, 5912-5920 (1977).

R. A. Brooker, S. C. Kohn, J. R. Holloway, and P. F. McMillan, "Structural controls on the solubility of CO_2 in silicate melts. Part II: IR characteristics of carbonate groups in silicate glasses," *Chem. Geol*. **174**, 241-254 (2001).

A. Bunde, K. Funke, and M. D. Ingram, "Ionic glasses: History and challenges," *Solid State Ionics* **105**, 1 (1998).

J.-C. Bünzli, "Europium in the limelight," *Nature Chem.* **2**, 696 (2010).

D. Canil and K. Muehlenbachs, "Oxygen diffusion in an Fe-rich basalt melt," *Geochim. Cosmochim. Acta* **54**, 2947-2951 (1990).

J. C. C. Chan, M. Bertmer, and H. Eckert, "Site Connectivities in Amorphous Materials Studied by Double-Resonanc NMR of Quadrupolar Nuclei: High-Resolution $^{11}B \leftrightarrow ^{27}Al$ Spectroscopy of Aluminoborate Glasses," *J. Am. Chem. Soc.* **121**, 5238-5248 (1999).

L. Q. Chen, L. Z. Wang, G. C. Che, G. Wang, and Z. R. Li, "Ionic conductivity enhancement during pre-crystallization in amorphous lithium ionic conductor $Li_2B_2O_4$," *Solid State Ionics* **14**, 149-152 (1984).

R. Conradt, "Chemical Durability of Oxide Glasses in Aqueous Solutions: A Review," *J. Am. Ceram. Soc.* **91**, 728-735 (2008).

G. B. Cook, R. F. Cooper, and T. Wu, "Chemical diffusion and crystalline nucleation during oxidation of ferrous iron-bearing magnesium aluminosilicate glass," *J. Non-Cryst. Solids* **120**, 207-222 (1990).

G. B. Cook and R. F. Cooper, "Iron Concentration and the Physical Processes of Dynamic Oxidation in an Alkaline Earth Aluminosilicate Glass," *Am. Mineral.* **85**, 397-406 (2000).

R. F. Cooper, J. B. Fanselow, and D. B. Poker, "The mechanism of oxidation of a basaltic glass: chemical diffusion of network-modifying cations," *Geochim. Cosmochim. Acta* **60**, 3253-3265 (1996a).

R. F. Cooper, J. B. Fanselow, J. K. R. Weber, D. R. Merkley, and D. B. Poker, "Dynamics of Oxidation of a Fe^{2+}-Bearing Aluminosilicate (Basaltic) Melt," *Science* **274**, 1173-1176 (1996b).

R. F. Cooper, R. L. A. Everman, J. W. Hustoft, and S.-H. D. Shim, "Mechanism and kinetics of reduction of a FeO-Fe_2O_3-CaO-MgO aluminosilicate melt in a high-CO-activity environment," *Am. Mineral.* **95**, 810-824 (2010).

B. Cordero, V. Gómez, A. E. Platero-Prats, M. Revés, J. Echeverría, E. Cremades, F. Barragán, and S. Alvarez, "Covalent radii revisited," *Dalton Trans.* 2832-2838 (2008).

G. de With, R. H. Brzesowsky, J. G. van Lierop, I. J. M. Snijkers-Hendrickx, and N. A. M. Sweegers, "Strengthening of glass by hybrid organicinorganic coatings," *J. Non-Cryst. Solids* **226**, 105–113 (1998).

P. G. Debenedetti and F. H. Stillinger, "Supercooled liquids and the glass transition," *Nature* **410**, 259-267 (2001).

G. Delaizir, J.-C. Sangleboeuf, E. A. King, Y. Gueguen, X.-H. Zhang, C. Boussard-Pledel, B. Bureau, and P. Lucas, "Influence of ageing conditions on the mechanical properties of Te-As-Se fibres," *J. Phys. D: Appl. Phys.* **42**, 095405 (2009).

S. Deriano, T. Rouxel, M. LeFloch, and B. Beuneu, "Structure and mechanical properties of alkali-alkaline earth-silicate glasses," *Phys. Chem. Glasses* **45**, 37-44 (2004).

M. P. Dickenson and P. C. Hess, "The structural role and homogeneous redox equilibria of iron in peraluminous, metaluminous and peralkaline silicate melts", *Contrib. Mineral. Petrol.* **92**, 207-217 (1986).

L. M. Donohoe and J. E. Shelby, "Formation and properties of soda-lime borate glasses," *Phys. Chem. Glasses: Eur. J. Glass Sci. Technol. B* **47**, 16-21 (2006).

R. H. Doremus, "Interdiffusion of Hydrogen and Alkali Ions in a Glass Surface", *J. Non-Cryst. Solids* **19**, 137-144 (1975).

R. H. Doremus, *Diffusion of Reactive Molecules in Solid and Melts*, John Wiley & Sons, New York (2002).

J. Dudowicz, K. F. Freed, and J. F. Douglas, "Fragility of Glass-Forming Polymer Liquids," *J. Phys. Chem. B* **109**, 21350-21356 (2005).

J. A. Duffy, "A review of optical basicity and its applications to oxidic systems," *Geochim. Cosmochim. Acta* **57**, 3961-3970 (1993).

J. A. Duffy and M. D. Ingram, "Establishment of an optical scale for Lewis basicity in inorganic oxyacids, molten salts, and glasses," *J. Am. Chem. Soc.* **93**, 6448-6454 (1971).

J. A. Duffy, E. I. Kamitsos, G. D. Chryssikos, and A. P. Patsis, "Trends in local basicity in sodium borate glasses and relation to ionic mobility," *Phys. Chem. Glasses* **34**, 153-157 (1993).

J. A. Duffy, B. Harris, E. I. Kamitsos, G. D. Chryssikos, and Y. D. Yiannopoulos, "Basicity Variation in Network Oxides: Distribution of Metal Ion Sites in Borate Glass Systems;" *J. Phys. Chem. B* **101**, 4188-4192 (1997).

T. Dunn, "Oxygen diffusion in three silicate melts along the join diopside-anorthite," *Geochim. Cosmochim. Acta* **46**, 2293-2299 (1982).

T. Dunn, “Oxygen chemical diffusion in three basaltic liquids at elevated temperatures and pressures,” *Geochim. Cosmochim. Acta* **47**, 1923-1930 (1983).

M. D. Dyar, “A review of Mössbauer data on inorganic glasses: The effects of composition on iron valency and coordination”, *Am. Mineral.* **70**, 304-316 (1985).

J. C. Dyre, P. Maass, B. Roling, and D. L. Sidebottom, “Fundamental questions relating to ion conduction in disordered solids,” *Rep. Prog. Phys.* **72**, 046501 (2009).

A. Ellison and I. A. Cornejo, “Glass Substrates for Liquid Crystal Displays,” *Int. J. Appl. Glass Sci.* **1**, 87-103 (2010).

R. L. A. Everman and R. F. Cooper, “Internal reduction of an iron-doped magnesium aluminosilicate melt,” *J. Am. Ceram. Soc.* **86**, 487-494 (2003).

M. E. Frary and C. A. Schuh, “Correlation-space description of the percolation transition in composite microstructures,” *Phys. Rev. E* **76**, 041108 (2007).

G. H. Frischat, *Ionic Diffusion in Oxide Glasses*, Trans Tech Publications, Germany (1975).

G. S. Fulcher, “Analysis of recent measurements of the viscosity of glasses,” *J. Am. Ceram. Soc.* **8**, 339-355 (1925).

G. J. Gao, S. Reibstein, M. Y. Peng, and L. Wondraczek, “Tunable dual-mode photoluminescence from nanocrystalline Eu-doped Li_2ZnSiO_4 glass ceramic phosphors,” *J. Mater. Chem.* **21**, 3156-3161 (2011).

A. N. Georoff and C. L. Babcock, “Relation of microindentation harndess to glass composition,” *J. Am. Ceram. Soc.* **56**, 97-99 (1973).

J. I. Gersten and F. W. Smith, *The Physics and Chemistry of Materials*, John Wiley & Sons, New York (2001).

E. L. Gjersing, S. Sen, and R. E. Youngman, “Mechanistic Understanding of the Effect of Rigidity Percolation on Structural Relaxation in Supercooled Germanium Selenide Liquids,” *Phys. Rev. B* **82**, 014203 (2010).

G. N. Greaves, “EXAFS and the structure of glass,” *J. Non-Cryst. Solids* **71**, 203-217 (1985).

G. N. Greaves and K. L. Ngai, “Reconciling ionic-transport properties with atomic structure in oxide glasses,” *Phys. Rev. B* **52**, 6358-6380 (1995).

G. N. Greaves and S. Sen, “Inorganic glasses, glass-forming liquids and amorphizing solids,” *Adv. Phys.* **56**, 1-166 (2007).

S. Greenblatt and P. J. Bray, “Nuclear magnetic resonance investigations of the system $BaO\text{-}B_2O_3$,” *Phys. Chem. Glasses* **8**, 190-193 (1967).

P. K. Gupta, “The Random-Pair Model of Four-Coordinated Borons in Alkali-Borate Glasses,” In: *Proceedings of the International Congress on Glass*, p. 1-10, New Delhi, unpublished (1986).

P. K. Gupta and J. C. Mauro, “Composition dependence of glass transition temperature and fragility. I. A topological model incorporating temperature-dependent constraints,” *J. Chem. Phys.* **130**, 094503 (2009).

D. K. Hale, ”Strengthening of Silicate Glasses by Ion Exchange,” *Nature* **217**, 1115-1118 (1968).

G. S. Henderson, “The Germanate Anomaly: What do we know?,” *J. Non-Cryst. Solids* **353**, 1695-1704 (2007).

A. Herrmann, S. Fibikar, and D. Ehrt, “Time-resolved fluorescence measurements of Eu^{3+}- and Eu^{2+}-doped glasses,” *J. Non-Cryst. Solids* **355**, 2093-2101 (2009).

L. M. Hirsch, T. J. Shankland, and A. G. Duba, "Electrical conduction and polaron mobility in Fe-bearing olivine," *Geophys. J. Int.* **114**, 36-44 (1993).

C. Huang and A. N. Cormack, "The structure of sodium silicate glass," *J. Chem. Phys.* **93**, 8180-8186 (1990).

H. Inoue, N. Aoki, and I. Yasui, "Molecular Dynamics Simulation of the Structure of Borate Glasses," *J. Am. Ceram. Soc.* **70**, 622-627 (1987).

S. Ishizuka, H. Hommoto, N. Kido, K. Hashimoto, A. Yamada, S. Niki, "Efficiency enhancement of $Cu(In,Ga)Se_2$ solar cells fabricated on flexible polyimide substrates using alkali-silicate glass thin layers," *Appl. Phys. Express* **1**, 092303 (2008).

C. M. Jantzen, K. G. Brown, and J. B. Pickett, "Durable Glass for Thousands of Years," *Int. J. Appl. Glass Sci.* **1**, 38-62 (2010).

J. R. Jurado-Egea, A. E. Owen, and A. K. Bandyopadhyay, "Electronic conduction in basalt glass and glass-ceramics – correlation with magnetic crystallization," *J. Mater. Sci.* **22**, 3602-3606 (1987).

E. I. Kamitsos, G. D. Chryssikos, A. P. Patsis, and J. A. Duffy, "Metal ion sites in oxide glasses: Relation to glass basicity and ion transport," *J. Non-Cryst. Solids* **196**, 249-254 (1996).

O. Kanert, R. Küchler, D. Suter, G. N. Shannon, and H. Jain, "Effect of devitrification on the ionic diffusion of Li-disilicate," *J. Non-Cryst. Solids* **274**, 202-207 (2000).

R. Kerner and J. C. Phillips, "Quantitative principles of silicate glass chemistry," *Solid State Commun.* **117**, 47-51 (2000).

W. D. Kingery, H. K. Bowen, and D. R. Uhlmann, *Introduction to Ceramics*, 2nd edition, Wiley, New York (1976).

C. A. Klein, "Anisotropy of Young Modulus and Poisson Ratio in Diamond," *Mater. Res. Bull.* **27**, 1407-1414 (1992).

C. R. Kurkjian, P. K. Gupta, and R. K. Brow, "The Strength of Silicate Glasses: What Do We Know, What Do We Need to Know?," *Int. J. Appl. Glass Sci.* **1**, 27-37 (2010).

R. A. Lange and I. S. E. Carmichael, "Densities of Na_2O-K_2O-CaO-MgO-FeO-Fe_2O_3-Al_2O_3-TiO_2-SiO_2 liquids: New measurements and derived partial molar properties," *Geochim. Cosmochim. Acta* **51**, 2931-2946 (1987).

W. T. Laughlin and D. R. Uhlmann, "Viscous flow in simple organic liquids," *J. Phys. Chem.* **76**, 2317-2325 (1972).

J. A. Liu, Y. Z. Yue *et al.*, unpublished data (2011).

H. X. Lu and R. Dieckmann, "Sodium tracer diffusion in glasses of the type $(CaO{\cdot}Al_2O_3)_x(2SiO_2)_{1-x}$," *J. Non-Cryst. Solids* **353**, 2528-2544 (2007).

P. Lucas, E. A. King, Y. Gueguen, J.-C. Sangleboeuf, V. Keryvin, R. G. Erdmann, G. Delaizir, C. Boussard-Pledel, B. Bureau, X.-H. Zhang, and T. Rouxel, "Correlation Between Thermal and Mechanical Relaxation in Chalcogenide Glass Fibers," *J. Am. Ceram. Soc.* **92**, 1986-1992 (2009).

M. E. Lynch, D. C. Folz, and D. E. Clark, "Use of FTIR reflectance spectroscopy to monitor corrosion mechanisms on glass surfaces," *J. Non-Cryst. Solids* **353**, 2667-2674 (2007).

V. Magnien, D. R. Neuville, L. Cormier, J. Roux, J.-L. Hazemann, D. de Ligny, S. Pascarelli, I. Vickridge, O. Pinet, and P. Richet, "Kinetics and mechanims of iron redox reactions in silicate melts: The effects of temperature and alkali cations", *Geochim. Cosmochim. Acta* **72**, 2157-2168 (2008).

J. D. Martin, S. J. Goettler, N. Fosse, and L. Iton, "Designing intermediate-range order in amorphous materials," *Nature* **419**, 381-384 (2002).

L.-M. Martinez and C. A. Angell, "A thermodynamic connection to the fragility of glass-forming liquids," *Nature* **410**, 663-667 (2001).

C. Martiny, S. Murugavel, B. Roling, F. Natrup, H. Bracht, and M. D. Ingram, "Mobilities of divalent ions in glass," *Glass Technol.* **43C**, 309-314 (2002).

J. C. Mauro, "Topological Constraint Theory of Glass," *Am. Ceram. Soc. Bull.* **90** (2011).

J. C. Mauro and A. K. Varshneya, "Modeling of Rigidity Percolation and Incipient Plasticity in Germanium-Selenium Glasses," *J. Am. Ceram. Soc.* **90**, 192-198 (2007).

J. C. Mauro, P. K. Gupta, and R. J. Loucks, "Composition dependence of glass transition temperature and fragility. II. A topological model of alkali borate liquids," *J. Chem. Phys.* **130**, 234503 (2009a).

J. C. Mauro, Y. Z. Yue, A. J. Ellison, P. K. Gupta, and D. C. Allan, "Viscosity of glass-forming liquids," *Proc. Natl. Acad. Sci. U.S.A.* **106**, 19780-19784 (2009b).

J. C. Mauro, D. C. Allan, and M. Potuzak, "Nonequilibrium viscosity of glass," *Phys. Rev. B* **80**, 094204 (2009c).

M. Micoulaut, J.-Y. Raty, C. Otjacques, and C. Bichara, "Understanding Amorphous Phase-Change Materials from the Viewpoint of Maxwell Rigidity," *Phys. Rev. B* **81**, 174206 (2010).

M. Moesgaard, H. D. Pedersen, Y. Z. Yue, and E. R. Nielsen, "Crystallization in stone wool fibres," *J. Non-Cryst. Solids* **353**, 1101-1108 (2007).

J. Nagler, A. Levina, M. Timme, "Impact of single links in competitive percolation," *Nat. Phys.* **7**, 265-270 (2011).

F. V. Natrup, H. Bracht, S. Murugavel, and B. Roling, "Cation diffusion and ionic conductivity in soda-lime silicate glasses," *Phys. Chem. Chem. Phys.* **7**, 2279-2286 (2005).

G. G. Naumis, "Energy landscape and rigidity," *Phys. Rev. E* **71**, 026114 (2005).

G. G. Naumis, "Glass transition phenomenology and flexibility: An approach using the energy landscape formalism," *J. Non-Cryst. Solids* **352**, 4865-4870 (2006).

M. Nogami, K. Watanabe, Y. Ito, H. Ito, and H. Nakano, "Hydrogen Gas Reaction with Eu^{3+}-Doped Al_2O^3-SiO_2 Glasses," *J. Am. Ceram. Soc.* **93**, 1663-1667 (2010).

V. N. Novikov and A. P. Sokolov, "Poisson's ratio and the fragility of glass-forming liquids," *Nature* **431**, 961-963 (2004).

W. C. Oliver and G. M. Pharr, "An improved technique for determining hardness and elastic-modulus using load and displacement sensing indentation experiments," *J. Mater. Res.* **7**, 1564-1583 (1992).

M. Y. Peng, Z. W. Pei, G. Y. Hong, and Q. Su, "Study on the reduction of $Eu^{3+} \rightarrow Eu^{2+}$ in $Sr_4Al_{14}O_{25}$: Eu prepared in air atmosphere," *Chem. Phys. Lett.* **371**, 1-6 (2003).

G. M. Pharr and A. Bolshakov, "Understanding nanoindentation unloading curves," *J. Mater. Res.* **17**, 2660-2671 (2002).

J. C. Phillips, "Topology of Covalent Non-Crystalline Solids. I: Short-Range Order in Chalcogenide Alloys," *J. Non-Cryst. Solids* **34**, 153-181 (1979).

J. C. Phillips, "The physics of glass," *Phys. Today* **35**, 27-33 (1982).

J. C. Phillips and R. Kerner, "Structure and Function of Window Glass and Pyrex," *J. Chem. Phys.* **128**, 174506 (2008).

J. R. Qiu, K. Kojima, K. Miura, T. Mitsuyu, and K. Hirao, "Infrared femtosecond laser pulse-induced permanent reduction of Eu^{3+} to Eu^{2+} in a fluorozirconate glass," *Opt. Lett.* **24**, 786-788 (1999).

S. L. Ratushnyak and N. O. Gonchukova, “Aging and Deformation of Metallic Glasses,” *Glass Phys. Chem.* **33**, 130-135 (2007).

B. S. Richards, “Enhancing the performance of silicon solar cells via the application of passive luminescence conversion layers,” *Sol. Energy Mater. Sol. Cells* **90**, 2329-2337 (2006).

P. Richet, M. Roskosz, and J. Roux, “Glass formation in silicates: Insights from composition,” *Chem. Geol.* **225**, 388-401 (2006).

K. Roselieb and A. Jambon, ”Tracer diffusion of Mg, Ca, Sr, and Ba in Na-aluminosilicate melts,” *Geochim. Cosmochim. Acta* **66**, 109-123 (2002).

P. S. Salmon, “Amorphous materials: Order within disorder,” *Nat. Mater.* **1**, 87-88 (2002).

S. Sastry, “The relationship between fragility, configurational entropy and the potential energy landscape of glass-forming liquids,” *Nature* **409**, 164-167 (2001).

H. Schmalzried, *Solid State Reactions,* Verlag Chemie, Weinheim (1984).

H. Scholze, “Der Einbau des Wassers in Gläser. I. Der Einfluss des im Glas gelösten Wassers auf das Ultrarot-Spektrum und die quantitative ultrarotspektroskopische Bestimmung des Wassers in Gläsern,” *Glastech. Ber.* **32**, 81-88 (1959).

H. D. Schreiber, S. J. Kozak, A. L. Fritchman, D. S. Goldman, and H. A. Schaeffer, “Redox kinetics and oxygen diffusion in a borosilicate melt,” *Phys. Chem. Glasses* **27**, 152-177 (1986).

H. D. Schreiber, N. R. Wilk, and C. W. Schreiber, “A comprehensive electromotive force series of redox couples in soda-lime-silicate glass,” *J. Non-Cryst. Solids* **253**, 68-75 (1999).

J. Sehgal and S. Ito, “Brittleness of glass,” *J. Non-Cryst. Solids* **253**, 126-132 (1999).

U. Senapati, K. Firstenberg, and A. K. Varshneya, “Structure-Property Inter-Relations in Chalcogenide Glasses and their Practical Implications,” *J. Non-Cryst. Solids* **222**, 153-159 (1997).

J. E. Shelby, *Handbook of Gas Diffusion in Solid and Melts*, ASM International, Materials Park (1996).

J. E. Shelby, *Introduction to Glass Science and Technology*, The Royal Society of Chemistry, Cambridge (2005).

B. Širok, B. Blagojević, and P. Bullen, *Mineral Wool*, Woodhead Publishing Limited, Cambridge (2008).

M. M. Smedskjaer and Y. Z. Yue, “Inward cationic diffusion in glass,” *J. Non-Cryst. Solids* **355**, 908-912 (2009).

M. M. Smedskjaer, J. Deubener, and Y. Z. Yue, “Inward Cationic Diffusion and Formation of Silica-Rich Surface Nanolayer of Glass,” *Chem. Mater.* **21**, 1242-1247 (2009).

R. J. Speedy, “Relations between a Liquid and Its Glasses,” *J. Phys. Chem. B* **103**, 4060-4065 (1999).

J. E. Stanworth, “Oxide Glass Formation from the Melt”, *J. Am. Ceram. Soc.* **54**, 61-63 (1971).

F. H. Stillinger, “Supercooled liquids, glass transitions, and the Kauzmann paradox,” *J. Chem. Phys.* **88**, 7818-7825 (1988).

D. R. Swiler, A. K. Varshneya, and R. M. Callahan, “Microhardness, Surface Toughness and Average Coordination Number in Chalcogenide Glasses,” *J. Non-Cryst. Solids* **125**, 250-257 (1990).

G. Tammann, *Der Glaszustand*, Voss, Leipzig (1933).

G. Tammann and W. Hesse, “The dependancy of viscosity on temperature in hypothermic liquids,” *Z. Anorg. Allg. Chem.* **156**, 245-257 (1926).

M. F. Thorpe, "Continuous deformations in random networks," *J. Non-Cryst. Solids* **57**, 355-370 (1983).

B. M. van der Ende, L. Aarts, and A. Meijerink, "Lanthanide ions as spectral converts for solar cells," *Phys. Chem. Chem. Phys.* **11**, 11081-11095 (2009).

A. K. Varshneya, *Fundamentals of Inorganic Glasses*, 2nd edition, Society of Glass Technology, Sheffield (2006).

A. K. Varshneya, "Chemical Strengthening of Glass: Lessons Learned and Yet To Be Learned," *Int. J. Appl. Glass Sci.* **1**, 131-142 (2010).

A. K. Varshneya and J. C. Mauro, "Comment on *Misconceived ASTM Definition of "Glass"* by A. C. Wrigth," *Glass Technol. Eur. J. Glass Sci. Technol. A* **51**, 28-30 (2010).

P. Vergeer, T. J. H. Vlugt, M. H. F. Kox, M. I. den Hertog, J. P. J. M. van der Eerden, and A. Meijerink, "Quantum cutting by cooperative energy transfer in $Yb_xY_{1-x}PO_4:Tb^{3+}$," *Phys. Rev. B* **71**, 014119 (2005).

T. A. Vilgis, "Strong and fragile glasses: A powerful classification and its consequences," *Phys. Rev. B* **47**, 2882-2885 (1993).

H. Vogel, "The temperature dependence law of the viscosity of fluids," *Z. Phys.* **22**, 645-646 (1921).

C. Wang, M. Y. Peng, N. Jiang, X. W. Jiang, C. J. Zhao, and J. R. Qiu, "Tuning the Eu luminescence in glass materials synthesized in air by adjusting glass compositions," *Mater. Lett.* **61**, 3608-3611 (2007).

R. F. Wendlandt, "Oxygen diffusion in basalt and andesite melts: Experimental results and a discussion of chemical versus tracer diffusion," *Contrib. Mineral. Petrol.* **108**, 463-471 (1991).

M. Yamane and J. D. Mackenzie, "Vickers Hardness of Glass," *J. Non-Cryst. Solids* **15**, 153-164 (1974).

Y. Z. Yue, "The iso-structural viscosity, configurational entropy and fragility of oxide liquids," *J. Non-Cryst. Solids* **355**, 737-744 (2009).

Y. Z. Yue, M. Korsgaard, L. F. Kirkegaard, and G. Heide, "Formation of a Nanocrystalline Layer on the Surface of Stone Wool Fibers," *J. Am. Ceram. Soc.* **92**, 62-67 (2009).

W. H. Zachariasen, "The Atomic Arrangement in Glass," *J. Am. Chem. Soc.* **54**, 3841-3851 (1932).

R. Zallen, *The Physics of Amorphous Solids*, Wiley Interscience, New York (1998).

E. D. Zanotto, "A bright future for glass-ceramics," *Am. Ceram. Soc. Bull.* **89**, 19-27 (2010).

J. Zarzycki, *Glasses and the Vitreous State*, Cambridge University Press, Cambridge (1991).

X. J. Zhao, Q. N. Zhao, J. G. Yu, and B. S. Liu, "Development of multifunctional photoactive self-cleaning glasses," *J. Non-Cryst. Solids* **354**, 1424-1430 (2008).

Q. J. Zheng, J. C. Mauro, A. J. Ellison, M. Potuzak, and Y. Z. Yue, "Universality of the High Temperature Viscosity Limit of Silicate Liquids," *Phys. Rev. B* **83**, 212202 (2011a).

Q. J. Zheng, R. E. Youngman, C. L. Hogue, J. C. Mauro, M. Potuzak, A. J. Ellison, M. M. Smedskjaer, and Y. Z. Yue, unpublished data (2011b).

J. J. Zhou, Y. Teng, G. Lin, X. Q. Xu, Z. J. Ma, and J. R. Qiu, "Broad-Band Excited Quantum Cutting in Eu^{2+}-Yb^{3+} Co-Doped Aluminosilicate Glasses," *J. Electrochem. Soc.* **157**, B1146-B1148 (2010).

E. S. Zouboulis, M. Grimsditch, A. K. Ramdas, and S. Rodriguez, "Temperature dependence of the elastic moduli of diamond: A Brillouin-scattering study," *Phys. Rev. B* **57**, 2889-2896 (1998).

List of Publications

In addition to the peer-reviewed journal articles listed in Section 1.3, the following papers have been published or presented:

M. M. Smedskjaer and Y. Z. Yue, "Inward Cationic Diffusion in Polyvalent Ion-Containing Silicate Glasses." Oral presentation: *8th Pacific Rim Conference on Ceramic and Glass Technology*, Vancouver, Canada (2009).

M. M. Smedskjaer, Y. Z. Yue, J. Deubener, and H. P. Gunnlaugsson, "Viscous Flow and Diffusion in Iron-Bearing Alkaline-Earth Silicate Glasses." Poster: *8th Pacific Rim Conference on Ceramic and Glass Technology*, Vancouver, Canada (2009).

M. M. Smedskjaer, "Gas and Glass." Oral presentation: *Danish Glass Symposium 2010*, Aalborg, Denmark (2010).

M. M. Smedskjaer, "A New Approach for Modifying Glass Surfaces." Invited lecture: *2010 Shandong Glass Symposium*, Jinan, China (2010).

M. M. Smedskjaer, "Inward Diffusion of Modifying Ions in Glasses and Glass-Ceramics." Norbert J. Kreidl award lecture: *2010 Glass & Optical Materials Division Meeting*, Corning, USA (2010).

M. M. Smedskjaer, J. C. Mauro, J. Deubener, and Y. Z. Yue, "Diffusion of Alkali and Alkaline Earth Ions in Silicate Glasses and its Correlation with Liquid Fragility." Oral presentation: *2010 Glass & Optical Materials Division Meeting*, Corning, USA (2010).

M. M. Smedskjaer, J. Deubener, S. Mørup, and Y. Z. Yue, "Formation of SiO_2-Rich Surface Layer on Glass Fibers." Poster: *2010 Glass & Optical Materials Division Meeting*, Corning, USA (2010).

M. M. Smedskjaer, J. C. Mauro, S. Sen, and Y. Z. Yue, "Network Topology in Soda Lime Borate Glass Systems." Oral presentation: *International Congress on Glass 2010*, Salvador, Brazil (2010).

M. M. Smedskjaer and Y. Z. Yue, "Percolative Inward Diffusion in Iron-Bearing Diopside Glass-Ceramics." Poster: *International Congress on Glass 2010*, Salvador, Brazil (2010).

M. M. Smedskjær, "Funktionelle Glasoverflader (popular science article in Danish)," *GLAS* **Vinter 01**, 14-15 (2011).

M. M. Smedskjaer, J. C. Mauro, and Y. Z. Yue, "Predicting the Composition Dependence of Glass Hardness." Oral presentation: *5th International Workshop on Flow and Fracture of Advanced Glasses*, St-Malo, France (2011).

M. M. Smedskjaer, J. C. Mauro, and Y. Z. Yue, "Understanding Glass Hardness from Constraint Theory." Invited lecture: *2011 Glass & Optical Materials Division Meeting*, Savannah, USA (2011).

M. M. Smedskjaer, J. C. Mauro, and Y. Z. Yue, "Predicting the Hardness of Glass Surfaces." Invited lecture: *Materials Science & Technology 2011 Conference & Exhibition*, Columbus, USA (2011).